PREPARATION, CHARACTERIZATION AND APPLICATION OF NANOPOROUS ACTIVATED CHARCOAL FROM PLANT RESOURCES

A THESIS SUBMITTED TO THE
CENTRAL DEPARTMENT OF CHEMISTRY
INSTITUTE OF SCIENCE AND TECHNOLOGY
TRIBHUVAN UNIVERSITY
NEPAL

FOR THE AWARD OF
DOCTOR OF PHILOSOPHY
IN CHEMISTRY

BY
DIBYASHREE SHRESTHA
NOVEMBER 2019

PREPARATION, CHARACTERIZATION AND APPLICATION OF NANOPOROUS ACTIVATED CHARCOAL FROM PLANT RESOURCES

A THESIS SUBMITTED TO THE

CENTRAL DEPARTMENT OF CHEMISTRY

INSTITUTE OF SCIENCE AND TECHNOLOGY

TRIBHUVAN UNIVERSITY

NEPAL

FOR THE AWARD OF
DOCTOR OF PHILOSOPHY
IN CHEMISTRY

BY

DIBYASHREE SHRESTHA
NOVEMBER 2019

DECLARATION

Thesis entitled **"Preparation, Characterization and Application of Nanoporous Activated Charcoal from Plant Resources"** which is being submitted to the Central Department of Chemistry, Institute of Science and Technology (IOST), Tribhuvan University, Nepal for the award of the degree of Doctor of Philosophy (Ph.D.), is a research work carried out by me under the supervision of Prof. Dr. Armila Rajbhandari (Nyachhyon), Central Department of Chemistry, Tribhuvan University. This research is original and has not been submitted earlier in part or full in this or any other form to any university of institute, here or elsewhere, for the award of any degree.

………………………..

Dibyashree Shrestha

RECOMMENDATION LETTER

This is to recommend that **Ms. Dibyashree Shrestha** has carried out research entitled **"Preparation, Characterization and Application of Nanoporous Activated Charcoal from Plant Resources"** for the award of Doctor of Philosophy (Ph. D.) **Degree in Chemistry** under my supervision. To my knowledge this work has not been submitted for any other degree.

She has fulfilled all the requirements laid down by the Institute of Science and Technology (IOST), Tribhuvan University, Kirtipur for the submission of the thesis for the award of Ph. D. degree.

……………………………………..
Prof. Dr. Armila Rajbhandari (Nyachhyon)
Supervisor
Central Department of Chemistry
Tribhuvan University
Kirtipur, Kathmandu, Nepal
November, 2019

LETTER OF APPROVAL

On the recommendation of **Prof. Dr. Armila Rajbhandari (Nyachhyon)**, this Ph. D. thesis submitted by **Ms. Dibyashree Shrestha** entitled **“Preparation, Characterization and Application of Nanoporous Activated Charcoal from Plant Resources”** is forwarded by Central Department Research Committee (CDRC) to the Dean, Institute of Science and Technology (IOST), T.U.

…………………………..

Dr. Ram Chandra Basnyat
Professor,
Head,
Central Department of Chemistry
Tribhuvan University
Kirtipur, Kathmandu
Nepal

ACKNOWLEDGEMENT

First of all, I would like to extend my profound gratitude to my supervisor Prof. Dr. Armila Rajbhandari (Nyachhyon), Central Department of Chemistry, Tribhuvan University, Kirtipur, Kathmandu, Nepal for her constructive feedback and valuable guidance. Her insightful comments at different stages of my research helped me to stay focused and on track.

I would also like to offer my sincere gratitude to Dean's Office, Institute of Science and Technology (IOST), Tribhuvan University, Nepal for permitting me to join Ph.D. in Central Department of Chemistry, T.U.

I am obliged to Prof. Dr. Megh Raj Pokhrel, former Head, Central Department of Chemistry, and Prof. Dr. Ram Chandra Basnyat, Head, Central Department of Chemistry, Tribhuvan University for providing laboratory facilities and encouragement during this study.

I acknowledge Patan Multiple Campus, Tribhuvan University, Nepal for their kind support for allowing me to join Ph.D. in Central Department of Chemistry, T.U.

University Grants Commission (UGC), Sanothimi, Bhaktapur, Nepal is highly acknowledged for providing partial financial support under Faculty Research Grants (FRG-1419).

In the similar fashion, sincere gratitude and credit goes to Prof. Dr. Soo Wohn Lee, Department of Environmental and Bio-chemical Engineering "Global Research Laboratory (GRL)" Sun Moon University (SMU), Republic of Korea for providing me laboratory facilities to conduct advanced instrumental characterization (TGS/DSC, XRD, Raman, FTIR, XPS, BET, BJH and SEM) of the samples. I am also grateful to Prof. Dr. Santi Maensiri, "Advanced Functional Materials Laboratory", Suranaree University of Technology, Ratchasima, Thailand for providing laboratory facilities to carry out electrochemical characterization of samples.

In the process of encountering "Instrumental Characterization" of samples at "Global Research Laboratory (GRL)"and the complete "Electrochemical Characterization" of samples at "Advanced Functional Materials Laboratory", I came across many difficulties. I am fortunate enough to have friends in both labs. So thanks also goes to Dr. Gobinda Gyawali, Dr. Bhupendra joshi, Dr. Sachindra Kumar Ray, Dr. Yubraj Khatri Kshetri, Dr. Khagendra Tripathi and Dr. Chhabi Regmi, Department of

Environmental and Bio-Chemical Engineering “Global Research Laboratory (GRL)” Sun Moon University (SMU), Republic of Korea. I would also like to gratitude Dr Unchita Wongpratat, Dr. Benjaporn Yotburut, Thongsuk Sichumsaeng, Kwanta Siwawongkasen and all the members of “Advanced Functional Materials Laboratory”, Suranari University of Technology (SUT) in Thailand, who helped me generously during laboratory work, data interpretation and analysis.

I would also like to express my admiration to all teaching and non-teaching staffs of the Central Department of Chemistry for their generous help.

I feel deeply obliged to my parents for being my backbone and main source of regulation throughout life. I’m deeply indebted to my husband for being there at every step of these journeys, for inspiring me, positively challenging me and giving so many reasons to get better promptly and accomplish my research project within the timeframe.

Dibyashree Shrestha
Ph.D. Scholar
Central Department of Chemistry
Kirtipur, Kathmandu, Nepal
2019

ABSTRACT

This study was undertaken to prepare Activated Carbon (AC) from an agro-waste, i.e. sawdust of *Shorea robusta* by chemical activation using phosphoric acid and characterized and applied this AC in energy related field.

The carbonization of wood powder of *Shorea robusta* was carried out at 400°C in an inert atmosphere of N_2 to prepare AC, which was chemically activated with H_3PO_4 and successfully tested as supercapacitor materials for the first time for its application in energy storage device. Thermogravimetric Analysis (TGA)/Differential Scanning Calorimetry (DSC), Scanning Electron Microscopy (SEM), X-ray diffractometer **(**XRD), Raman spectra, Fourier Transform Infrared Spectroscopy (FTIR), Brunauer–Emmett–Teller (BET), and X-ray Photoelectron Spectroscopy **(**XPS) are the methods that have been utilized to characterize as prepared AC.

Thermal decomposition behavior (TG curve) coupled with endothermal peak of DSC curve confirmed that 400^oC was the adequate temperature for carbonization of raw sawdust powder, since no significant weight loss occurred after 400^oC, which confirms the completion of carbonization process. FTIR spectra clearly confirmed the presence of oxygenated functional groups such as hydroxyl (-OH), aldehyde/ketone (-CHO/C=O) and ether (C-O-C), at the surface of as prepared AC. Similarly, XPS shows a broad peak at 532.6 eV for O 1s, indicating the presence of different chemical states of oxygen and the three deconvoluted peaks for oxygen at the binding energies 531 eV, 533.04 eV and 533.12 eV shows the presence of phosphatic oxygen (PO_4^{3-}), hydroxyl group (-OH) and silicon dioxide (SiO_2) respectively. XPS spectra confirmed that as prepared activated carbon (Sa-H_3PO_4) was well functionalized after H_3PO_4 activation and consists of more acidic functional groups as aldehydes/ketones, ethers, hydroxides. This aligns with the FTIR results, where activated carbon (Sa-H_3PO_4) showed high intensities for hydroxyl (-OH), aldehyde/ketone (-CHO/C=O) and ether (C-O-C) functional groups. XRD-pattern showed the amorphous structure of carbon having 002 and 100 plane, whereas Raman spectra clearly displayed G and D band which further confirms the amorphous nature of carbon. The G/D intensity ratio was found to be approximately 1, which indicated the presence of graphitic degree and defects in equal proportion. BET method of surface area determination showed the high specific surface area of 1270 m^2g^{-1} ($\underline{+}$ 0.57 %).

Electrochemical characterization was performed in 6M aqueous KOH using Cyclic Voltammetry (CV), Galvanostatic Charge-Discharge (GCD) and Electrochemical Impendance Spectroscopy (EIS). The specific capacitance acquired from GCD at 1 A g^{-1} was found to be 136.3 Fg^{-1} (± 0.15 %) with 0.44 Ω (± 0.02 %) ESR. The 97 % capacitance retention was observed after 1000 cycles. The energy density of as prepared carbon electrode was found to be 3.0 (± 0.25 %) $Whkg^{-1}$ at 100.5 (± 0.20 %) Wkg^{-1} power density. Then the working carbon electrode was replaced by hybrid-composite-electrode which showed the ideal capacitive behaviors having specific capacitance of 480.4 (± 0.20 %) Fg^{-1}, specific energy density of 24 (± 0.26 %) $WhKg^{-1}$ at power density of 149.3 WKg^{-1} and low ESR value of 0.41 (± 0.02 %) Ω. The obtained results revealed that the desirable electrochemical capacitive performances enable the hybrid composite to act as a new bio-material for high performance supercapacitors and energy storage devices.

Keywords: hybrid composite, capacitive behavior, energy density, power density

LIST OF ACRONYMS AND ABBREVIATIONS

AC	Activated Carbon/ Activated Charcoal
ACC	Activated Carbon Cloth
ACF	Activated Carbon fiber
BAC	Bead Activated Carbon
Bio-AC	Biochar Activated Carbon
BJH	Barrett, Joyner, Hallenda
BET	Brunauer, Emmet, Teller
CAC	Cylindrical Activated Carbon
CCCD	Constant Current Charge/Discharge
Cdl	Double layer capacitance
CPE	Constant phase element
CSB	Charred Sugarcane Bagasse
CNF	Carbon Nano Fibers
CNT	Carbon Nano Tubes
CV	Cyclic Voltammetry
Cs	Specific capacitance
DSC	Differential Scanning Calorimetry
EAC	Extruded Activated Carbon
EC	Electrochemical Capacitor
EDLC	Electrochemical Double Layer Capacitor
EES	Electrochemical Energy Storage
EIS	Electrochemical Impedance Spectroscopy
ES	Energy Storage
FS	Faradiac Supercapacitance
FT-IR	Fourier Transform Infrared Spectroscopy
GAC	Granular Activated Carbon
GCD	Galvanostatic Charge/Discharge
HLPC	Honeycomb-Like Porous Carbon
IAC	Impregnated Activated Carbon
MnO_2	Manganese dioxide
NMP	N-Methyl-2-pyrolidone
PAC	Pellet Activated Carbon

PwAC	Powdered Activated Carbon
PC	Pseudo-Capacitance
PCAC	Polymer-Coated Activated Carbon
PVDF	Polyvinlidine fluoride
RSB	Raw Sugarcane Bagasse
Rs	Solution resistance
Rct	Charge transfer resistance
RuO_2	Ruthenium oxide
SC	Supercapacitor
SEM	Scanning Electron Microscopy
TGA	Thermo Gravimetric Analysis
W	Warburg Impedance
XRD	X ray Diffraction
XPS	X-ray Photoelectron Spectroscopy

LIST OF SYMBOLS

α	Alpha
°C	Degree centigrade
H	Hour
Ω	Ohm
Fg^{-1}	Farad per gram
A g^{-1}	Ampere per gram
m^{2}**g**$^{-1}$	Meter square per gram
Wkg^{-1}	Watt per kilogram
Whkg^{-1}	Watt hour per kilogram
Hz	Herz
MHz	Mega Herz
KHz	Kilo Herz
Z’	Real resistance
Z”	Imaginary resistance

LIST OF TABLES

LIST OF FIGURES

TABLE OF CONTENTS

CHAPTER – 1

1. INTRODUCTION

1.1 Introduction

Carbon is a unique and adaptable element of the entire world's flora. The atomic structure of carbon allows special bonding potentials leading to various structures with divergent properties. It is hard to determine the particular era of the commencement of carbon because carbon materials have been used for so long.

Carbon, in activated form, facilitates well pore structure having high surface area, which may be useful to integrate materials. It has numerous different allotropic modifications like diamond, graphite, carbon fibres, carbon black, activated carbon etc. Among all, activated carbon/activated charcoal (AC) is one of the striking allotropic forms of carbon.

1.2. Activated carbon

Activated carbon/Activated Charcoal (AC), is a carbon-based high quality adsorbent material which has been processed to capitalize on its adsorptive properties. AC has a remarkable pore structure which causes it to have a very high specific surface area, which captures and holds materials. It can be produced from a number of carbon-rich lignocellulosic organic material which are basically considered as precursor such as wood, coconut shells, coal peat, tobacco stems, bean husks, hazelnut shell, banana peels, mangosteen shells, sawdust, rice husk and so on. Lignocellulosic materials if heated in an inert atmosphere, their polymeric structures hemicellulose, cellulose and lignin undergo decomposition as a result of hundreds of concurrent and consecutive reactions. During the course of reaction most of the non-carbon elements, mainly hydrogen, oxygen and nitrogen get liberated in the form of liquid tars**,** chars and gases, leaving behind a rigid carbon skeleton in the form of aromatic sheets and strips (Jagtoyen & Derbyshire 1998). The elementary carbon atoms which get freed from bulk material of precursor, come together into organized crystallographic form i.e. elementary graphitic crystallites along with chars. Char is a non-volatile carbon rich solid residue, which consist of ~30% of carbon and are therefore suitable for the production of AC. By developing internal properties such as surface area, pore volume and pore size distributions in char, AC could be produced which is done by activation along with carbonization.

Besides this it is customary to say that agro-industrial byproducts, agricultural wastes, biomass residues etc. are considered to be the precursors for the production of AC which is reported in different literatures, such as corn cobs (Jonglertjunya, 2008), palm shells (Noor & Nawi, 2008), tropical wood (Acharya et al., 2009; Janoš & Coskun, 2009), walnut shells (Yang & Qiu, 2010), durian peel (Nuithitikul et al., 2010; Saueprasearsit, 2011; Srikun et al., 2011), rice husk (Rahman et al., 2013; Alvarez et al., 2014), watermelon (Banerjee et al., 2012), as coal, jujube seeds (Bae et al., 2014), coconut shells (Boopathy & Karthikeyan, 2013; Bernard et al.; 2013; Floyd et al., 2014; Shaheed et al., 2015), sawdust (Kini et al., 2015) tobacco stems, bean husks, hazelnut shell, banana peels, mangosteen shells and many more (Ioannidou &, Zabaniotou, 2007). Moreover, even non-agricultural products like waste-automobile tires are also found as cheap sources of AC (Behnamfard & Salarirad, 2013).

These carbonaceous raw materials are generally washed, air dried, crushed into fine powder and sieved to get appropriate particle size. Then it is subjected to carbonization (pyrolysis) and activation by adjusting different parameters like temperature, heating rate, holding time, inert environment and activating agents etc. to get amorphous form of carbon. The detail of carbonization is discussed here.

1.2.1. Carbonization

Carbonization is the process of heating in closed system using inert atmosphere. Generally, carbonization of lignocellulosic materials begins from 170^{o}C and completed nearly at around 400^{o}C- 600^{o}C. The rate of pyrolysis is largely influenced by the moisture content of the starting material as well as the heating rate, temperature, holding time of carbonization.

The product formed after carbonization showed the uneven mutual arrangement of the crystallites and resulted the free interstices between them. However, as a consequence of deposition and decomposition of tarry substances, these interstices become filled or at least blocked by amorphous carbon. The resulting carbonized product has small adsorption capacity. In order to enhance the adsorptive properties, internal properties such as surface area, pore volume and pore size distributions should be developed, which can be done by activation along with carbonization. During carbonization, the volatile compounds are driven away initially from the transforming carbon and the non-carbon elements (heteroatoms). Besides this, precursor consists of inorganic ash contents as well, which may act as catalysts for some of the pyrolytic processes. After completion of heating process AC produced having some micropores. Thus, obtained carbon is further subjected to activation process to increase the porosity and surface area.

1.2.2. Activation

Activation is the process to enlarge the diameters of the pores and to increase surface area. It is generally done by two different processes (a) physical activation i.e., heat treatment along with some oxidizing agents like CO_2, steam and (b) chemical activation using different chemicals like H_3PO_4, KOH, $ZnCl_2$ etc. during carbonization. It is generally carried out to remove the disorganized carbon blockings in the pores of activated carbon**.** Apart from this, it helps to enlarge the diameters of the pores, and to create some new porosity (Cagnon et al., 2009). Consequently, a well-developed and readily accessible pore structure with large internal surface area can be produced (Noor & Nawi, 2008).

The activation can be done by one of the following methods.

1.2.2.1. Physical activation

Physical activation is a thermal activation. It is generally carried out in two consecutive heating steps. First one is carbonization under inert atmosphere (usually nitrogen) to devolatilize the raw material and second one is activation by using high temperature along with oxidizing agents like steam, carbon dioxide or a mixture CO_2 and steam which may result the formation of the porous network. Actually, these agents act as extractants of carbon atoms from other hetero atoms (Marsh & Rodríguez-Reinoso, 2006). Carbon dioxide is the preferred gas for physical activation, because it can be easily controlled and it is largely available in different levels of purity. On the other hand, activation with steam has the advantages of being less expensive than activation with carbon dioxide. Likewise, the activation process with these agents can be more easily controlled because the reactions with both carbon dioxide and steam are endothermic and consequently slow. (Marsh & Rodríguez-Reinoso, 2006; Ioannidou & Zabaniotou, 2007). The reactions of carbon materials with both CO_2 and steam can be described as follows:

$C + O_2 \rightarrow 2CO \quad \Delta H = +159\ kJ\ mol^{-1}$……………………...(1)

$C + H_2O \rightarrow CO + H_2 \quad \Delta H = +117\ kJ\ mol^{-1}$……………….(2)

$C + 2H_2O \rightarrow CO_2 + 2H_2 \quad \Delta H = +75\ kJ\ mol^{-1}$…………….(3)

In general, the activation with CO_2 leads to the creation and widening of micropores, whereas activation with steam only widens the existing micropores in the char structure (Rodríguez-Reinoso & Molina-Sabio, 1998), which produces activated carbons with meso- to macropore structures. Irrespective of the use of activating agent, molecular oxygen will be always present in the gases and some burning of the carbon will essentially occur in accordance with equations (4) and (5).

$$\mathbf{2C_f + O_2 \rightarrow 2CO \ldots\ldots (4)}$$

$$\mathbf{C_f + O_2 \rightarrow CO_2 \ldots\ldots (5)}$$

In the above, equation, $\mathbf{C_f}$ refers to a carbon atom, which is free from bonding with heteroatoms. These reactions are highly exothermic, making it difficult to control, and because they occur mostly at the outside surface, little or no enhancements in microporosity are observed. Thus, oxygen (air) is not commonly used as an activating agent. Due to this issue and for the safety, oxygen activation is barely used. However, low amounts of oxygen (or air) can be added during thermal activation with steam or carbon dioxide to help maintaining the high temperatures by reacting with the gases produced during activation (i.e. CO and H_2) (Sugumaran et al., 2012). This approach has the advantage of lowering the pressure of CO and H_2, both inhibiting gases for the activation, and increasing the partial pressure of the activating agent (Sugumaran et al., 2012).

1.2.2.2. **Chemical activation**

The term, chemical activation is referred to the pyrolysis of the starting material in which some chemicals such as phosphoric acid or sulphuric acid, potassium hydroxide, zinc chloride etc. have been previously added which restrict the formation of tar. As a result, a carbonized product with a well-developed porosity may be obtained in a single procedure.

All the agents involved in the chemical activation have a common feature of being dehydrating agents, which influence during the pyrolytic decomposition and impede the formation of tar increasing the production of carbon. The production and properties of AC depend on the impregnation conditions, such as impregnation ratio of weight of activating reagent and weight of carbon precursor, time of pre-drying impregnated materials, as well as pyrolysis conditions, such as temperature, soaking time (period of time the sample and chemical are in contact) and atmosphere. All these process variables vary with the type of carbon precursor and the activating agent.

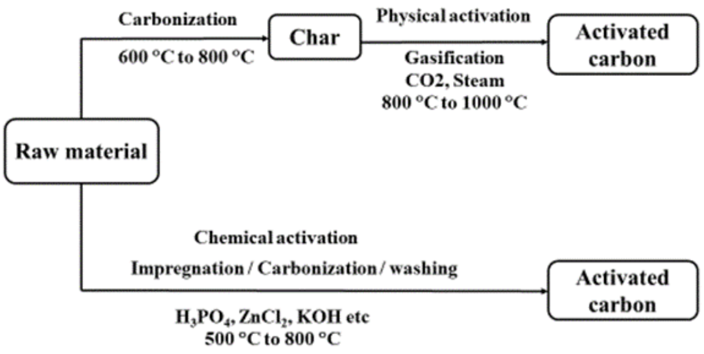

Figure 1: Flow chart diagram of production of AC showing carbonization and activation steps.

The two competing mechanisms of pore evolution in the carbon structure that occur during chemical activation is believed to be as follows:

a. The first one is the insertion of chemicals into the lignocellulosic structure which created the micropores and

b. The second one is the insertion of chemical into the lignocellulosic structure which effects in widening of pores. However it is reported that when the chemical ratio is reasonably high (Stoller et al., 2008) there is a chances of formation of meso as well as macro pores by breaking the walls of pores. Several researchers (Jabit, 2007; Bolotin et al., 2008) reported that activated carbons obtained at low impregnation ratios were essentially microporous and when the amount of impregnation agent increases to some extent, the activated carbon becomes predominantly mesoporous.

Various literatures suggested that H_3PO_4 (Olivares-Marin et al., 2006; Prahas et al., 2008) $ZnCl_2$, KOH, H_2SO_4, NaOH, K_2CO_3, HNO_3 etc. are used as chemical agents for the activation of precursors (Park & Jung, 2003). Some of the common activating agents are discussed below.

1.2.2.2.1. Potassium hydroxide

This agent is an inorganic compound with the formula KOH. It is a strong base and is used in several industrial applications. It is extremely reactive towards acids and corrosive in nature. During the 1970´s, the ACs were prepared using KOH chemical to produce “super ACs” achieving specific surface areas of 3000 m^2g^{-1}. The oxygen of the KOH supports to remove the cross-linking and stabilizing carbon atoms in crystallites, whereas K metal may be intercalated. Then the potassium and carbon atoms are removed from the internal volume of the carbon by washing properly and through activation reaction finally create the microporosity in AC as new structure.

Although KOH develops large microporosity, the production of activated carbon is lower i.e. the carbon content is less than fixed carbon in the initial precursor and thus high temperature of 650 °C is needed for carbonization. The intercalation of metallic potassium in carbon matrix may also affect the lower production of activated carbon (Prahas et al., 2008). With potassium hydroxide, the process is more complex since there is the disintegration of the structure followed by intercalation of the metallic potassium (Prahas et al., 2008) into the “graphitic” laminar structure, breaking down particles and limiting GACs synthesis. Concurrently, there is also some gasification of carbon atoms due to reaction with CO_2 and H_2O, resulting from the redox reaction of carbon with potassium compounds (Prahas et al., 2008).

1.2.2.2.2. Zinc chloride

Zinc chloride is the name of chemical compound with the formula $ZnCl_2$. This product was employed in the 1970´s especially for wood wastes. However, it is no longer used because it is environmentally unfriendly or it is not considered as green chemical agent/compound. Impregnation with $ZnCl_2$ produces a degradation of the cellulosic material, during the carbonization results in charring and aromatization of the carbon skeleton and creation of the pore structure (Caturla et al., 1991). Similarly, the problems of corrosion and inefficient chemical recovery are also associated with it. Moreover, the ACs obtained, using $ZnCl_2$ cannot be used in pharmaceutical and food industries as they may contaminate the product (Caturla et al., 1991).

1.2.2.2.3. Phosphoric acid

Phosphoric acid, also known as ortho-phosphoric acid is a mineral acid having the chemical formula H_3PO_4. It is the most favored and broadly used impregnating agent for the activation of lignocellulosic materials.

The mechanisms for chemical activation of lignocellulosic materials impregnated with H_3PO_4 were widely studied by many researchers (Molina-Sabio et al. 1995a; Jagtoyen and Derbyshire, 1998; Fierro et al., 2005; Olivares-Marín et al., 2006). Several mechanisms were proposed for the action of H_3PO_4 on the carbon structure of lignocellulosic precursor, which involves; (i) acid catalysis to promote bond cleavage, (ii) hydrolysis, (iii) dehydration and condensation, and (iv) formation of phosphate linkages (e.g., phosphate and polyphosphate esters) that promote the cross-linking between phosphoric acid and the lignocellulosic biopolymers (mostly cellulose and hemicellulose) (Zuo et al., 2009).

According to Jagtoyen and Derbyshire (1998), in phosphoric acid activation, the dehydration of the lignocellulosic material starts at lower temperatures around 75°C. At this temperature, oxygen and hydrogen got removed from the carbon matrix through elimination of water. During phosphoric acid activation of lignocellulosic precursors, an overall structural dilation and the simultaneous development of microporosity is usually observed for temperatures in the range of 150 to 350°C. When temperature increases, mesopore formation also increases, which is mostly through widening of the existing micropores (Molina-Sabio et al. 1995a; Jagtoyen & Derbyshire, 1998).

The formation of phosphate ester linkages between cellulose chains is considered to be the major contributor to the dilation of the carbon structure since these linkages are based on the insertion of phosphoric acid molecules in between the cellulose chains, which further separates them. Dilation can be further enhanced by the formation and subsequent insertion of polyphosphates into the structure through ester linkages with cellulose chains, which in turn is considered to be one of the major contributors to the development of mesopores as can be seen in **Figure 2 and 3.** At temperatures higher than 450°C, the phosphate ester linkages are thermally unstable and start to breakdown which leads to a shrinkage of the carbon structure.

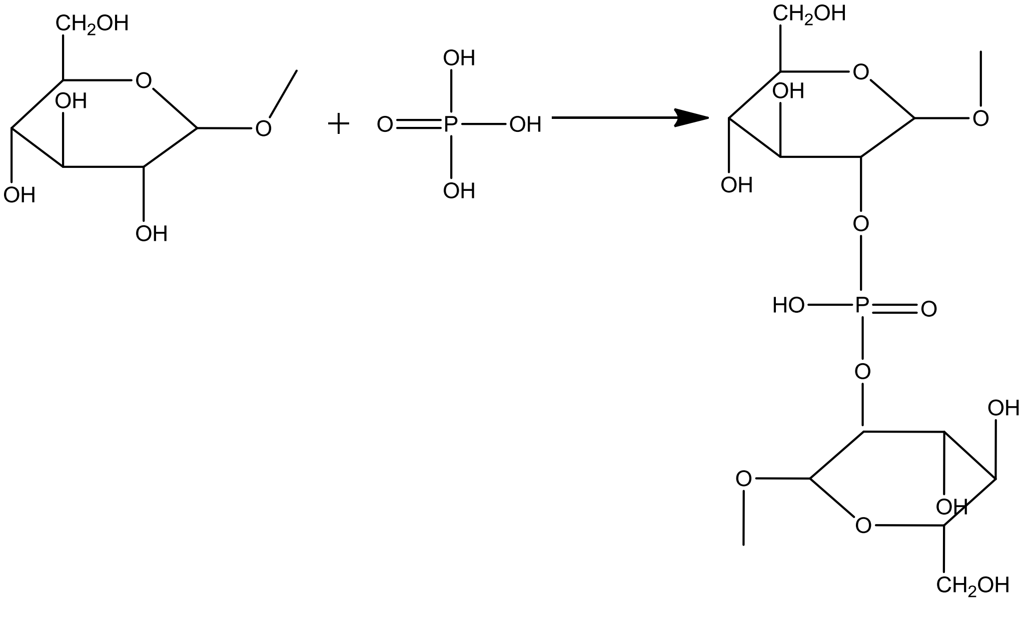

Figure 2: Mechanism of Cellulose linkage with phosphoric acid (Jagtoyen and Derbyshire, 1998).

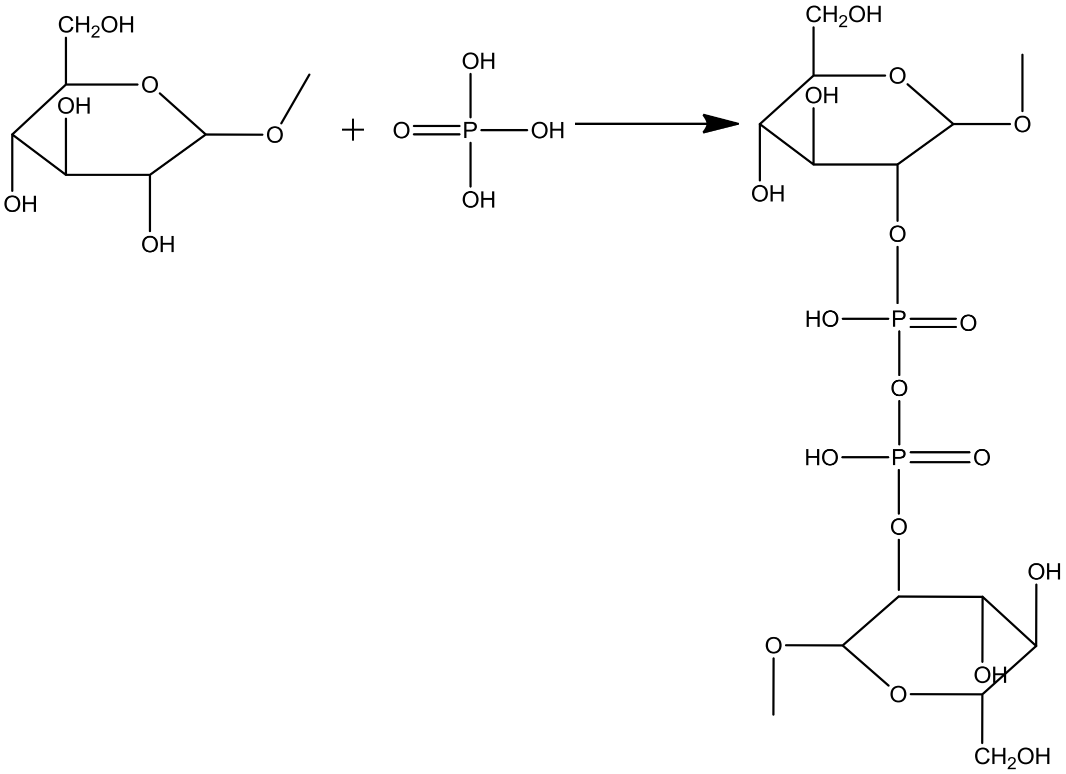

Figure 3: Structure of cellulose ring intact with polyphosphate (polyphosphate ester formation with cellulose (T < 450°C) (Jagtoyen and Derbyshire, 1998).

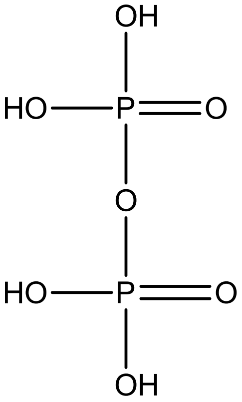

Figure 4: Structure of Polyphosphate

Generally, during impregnation and successive activation of lignocellulosic materials, the acid will firstly attack the amorphous polymers i.e. lignin and hemicellulose. Both lignin and hemicellulose are more easily available than cellulose. The activation of lignin and hemicellulose produces usually micropores, whereas the activation of crystalline i.e. cellulose produces a more extensive range of pore sizes. Crystalline cellulose was believed to present a much greater potential for expansion of pores than their lignin and hemicellulose due to the fact that it is more prone to higher degrees of esterification with phosphates and polyphosphates. After activation of phosphoric acid, it is a common practice to wash the carbon with water to recover the acid. Water hydrolyzes the phosphate crosslinks and removes the phosphoric acid formed, together with that which was converted to hydrated phosphorus pentoxide ($P_2O_5.xH_2O$). The phosphorus pentoxide, then driven off upon high temperature carbonization, leaving behind a vacant space (voids), which includes a micropore with a volume that corresponds to that of the removed phosphoric acid (Molina-Sabio et al. 1995a; Jagtoyen and Derbyshire, 1998). Thus, it can be stated that, aside from its chemical action, phosphoric acid also acts as a template for micropore formation.

1.2.2.3. Some key factors affecting the activation process are as follows

1.2.2.3.1. Pyrolysis temperature:

The pyrolysis temperature is one of the important factors during activation process. The temperature ranges commonly from 400 to 900ºC. The optimum pyrolysis temperature for manufacturing AC from lignocellulosic materials is 500ºC (Spahis et al., 2008). Some studies (Moreno-Castilla et al., 2001) explored that by increasing the pyrolysis temperature, an increase in the mesopore volume corresponded to a decrease in microporosity. However, after a certain high temperature, the surface area may get decreased due to contraction of the carbon porous structures and also there is a chance of ash formation in consistent with nature of the precursor used.

1.2.2.3.2. Pyrolysis time:

Pyrolysis time is referred to the amount of time required for burning off the sample. It is a critical parameter that affects the quality of AC. In most of the literatures (Marsh et al., 1984, Spahis et al., 2008) reported that the 1 to 3 hour pyrolysis time is sufficient for the preparation and chemical activation of activated carbon.

1.2.2.3.3. Soaking time:

Generally, a soaking time of activating agent by carbon powder is more than 1 hour so as to widening of pores and enhancement of surface area during chemical activation. If precursor does not get soaked properly, there is a chance of collapses of smaller pores which leads to the reduction in both surface area and total pore volume.

1.2.2.3.4. Activating agents:

As described earlier, activating agents are the prominent factor that affects the activating process. Pore development is enhanced by appropriate activating agents to the raw carbon powder in AC. There are many different activation agents, but the most applied ones are H_3PO_4, $ZnCl_2$ and KOH.

1.2.3. Types of activated carbon (AC)

AC is a complex product, which is difficult to classify on the basis of their behavior, surface characteristics, and preparation methods. However, some broad classification is made for general purpose based on their physical characteristics.

1.2.3.1. Powdered activated carbon

Powdered Activated Carbon (PwAC) is granular form of carbon having < 1mm of size. Their average pore diameter is approximately 0.25 mm. PACs are typically used in liquid-phase adsorption applications and offer reduced processing costs and flexibility in operation.

1.2.3.2. Granular activated carbon

Granular Activated Carbon (GAC) is 0.2 mm to 5 mm in size which is relatively larger than powdered activated carbon. It exhibits a lower surface area than PAC. GAC is usually used for the adsorption of gases and vapors (Chen et al., 2016) It is also used for deodorization, water treatment and separation of components in a flow system (Fang et al., 2014).

1.2.3.3. Extruded activated carbon

Extruded Activated Carbon (EAC) is cylindrical shaped activated carbon having the diameters from 0.8 to 130 mm. Since they are bigger in size, they have high mechanical strength, low dust content and low pressure drop during their application. Hence, they are used for gas phase applications.

1.2.3.4. Impregnated activated carbon

These are porous ACs that are impregnated with inorganic elements such as I, Ag or cations such as Al, Mn, Zn, Fe, Li, and Ca. These are used for adsorption of gases and water purification systems too.

1.2.3.5. Polymer-coated activated carbon

Polymer-Coated Activated Carbon (PCAC) can be prepared by coating ACs with a biologically compatible polymer in order to give a smooth and permeable coat, which does not block the pores. It is used as an absorbent in hemoperfusion where large volumes of the patient's blood are passed over an adsorbent substance to remove toxic substances from the blood.

1.2.3.6. Pellet activated carbon

Pellet Activated Carbon (PAC) is compact, hard carbon having very high surface area. They usually have 20 to 40 mm length and 5 to 10 mm diameter. Their pore size distribution is unique having enhanced mesoporosity. They are generally used in high pressure operations and high volumetric adsorption.

1.2.3.7. Activated carbon cloth

Activated Carbon Cloth (ACC) is also available in cloths and fibers. ACC is used by the military for Nuclear Biological Chemical (NBC) protective clothing, socks and gloves. It is also used in wound dressings, protective masks, protection of artifacts from tarnish and degradation, oil mist filters for compressors, gas sensors, electrodes, water purification and so on.

1.2.3.8. Biochar activated charcoal

Biochar Activated Charcoal (BioAC) is that activated carbon which is produced by a pyrolysis of biomass, typically wood, under limited oxygen conditions with extremely low carbon emissions. Carbon retention is around 96% from pyrolysis, compared to 50% from conventional methods.

1.2.3.9. Activated carbon fiber

Activated Carbon Fibers **(**ACF) are porous carbons in fiber shape with aspect ratio higher than 10 and contains a well-defined porous structure with high adsorption capacity (Linares-Solano & Carorla- Amoros, 2008). ACFs are basically prepared from general-purpose carbon fibers through a heat treatment to achieve high porosity to fulfill requirement of specific applications. One of the interesting characteristics of ACF is having extremely high surface area around 2000 m^2g^{-1} (Diefendorf, 2000). With such high surface area, ACF has been the latest additional advantage in family of porous carbon for adsorption. ACFs are promising solid materials which exhibit excellent properties in comparison to other two carbons viz. powdered activated carbons (PAC) and granular activated carbons (GAC). The main characteristics and advantages of the ACFs are: (a) extremely high surface area and adsorption capacity. According to Mays (1999) high adsorption capacities in ACF are due to the lack of non-adsorbing macropore and minimum mesopore spaces.

ACFs are normally applied in removal of SO_2 and NO_2 from atmosphere (Linares-Solano & Carorla- Amoros, 2008) and they have reviewed the applicability of activated carbon fibers for the removal of SO_2 and NO_2. It was found that pitch-based ACF with heat treatment in nitrogen at temperatures ranging from 600^{o}C to 900^{o}C exhibited the highest activity for SO_2 reduction in the presence of water at temperature 25^{o}C. Reduction of atmospheric NO_2 to harmless N_2 was successfully achieved using the pitch-based ACF through cooperation of the TiO_2 photocatalyst and urea.

1.2.3.10. Bead activated carbon

Bead Activated Carbon (BAC-2) is made from petroleum pitch. It is spherical in shape having diameter of nearly 0.35 to 0.80 mm. It is preferred for liquidized bed applications such as water filtration due to its spherical shape.

1.2.4. Surface area

Surface area is the major characteristics of porous material where the reaction takes place between any chemical and the surface of the bulk mass of it. The rate of a chemical reaction is determined by the size of the surface area. The larger the surface area, the faster the rate of reaction. The most widely used commercial AC has a specific surface area of ranging from 600 to 1200 m^2g^{-1} (Hassan et al., 2011). The surface area limits the amount of material to be adsorbed, assuming a suitable molecular size (Thommes et al., 2015).

The specific surface area is measured in m^2g^{-1}. It is commonly determined using the BET theory (Gregg & Sing, 1982) by measuring adsorption of gas and is based on the interpretation of adsorption isotherm. The recommended adsorptive gas is N_2 at its boiling point of 77K, although argon at 77K has also been used.

1.2.5. Surface functional group of activated carbon

The functional groups that present on the surface of organic matrix is called as surface functional group which confer specific chemical properties. Functional groups are mostly found along the “carbon backbone” of macromolecules, which is formed by chains and/or rings of carbon atoms with the occasional change of an element such as nitrogen or oxygen. A functional group can take part in some particular chemical reactions. Some of the major functional groups in biological molecules are hydroxyl, methyl, carboxyl, carboxyl anhydride, lactone, phenolic hydroxyl, ether, carbonyl, quinine, amino and phosphate groups (Hassan et al., 2011). Different surface functional groups having oxygen, nitrogen and other heteroatoms on matrix of AC have been shown in **Figure 5**.

The hetero-atoms bound to the surfaces take up the character of the functional groups typically found in aromatic compounds, and they react in similar ways with many reagents. These surface groups play a key role in the surface chemistry of activated carbon (Hassan et al., 2011).

A number of methods such as Boehm titrimetric method, IR spectroscopic technique have been used to determine the surface functional groups. **Figure 5** shows several IR- active functional groups that can be found at the edges of and within graphene layers after the oxidative treatment of AC.

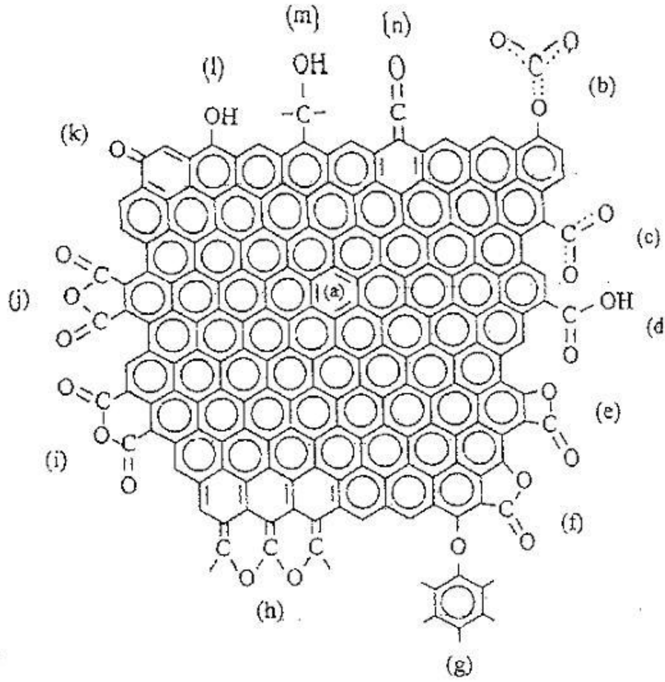

Figure 5: IR- active functionalities on carbon surfaces: (a) aromatic C=C stretching; (b) and (c) carboxyl-carbonates; (d) carboxylic acid; (e) lactone (4-membered ring); (f) lactone (5- membered ring); (g) ether bridge; (h) cyclic ether; (i) cyclic anhydride (5- membered ring); (j) cyclic anhydride (6-membered ring); (k) quinine; (l) phenol; (m) alcohol; and (n) ketene (Khan & Ansari, 2009).

All functional groups play crucial role to determine the particular chemical properties of the molecules. However, oxygen functional groups are one of the most important subjects in the study of electrochemical properties of carbon materials. These materials can change the wettability, conductivity and pore size distributions of carbon materials, and can bring redox reactions. In the electrode materials of carbon-based supercapacitors, the oxygen functional groups have widely been used to improve the capacitive performance (Hassan et al., 2011).

1.2.6. Pore structure

Activated carbons are complex products which are difficult to classify based on their behavior, surface characteristics and other fundamental criteria. However, they are broadly classified for general purpose based on their preparation methods, pore-size and industrial applications.

In this context, a pore is a class of void connected to the external surface of a solid and allows the passage of fluids into, out of, or through a material. Marsh (1989), stated that the scientific literature on porous solids use the terms ‘open pore’ and ‘closed pore’, the former being a non- connected pore. The **Figure 6** shows the example of different types of pore types schematically.

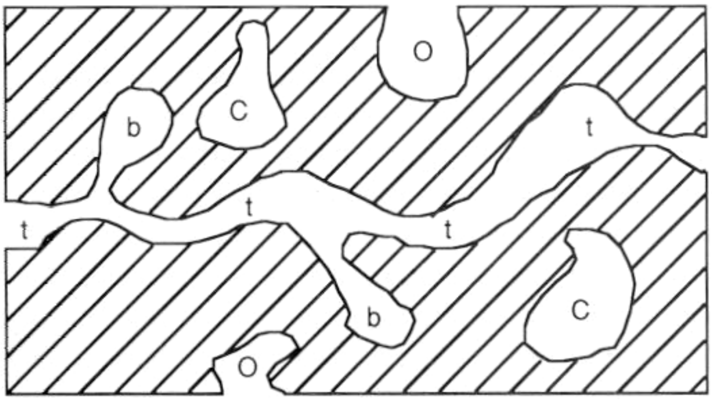

Figure 6: Different types of porosity in a porous solid (Marsh, 1989) O-open pores; C- closed pores; t-transport pores; b-blind pores.

A concentration gradient exists during steady state in the transport pores or time-independent fluid flows through the material. Blind pores are connected to transport pores by a single opening so that the gradients concentrate in them and hence the fluid flows only during unsteady state of independent flow.

Porosity is undoubtedly the most important physical property of nanoporous carbon materials. IUPAC defines nanopores as a pore of nanometer size and, according to their size, they are classified as **micropores**, which have pores with width less than 2 nm, **mesopores,** having pores with width between 2 and 50 nm and **macropores** are the pores with width greater than 50 nm (Thommes et al., 2015).

Micropores can be further distinguished into ultramicropores with width <0.7 nm and supermicropores with width between 0.7 and 2 nm (Thommes et al., 2015). It is hard to measure its size. So pore filling mechanisms has been used to measure their size.

Thommes et al., 2015 used nitrogen adsorption-desorption data at −196°C for ultra and supermicropores. The isotherm profile was also given by Gregg & Sing in 1982 to measure the size of pore where pore size resembles according to pore filling mechanisms. Actually, micropore filling is regarded as a primary physisorption process and occurs at low relative pressures. In isotherm profile, it can be observed that initial adsorption occurs at very low relative pressure indicating ultramicropores filling, where there is an overlapping of the adsorption forces favoring the enhancement of the adsorbent-adsorbate interaction due to the close vicinity of pore walls. This process is termed 'primary micropore filling'. After this initial filling in the most energetic sites, the cooperative adsorbent-adsorbate interactions inside the supermicropores become more relevant called as secondary micropore filling occurring up to relative pressures ≈ 0.15 (Thommes et al., 2015).

In regard to mesopores, a hysteresis loop in isotherm profile is the indication of mesopore filling (Gregg & Sing, 1982). In mesopore filling, all adsorbate molecules are in contact with the surface of the adsorbent which is said to be monolayer adsorption and followed by multilayer adsorption (consecutive adsorbate layers) and finishing with capillary condensation (Thommes et al., 2015).

Regarding to macropores, pore size is so wide that they behave as an open space. They do not allow capillary condensation and cannot be characterized by nitrogen adsorption profile whose maximum relative pressure occurs near the unity (Gregg & Sing, 1982).

1.2.7. Characterization of AC

AC was instrumentally characterized by TGA/DSC, SEM, XRD, Raman, FTIR, XPS, and BET.

1.2.7.1. Thermogravimetric analysis (TGA)/ Differential scanning calorimetry (DSC)

Thermogravimetric analysis (TGA), coupled with differential scanning calorimetry (DSC) were used to investigate the thermal decomposition of lignocellulosic raw materials. Theoretically, TGA measures mass/weight change as a function of temperature and whereas DSC, allows for the measurement of a change in enthalpy as a function of time. Both technique are measured simultaneously. A simultaneous DSC-TGA device that can be used to characterize any material exhibiting a weight change or a phase change between ambient temperature and 1500°C, i.e. the mass of a substance and the difference in energy inputs into a substance and a reference material are both measured simultaneously as a function of temperature while the substance and reference material are subjected to a controlled temperature program.

1.2.7.2. Scanning electron microscopy (SEM)

The scanning electron microscopy (SEM) is a type of electron microscopy which produces image of sample by probing it with a focused beam of electron that is scanned across a rectangular area of the sample. When the electron beam interacts with the sample, it loses energy by a variety of mechanisms. The lost energy is converted into alternative forms such as heat, emission of low energy secondary electrons and high-energy backscattered electrons, light emission or x-ray emission, all of which provide signals carrying information about the properties of the sample surface, such as its topography and composition.

1.2.7.3. X-ray diffraction (XRD)

X-ray scattering technique is a non-destructive analytical technique which reveals the information about the crystallographic structure, chemical composition, and physical properties of materials and thin films. The technique is based on observing the scattered intensity of an X-ray beam hitting on the sample as a function of incident and scattered angle, polarization and wavelength or energy.

The main principle of X-ray diffractionis according to Bragg’s law, which is represented as follows

$$2d \sin\theta = n\lambda \qquad (6)$$

Where, d is the spacing between diffracting planes, θ is the incident angle, n is any integer, and λ is the wavelength of the beam.

1.2.7.4. Raman scattering

Raman spectroscopy is a standard non-destructive tool for the characterization of crystalline, nano crystalline, and amorphous carbons. The technique is based on inelastic scattering of monochromatic light, usually from a laser source. Photons of the laser light are absorbed by the sample and then re-emitted. Frequency of the re-emitted photons is shifted up or down in comparison to original monochromatic frequency, which is called the Raman Effect. This shift provides information about vibrational, rotational and other low frequency transitions in molecules.

When a sample is normally illuminated with a laser beam, light will be scattered and is collected with a lens and is sent through interference filter or spectrophotometer to obtain Raman spectrum of a sample.

As every band in the Raman spectrum corresponds directly to a specific vibrational frequency of a bond within the molecule, in amorphous carbon, a relatively broad band around 1400 cm^{-1} and 1550 cm^{-1} is observed, which are called D and G band respectively. The variation in the position, width, and intensity ratio (ID/IG) has been often examined as a function deposition conditions and some properties measured from other techniques. Especially, the intensity ratio (ID/IG) is used as the most useful parameter indicating the sp^2 cluster size, or the sp^3 to sp^2 bonding ratio in hydrogenated amorphous carbons.

1.2.7.5. Fourier transform infrared spectroscopy (FTIR)

FTIR is one of the useful techniques to determine the various surface functional groups present in the sample. In this technique, spectrums are observed after absorption of IR wavelengths. Analysis of these absorption spectra reveals the functional groups present in the sample. When the frequency of the IR is same as vibrational frequency of a bond absorption occurs. Only IR active compound gives the spectra.

1.2.7.6. X-ray photoelectron spectroscopy (XPS)

X-ray photoelectron spectroscopy (XPS) is a classical method for the semi-quantitative analysis of surface composition. It is also stated as Electron Spectroscopy for Chemical Analysis (ESCA). It is based on the photoelectric effect, i.e., emission of electron following excitation of core level electrons by photons. It is surface sensitive because of the low inelastic mean free path of electrons. An XPS setup consists of X-ray source, a sample chamber and an electron analyzer. XPS requires a monochromatic source of X-rays, i.e., either from a lab based anode or from a synchrotron, with X-ray monochromator in both cases. Traditionally, XPS works only in ultrahigh vacuum because of scattering of electrons in gases. Since recently, XPS can also be performed in the mbar pressure range.

1.2.7.7. Nitrogen adsorption-desorption isotherm

Adsorption is the process in which atoms, ions or molecules from a gas, liquid or dissolved solid adheres to the surface of solid. The process of adsorption is usually studied through graph known as adsorption isotherm. The graph was plotted between the amounts of adsorbate (x) adsorbed on the surface of adsorbent (m) and pressure at constant temperature. Different types of isotherm models have been discussed such as Langmuir adsorption isotherm, Freundlich adsorption isotherm, BET adsorption isotherm. Langmuir adsorption isotherm provides information about homogenous monolayer adsorption; Freundlich adsorption isotherm states about heterogenous monolayer adsorption of molecules whereas BET adsorption describes multilayer adsorption of molecules. The BET theory was put forwarded by Brunauer, Emmett and Teller. The theory explains the formation of multilayer during the process of physical adsorption. Under the condition of high pressure and low temperature, thermal energy of gaseous molecules decreases and more and more gaseous molecules would be available per unit surface area. Due to this, multilayer adsorption would occur.

There are five different types of adsorption isotherm generally used which is described below:

1.2.7.7.1. Type I adsorption isotherm:

Type I adsorption isotherm is shown in **Figure 7.** This isotherm illustrates the monolayer adsorption isotherm which is well explained by using Langmuir adsorption isotherm when P/Po<<1 and C >>1 in BET equation, then it leads to monolayer formation and Type I adsorption isotherm is obtained.

The adsorption of nitrogen (N_2) or Hydrogen (H_2) on charcoal at temperature near to -180 ºC can be taken as an example of Type-I adsorption.

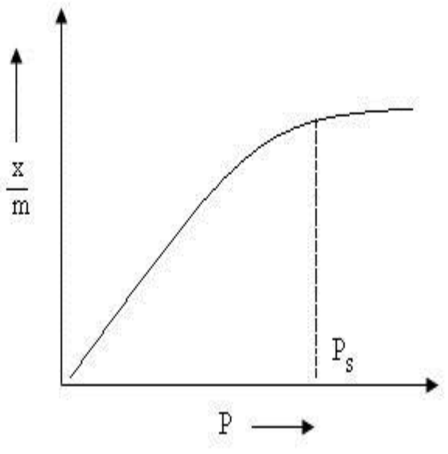

Figure 7: Type I adsorption isotherm.

1.2.7.7.2. Type II adsorption isotherm:

Figure 8 demonstrates the Type II adsorption isotherm. It shows large deviation from Langmuir model of adsorption. The intermediate flat region in the isotherm corresponds to monolayer formation. In BET equation, value of C has to be very large in comparison to 1.Typical examples of Type-II adsorption are: nitrogen gas adsorbed at -195 ºC on iron (Fe) catalyst, and nitrogen gas adsorbed at -195 ºC on silica gel.

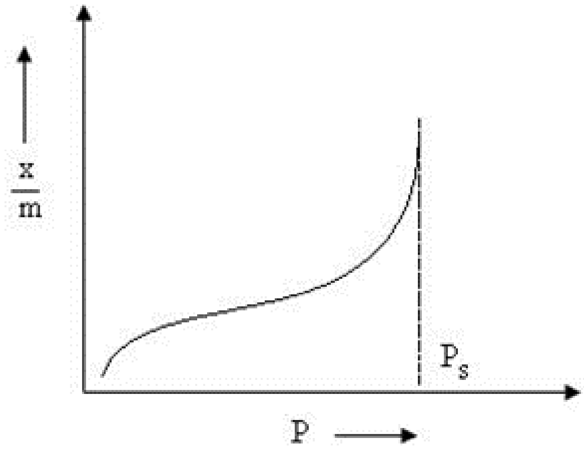

Figure 8: Type II adsorption isotherm.

1.2.7.7.3. Type III adsorption isotherm:

Type III Adsorption Isotherm also demonstrates the large deviation from Langmuir model. It is shown in **Figure 9**. In BET equation, if value of C <<< 1 Type III adsorption isotherm is obtained. This isotherm explains the formation of multilayer. The absence of flattish portion in the curve indicates that monolayer formation is missing. One of the good example of Type III adsorption isotherm is bromine (Br_2) at 79 ºC on silica gel or iodine (I2) at 79 ºC on silica gel.

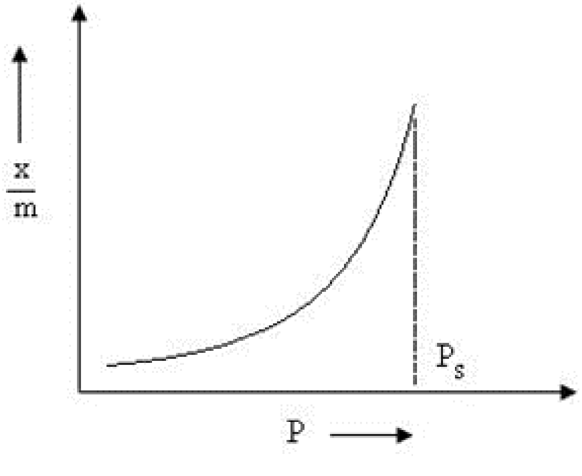

Figure 9: Type III adsorption isotherm.

1.2.7.7.4. Type IV adsorption isotherm:

Type IV adsorption isotherm is shown in **Figure 10.** In the figure, it is clearly seen that the lower pressure region is quite similar to that of Type II. This explains formation of monolayer followed by multilayer adsorption. The saturation level reaches at a pressure below the saturation vapor pressure. This can be explained on the basis of a possibility of gases getting condensed in the tiny capillary pores of adsorbent at pressure below the saturation pressure (PS) of the gas. The well-known examples of Type IV adsorption isotherm are: adsorption of Benzene on Iron Oxide (Fe_2O_3) at 50 ºC and adsorption of Benzene on silica gel at 50 ºC.

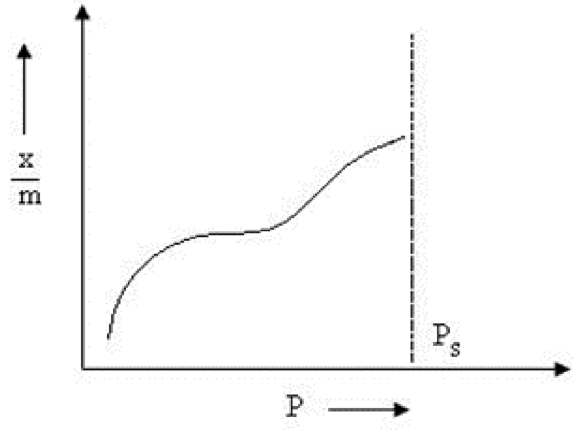

Figure 10: Type IV adsorption isotherm.

1.2.7.7.5. Type V adsorption isotherm:

Explanation of Type V graph is similar to type IV which is shown in **Figure 11.** Adsorption of water (vapors) at 100 ºC on charcoal can be taken as example of Type V adsorption isotherm. The phenomenon of capillary condensation of gas can be studied by Type IV and V adsorption isotherm.

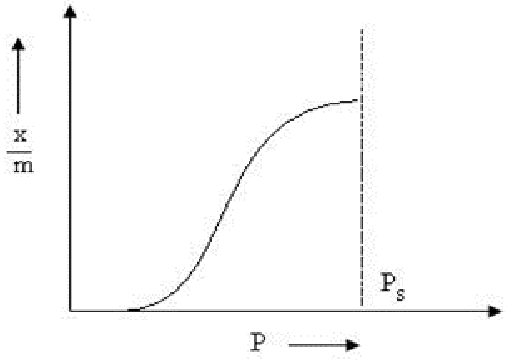

Figure 11: Type V adsorption isotherm.

1.2.8. Electrochemical characterization

1.2.8.1. Cyclic Voltammetry

Cyclic Voltammetry *(*CV) is a type of potentiodynamic electrochemical measurement. In Cyclic Voltammetry (CV), the current response of a small stationary electrode in an unstirred solution is excited by a triangular voltage waveform. The potential is first varied linearly versus reference electrode. When the extreme of potential is reached, the scan direction is reversed, and the potential is returned to its original value. This excitation cycle is often repeated several times. The extreme voltage at which reversal takes place are called switching potentials. The range of switching potentials chosen for a given experiment is one in which a diffusion-controlled oxidation or reduction of one or more analyte occurs. The direction of the initial scan may be either negative or positive depending on the composition of the sample. A scan in the direction of more negative potential is termed a forward scan whereas scan in opposite direction is termed as reverse scan. Generally, cycle times ranges from 1 to 100 s or more. The resulting current at the working electrode is plotted as a function of applied voltage to record the cyclic voltammogram.

In two-electrode systems, CV provides idea of change in electric potential between positive and negative electrodes while in three-electrode system, it provides electric potential between reference and working electrode**.** The speed of the potential change in mVs^{-1} is labeled as the sweep rate or scan rate, ν, and the range of potential change is called the potential window or operating potential. The instantaneous current recorded during the cathodic and anodic sweeps is to describe the electrochemical reactions involved. The data are plotted as current (A*)* vs. potential (V) or sometimes as current (A) or potential (V) vs. time (s) (Bard & Faulkner, 2000).

CV testing with the three-electrode setup is regarded as the most suitable approach (Liu et al., 1998; Conway, 1999), to study the charge storage mechanisms in Supercapacitor (SC) materials where Electric double layer capacitor (EDLC) and Pseudocapacitor (PC) behaviors can be distinguished. The test results can be analyzed firstly by examining the shape of the CV curves. EDLC materials generally shows, rectangular CV curves, whereas for some PC materials, pronounced redox peaks may occur in a highly reversible manner (Simon et al., 2014). Therefore, it is not enough to distinguish EDLC and PC materials by solely observing the shape of CV curves.

The specific capacitance from CV can be calculated by the formula;

$\mathbf{C_S}$ (from **CV**) = $\frac{1}{m\Delta V}\int I(t)dt$**………………(7)**

Where,

$\mathbf{C_S}$ **(Fg^{-1})** = Specific Capacitance (from CV)
I(A) = Current

m(g) = sample mass

ΔV(V) = Potential Window

Δt (s) = Duration time

1.2.8.2. Galvanostatic Charge/Discharge (GCD)

1.2.8.2.1. Charge/discharge time

The GCD technique measures the potential with respect to time at a constant current density (e.g., Ag^{-1}). Generally, the working electrode is charged to a preset potential and the discharge process is then monitored to assess the capacitance. The EDLC materials shows linear charge/discharge behavior, while PC shows the nonlinear behavior due to the redox reactions (Stoller & Ruoff, 2010)

1.2.8.2.2. Specific Capacitance

Furthermore, the specific capacitance SC materials can also be obtained by using a three-electrode setup via GCD test. The specific capacitance from GCD can be calculated by using the formula;

$\mathbf{C_S} = \frac{I\Delta t}{m\Delta V}$**………………(8)**

Where,

$\mathbf{C_S}$ **(Fg^{-1})** = Specific Capacitance (from GCD)

I(A) = Current

m(g) = sample mass

ΔV(V) = Potential Window

Δt (s) = Duration time

Besides these, GCD technique measures power density and energy density. It can also be conveniently used to study the cyclic stability (% capacity retention) of SC devices.

1.2.8.2.3. Power density and energy density

Power density and energy density are the most directly significant to the end applications and hence are the parameters used most often for performance evaluation. They normally are evaluated gravimetrically or volumetrically in Wkg^{-1} or WL^{-1} for power density to describe the efficacy in energy uptake/delivery; and in Wkg^{-1} or WL^{-1} for energy density to demonstrate the amount of electrical energy stored or deliverable. The diagonal time line, so-called 'characteristic time' (Park et al., 2002) in Ragone plot (Chen et al., 2010) can describe effective comparison with other EES devices, a reflection of running time of the devices at the rated power. The actual running times of EES devices vary hugely, depending on the load or discharging rate.

Energy and power densities are calculated by using equation **(4)** and **(5).**

$$\mathbf{E} = \frac{1}{2} C_{SP} \Delta v^2 \text{ ....} \mathbf{(9)}$$

$$\mathbf{P} = \frac{E}{\Delta t} \text{ ....} \mathbf{(10)}$$

Where, E is the energy density in W h kg^{-1}, P is the power density in W kg^{-1}, Csp is the specific capacitance in F g^{-1}, ΔV is the potential window (V), whereas Δt (s) is the time of discharge

1.2.8.2.4. Cyclic stability (% Capacity Retention)

One of their major merits of SC devices is the long cycle life, which are greatly anticipated for certain applications. However, the drawback of this extremely long cycle life (>1000000 cycles) is difficult to measure it directly. In other words, the capacitance retention rate is therefore used to indirectly estimate the cycle life of SCs. It is easily obtained in GCD test by comparing the capacitance after given thousands of cycles with that of the first cycle.

1.2.8.3. Electrochemical impedance spectroscopy (EIS)

Electrochemical techniques, including electrochemical impedance spectroscopy (EIS) is a powerful technique for characterizing a wide variety of electrochemical systems and for determining the contribution of electrode or electrolytic processes in these systems.

EIS measures the impedance of a power cell as a function of frequency by applying a low-amplitude alternative voltage (normally 5 mV) superimposed on a constant potential. The resulting data are usually expressed graphically in a Nyquist plot to show the imaginary and real parts of the cell impedances on a complex plane (Miller et al., 2010; Du & Pan, 2006).

In addition to the frequency response and impedance, EIS has also been used to characterize the charge transfer resistance (Rct), solution resistance (Rs), Wargburg impedance (W) and double layer capacitance (Cdl) (Taberna et al., 2003; Choi et al., 2006).

1.2.8.3.1. Double layer capacitance (Cdl)

Double layer capacitance (Cdl) indicates an electrical double layer exists on the electrode and electrolyte interface. This double layer is formed by the ions or charges from the solution, which stick on the electrode surface. The charged electrode is separated from the ions/charges. The separation is very small, often on the order of angstroms.

The value of the double layer capacitance depends on many variables. Electrode potential, temperature, ionic concentrations, types of ions, oxide layers, electrode roughness, impurity and adsorptions. The Cdl can be estimated from the frequency at which maxima occurs in Nyquist plot by using this equation.

$$\mathbf{Cdl = \tfrac{1}{2}\pi f\ R} \ \ldots\ldots\ldots\ldots\ldots\ldots\ldots\ldots\ldots\ldots\ldots\ldots \mathbf{(11)}$$

Where, f is the frequency in Hz and R is the resistant

1.2.8.3.2. Solution resistance (Rs)

The opposition to current flow through the solution/electrolyte by the migration of ions is called Solution resistance (Rs). In general, the solution resistance is considered to decrease with increase in microbial growth of charges.

1.2.8.3.3. Charge transfer resistance (Rct)

Charge transfer resistance is the process of electron transfer from one phase (e.g. electrode) to another (e.g. liquid). Charge transfer resistance (Rct) can also be defined as contact resistance between the electrode material and the current collector and interparticle resistance of Alternating Current (a.c.).

In practical terms, it is at high frequency and small amplitude perturbation. It has the same value at any frequency.

1.2.8.3.4. Warburg impedance (diffusion impedance)

The Warburg impedance is an example of a constant phase element (CPE) for which the phase angle is a constant 45° and independent of frequency. The magnitude of the Warburg impedance is inversely proportional to the square root of the frequency as one would expect for a CPE with an n-value of 0.5.

1.2.8.3.5. Analysis of data by EIS: Nyquist plot and equivalent circuit model

A Nyquist plot (or Nyquist Diagram) is a frequency response plot used in control engineering and signal processing. In the plot, the real resistance (Z') of the transfer function is plotted on the X axis, and the imaginary resistance (Z″) is plotted on the Y axis. The intersection of the impedance curve at the x-axis corresponds to the Equivalent series resistance (ESR).

Getting meaningful information about the electrode/electrolyte interface from EIS data requires a level of mathematical skills. When the necessary mathematical skills are present, the EIS can differentiate between closely related phenomenon taking place at the interface. However, this limitation of having good mathematical skill can be overcome by using an appropriate electrical circuit equivalent of electrode/electrolyte interface. It is worth mention that an electrode/electrolyte interface undergoing an electrochemical reaction is typically analogous to an electric circuit consisting of a specific combination of resistors and capacitors.

One can take advantage of this analogy by using established ac circuit theory to characterize the electrochemical system in terms of its equivalent circuit. These models are prepared with the help of well-known passive elements such as resistors, capacitors, and inductors and distributed elements such as constant phase element and Warburg impedance. These elements can be combined in series and parallel to give complex equivalent circuits. A certain physical meaning is then assigned to the various elements of the equivalent circuit.

Electrochemical reaction often is control by the diffusion of the reacting species either onto the electrode surface from the bulk or from the surface of the electrode towards solution bulk. Since the diffusion process is slow, it's effect can be seen only at low frequency in the form of a straight line at a phase angle of 45 degree. For common electrochemical system, if diffusion impedance is present in the system the equivalent circuit is represented as shown in **Figure 12**, where a diffusion impedance (called

Warburg impedance) is placed in series with Rc. The diffusion impedance depends upon the frequency of the potential perturbation. At high frequencies, the Warburg impedance is small since diffusing reactants do not have to move very far. At low frequencies, the reactants have to diffuse farther, increasing the Warburg impedance. At high frequency region, a semicircle could be seen representing charge transfer resistance Rct.

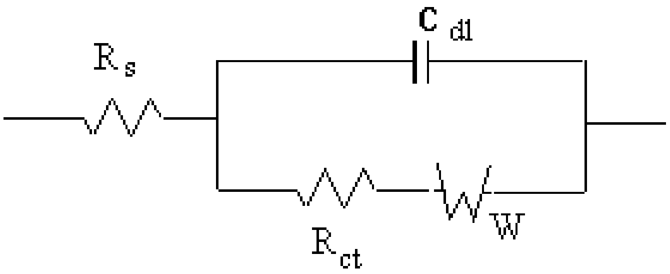

Figure 12: Equivalent RCW Circuit.

This circuit models a cell where polarization is due to a combination of kinetic and diffusion processes. The Nyquist plot for this circuit is shown in **Figure 13.**

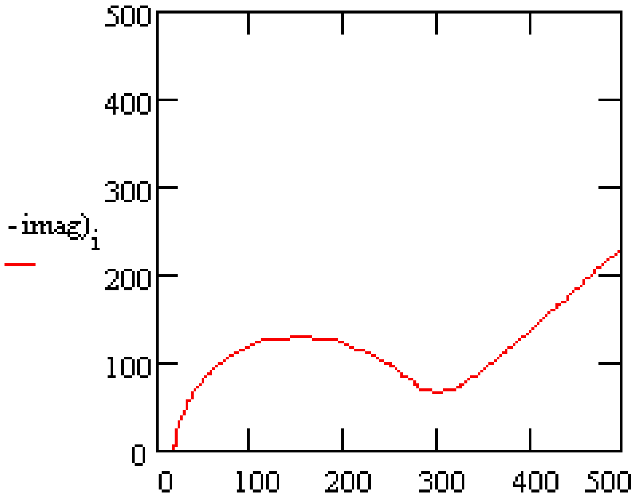

Figure 13: Nyquist Plot of RCW circuit.

Nyquist plot is based on frequency. At high frequency region, a semicircle could be seen representing charge transfer resistance. Since the diffusion process is slow, it's effect can be seen only at low frequency in the form of a straight line at a phase angle of 45°.

1.3. Application of activated carbon (AC)

AC is one of the most explored agents in the 21st century. It has got multipurpose application in

(a) Environmental pollution remediation to remove an extensive variety of pollutants such as dyes, heavy metals, pesticides from air and water sources,

(b) Industrial sector such as food, oil, pharmaceutical, chemical, mining and especially in water treatment processes,

(c) Energy storage and harvesting such as batteries, solar cells, sensors, supercapacitors.

1.3.1. Energy storage and harvesting

According to the "World Energy Outlook 2014", global energy demand will grow by 37% by 2040 (Asif & Muneer, 2007). Meanwhile, nearly 80% of today's world energy is supplied by fossil fuels, including oil, gas and coal. These non-renewable fossil fuels produce exhaust in the form of CO_2 and are projected to rise to 45 billion metric tons by 2040, contributing largely to global warming (Sieminski, 2013).

Limited and decreasing availability of fossil fuel resources and the destructive climate change strongly calls for the need of clean, sustainable and renewable energy resources.

As a result, the utilization of green and clean natural energy sources like wind, hydro and solar energy has become more and more important to reduce the dependence on fossil fuels for global energy demands. Likewise, the development of electric vehicles or hybrid electric vehicles with low CO_2 emissions are needed (Simon & Gogotsi, 2008). The solar energy devices are unable to generate electricity during the night as the sun does not shine during the night but may generate surplus amount of energy during the day. Similarly, the wind does not blow as per our demand and we all expect to drive our vehicle with at least a few hours of autonomy. Therefore the energy harvesting and storage systems play significant role in our lives.

Energy can be stored in various forms like thermal, chemical, electrical and electrochemical energy (Jian et al., 2014). Thermal energy provides cooling (air condition) or heating (geezers), which run on electricity. Similarly, wind and solar energy are the universal natural resources that provide electrical energy. Fossil fuels store energy in chemical form while in case of electrochemical energy storage, the electrical and chemical energies are interconvertible within a fraction of time (Wei et al., 2017). The most common energy storage systems which are heavily investigated are batteries, supercapacitors, solar cells, and fuel cells and is called as primary energy storage devices (Le et al., 2017; Xu et al., 2017; Dobrota et al., 2017; Zhao et al., 2017). Their applications are growing hugely; from smart micro batteries to large-scale electric vehicles. Consequently, a high performance, smaller, lighter, versatile and more economically viable energy storage devices (ESD) are essential in the future to fulfill the requirement. A variety of organic and inorganic or their nano-composites are broadly being used as a material for ES devices. These materials include metal oxides, conducting polymers, graphene, activated carbon, CNTs, metal organic framework etc. (Iqbal & Ahmad, 2018;Liu et al., 2013;Mai et al., 2013;Cao et al., 2016). However, the development of energy conversion and storage applications depend on nanostructured materials and thus they have critical roles in it. They possess a characteristic dimensions with new properties and possibilities.

1.3.2. Energy storage devices

1.3.2.1. Batteries

Electrochemical batteries are the most common electrical ES device, which can store large amount of energy in a relatively small volume and weight, and also providing suitable levels of power for many applications and requirements of everyday life. It produces electricity by releasing the potential energy stored in the chemicals of the battery. A traditional battery consists of two electrodes (cathode and anode), an electrolyte, and a separator (insulating and porous material) (Winter & Brodd, 2004). However, increasing demand of portable electronic devices has led to drastic improvements in their performance. In this backdrop, lithium-ion batteries have gained considerable attention and have diverse applications. The pioneering work in 1991 by Sony Corporations has introduced a high performance Li-ion battery with high-voltage, and high-energy for portable electronic applications.

1.3.2.2. Fuel cells

Fuel cell is an electrochemical device that converts chemical energy directly into electrical energy (Olabi et al., 2017). In architecture, fuel cell also resembles a battery i.e. consisting of two electrodes and an electrolyte. Nevertheless, fuel cell is different from battery because fuel cell does not require charging as the species consumed during the electrochemical reactions are continuously replaced (Ellis et al., 2001). Fuel cells have converted global materials of 21st century for ES applications ranging from cell phones to automobile and power plants due to their high productivity, excellent load performance, low pollutant's emission and wide range of a size.

1.3.2.3. Supercapacitors / Electrochemical capacitors

Supercapacitors (SCs) are also one of the most accessible, workable, efficient high power rechargeable energy storage devices. In architecture point of view, although SCs are very similar to solid electrode batteries, they have thousands of times high power density, low maintenance, and long life cycle (Faggioli et al., 1999; Ates et al., 2011). It consists of two electrode-containing electrolytes, which are separated by a separator (Ashok Kumar & Baek, 2014). The overall performance of a SC is mainly governed by the type of electrodes, separator, current collector, and electrolytes, while high power density (>10 Wh Kg^{-1}), long cycle life (100 times more than batteries), charging-discharging within seconds, low self-discharging are also the key parameters that evaluate the performance of SC (Tyagi et al., 2015).

SCs can replace batteries in numerous high power applications ranging from wind turbines to hybrid engine for vehicles. They offer uninterruptable power supplies to electronic devices and pulse-power applications in the aerospace and defense industries. The global market share of SCs is rapidly growing, and newer model SCs have higher energy density compared to their predecessors.

In recent years, electrochemical SCs have drawn attention fascinatingly due to their noble characteristics, including rapid charging-discharging rate, high power density, and longer cycle of life (Largeot et al., 2008; Kandalkar et al., 2010). The higher power density of electrochemical SC leads to wide-ranging commercial applications such as electrical batteries, electronic gadgets like laptop, mobiles and in energy storage vehicles (Jayalakshmi & Balasubramanian, 2008; Li et al., 2003; Pandolfo & Hollenkamp, 2006; Taer et al., 2011)., high capacitive behavior.

The capacitive behavior of electrochemical SCs can be classified into two categories based on the charge storage mechanisms: (i) Electrical/ Electrochemical Double Layer

Capacitance (EDLC) and (ii) Pseudo-Capacitance (PC)/ Faradiac Supercapacitance (FS).

In electrochemical double layer capacitor (EDLC), the storage of charge arises from pure electrostatic attraction between ions and the charged surface of an electrode (such as carbon materials) at electrode-electrolyte interface. While in pseudo capacitor (PC), charge is stored via fast and reversible oxidation/reduction (redox) or faradaic charge transfer reactions of the electro-active species on the surface of the electrode; for instance, transition metal oxides and conducting polymers (Taer et al., 2011).

1.3.2.3.1. Principles of Operation of Supercapacitors

The SCs store energy in three different ways:

i) SCs store energy in the electric field of the interfacial double layer of the electrode/electrolyte interfaces. It refers to "Electric Double Layered Capacitance (EDLC)". This concept was introduced by Hermann Von Helmholtz. This is completely non-faradaic process, which does not involve any making or breaking of chemical bonds (Fan et al., 2011). However, the charges are stored in the electric field, formed between electrons on the surface of the electrode and ions in the electrolyte that are adsorbed at the electrode surface. Helmholtz's model fell short in explaining the multitude of processes occurring at the electrode/electrolyte interface. Gouy (1910) presented a model of the double layer effect accounting for the diffusion of the ions in the electrolyte called a diffusion layer. Later, Stern (1924) combined both models and presented a more refined model, which is named as Stern Layer.

ii) SCs store energy through electro sorption and surface redox reactions (pseudo-capacitance) on p-doped (3-p valent doping) or n-doped (5-n valent doping) electrodes, which have been reported to match and sometimes surpass the performance of EDLC (Mastragostino et al., 2001). It refers to the Pseudo-capacitor (PS) or Faradiac supercapacitors (FS). When a potential is applied onto the FS, fast and reversible faradaic reactions (redox reactions) take place on the electrode materials. It involves the passage of charge across the double layer, similar to the charging and discharging processes that occur in batteries, resulting in faradaic current passing through the supercapacitor cell. Materials undergoing such redox reactions include conducting polymers and several metal oxides, including RuO_2, MnO_2, and Co_3O_4 (Frackowiak & Béguin, 2001; Mastragostino et al., 2001; Sharma

& Bhatti, 2010; Wang et al., 2014). There are three types of faradaic processes occurring at FS electrodes; reversible adsorption (for example, adsorption of hydrogen on the surface of platinum or gold), redox reactions of transition metal oxides (e.g. RuO_2), and reversible electrochemical doping–dedoping in conductive polymer based electrodes (Mastragostino et al., 2001).

These faradaic electrochemical processes have been demonstrated not only to extend the working voltage but also to increase the specific capacitance of the SCs (Troshin et al., 2011). Since the electrochemical processes occur both on the surface and in the bulk near the surface of the solid electrode, FS shows far greater capacitance values and energy density than an EDLC. As reported by Conway et al. (1999), the capacitance of an FS can be 10 to 100 times greater than the electrostatic capacitance of an EDLC. However, an FS usually suffers from comparatively lower power density than EDLC because faradaic processes are normally slower than non-faradaic processes (Wang & Kaskel, 2012).

iii) SCs store energy by utilizing both the faradaic electrode and non-faradaic electrode processes. It refers to the “**Hybrid capacitor**” (Hayashi et al., 2000). As redox reactions occur at the electrode, an FS often lacks stability during cycling, similar to batteries. It is worth mentioning that hybrid ES with an asymmetrical electrode configuration (e.g. one electrode consists of electrostatic carbon material while the other consists of faradaic capacitance material) have been extensively studied recently to capitalize on both electrode materials’ advantages in improving overall cell voltage, energy, and power densities (Lewandowski & Galinski, 2004; Fan et al., 2011). In this kind of hybrid supercapacitor, both electrical double-layer capacitance and faradaic capacitance mechanisms occur simultaneously, but one of them plays a greater role.

1.3.2.3.2. Composition of supercapacitor

Supercapacitor generally consists of positive / negative electrodes which collect current, electrolyte resides in between electrodes and a separator which electrically isolates the electrodes. Besides this three electrode system is in practice where there is a reference electrode, a counter electrode and a working electrode. The detail of electrode, electrolyte are discussed in **section 1.3.2.3.3, 1.3.2.3.4,** respectively.

1.3.2.3.3. Electrode for supercapacitor

The electrode is the heart of the cell that regulates the performance of SC in terms of self-discharge, life expectancy, capacity, resistance, and so on. In general, the silver-silver chloride electrode act as reference electrode, platinum act as counter electrode and carbon/metal oxide etc. electrode as working electrode in three electrode system.

The working electrode in supercapacitor is fabricated from nanoscale materials that have high surface area and high porosity. Charges can be stored and separated at the interface between the conductive solid particles such as carbon particles or metal oxide particles and the electrolyte. This interface can be treated as a capacitor with an electrical double-layer capacitance.

As described earlier, the electrode material, such as carbon particles in electrochemical super capacitor (ESC), is not electrochemically active i.e., electrochemical reaction does not take place on the electrode material during the charging and discharging processes. In such case, pure physical charge accumulation occurs at the electrode/electrolyte interface. Whereas in Faradiac supercapacitor (FS)/ Pseudocapacitor (PC), the electrode material is electrochemically active as for example if metal oxide as electrode material, it can directly store charges during the charging and discharging processes (Ellis et al., 2001; Asif & Muneer, 2007; Le et al., 2017). Hence, the selection of a working electro-active material is an important task of research.

Some key requirements for the selection of electro-active material based on the principles of the electrochemical capacitors are high specific surface area with open porosity, high electronic conductivity, good wettability to electrolyte, good electrochemical stability, low cost and good process ability.

Carbon based materials, which are normally used as electrode materials in the fabrication of EDLC, are activated carbon, carbon aerogels, mesoporous carbon, carbon onions and carbon nanotubes (CNTs). It is due to their properties like (i) high surface area (ii) low cost (iii) availability (iv) established electrode production technologies. Besides, these carbonaceous materials are chemically and thermally stable and environmentally friendly (Thommes et al., 2015). In carbon based materials, its surface area is accessible to electrolyte ions so that electrochemical double layer will be formed at electrode/electrolyte interface. Henceforth, the electrical double layer at electrode/electrolyte interface is the main part of mechanism of charge storage or capacitance in carbon based electrodes. In along with surface area, pore structure, pore size distribution, surface functionality and electrical conductivity are five important factors that influencing on electrochemical performance (Conway et al., 1997; Kisacikoglu et al., 2009; Chuang et al., 2010).

1.3.2.3.4. Electrolyte

Besides electrodes, electrolytes, is also one of the most important components in electrochemical Super capacitor, which reside inside the active material layers. The requirements for an electrolyte in ESC include: availability at high purity, wide voltage window, high electrochemical stability, high ionic concentration and low solvated ionic radius, less resistivity, minimum viscosity, stumpy volatility, less toxicity, low cost.

1.4. Statement of the problem

In order to meet the emergent energy demand of the current society, there is a need of high-performance, low cost and environmentally-friendly energy storage and production systems. In these days, many research effort have been done in this area to improve the performance of energy storage devices, such as supercapacitors and batteries especially Li-ion batteries, and energy production systems such as fuel cells. Such target has been achieved by designing novel materials and developing synthesis processes by many researchers. It has also been touched that, there is a need of precise control over the structural and chemical characteristics of the material synthesis. Most of the researchers are seeking for greener and cost effective material synthesis processes to use in energy related field like solar energy, flashlight, solar watch, remote control and in memory back- up system like mobile phone, digital camera, wireless device, audio player etc. and in case of power supporter devices like motor starter, hybrid car, smart meter, controller, copy machine, digital camera as well. For this purpose, carbon-based materials such as carbon nanotubes, graphite, carbon felt, carbon foam, carbon papers, carbon brush and carbon cloth activated carbons have attracted significant interest in many energy related applications due to their availability, chemical and thermal stability, processability and the possibility of tuning their textural and structural characteristics. In particular, activated carbon has been reported to be a prominent material due to their large surface area (> 1000 m^2g^{-1}) and pore volume (> 0.5 cm^3g^{-1}), and relatively low material and processing cost. In market, different brands of commercial ACs are available, however they may be expensive.

Hence, environmentally friendly, low cost AC has been searched by different scientists from agricultural by products and biochemical wastes. In such fields, many cost effective and sustainable techniques have been developed, such as EDLC, pseudo-capacitor or hybrid capacitor techniques. Among them, hybrid capacitors are more preferable for storing energy for many devices. In these days, preparation of activated carbon from low cost precursors and simple method of preparation has been investigating.

In present study, an effort has been made to address these problems and tried to explore the preparation and characterization techniques of low cost AC from locally available agricultural waste ie, sawdust of *Shorea robusta* and applied as an electroactive material for energy storage devices, specifically supercapacitor.

Shorea robusta is a huge tree, belonging to the family of Dipterocarpaecea. It is an indigenous plant of Nepal, Myanmar, India and Bangladesh. In Nepal, it is mostly available in the terai region, particularly, in the churia range in the subtropical climate zone. This tree is believed to be the most valuable among tree species for the rural population of Nepal for their day to day life (World Resources Institute, 1996). It is the major source of fuel wood as well as raw material for construction and carpentry works. The trunk is the main stem of the tree from which timber sections are cut and timber based broad materials are manufactured. Hence, sawdust obtained from timber section of *Shorea robusta* tree collected from local sawmill/carpentry has been used as a precursor for this study.

From the carpentry work, waste byproducts like sawdust and splinters of wood are achieved. In fact, these byproducts consist of high carbon content in lignocellulosic form and have got distinctive chemical composition such as low content of inorganic materials and comparatively high content of volatile matters. Hence, in this research work, these wood residues have been used as a precursor for the preparation of activated carbon. Subsequently, these materials are used to investigate their electrochemical capacitive performances. **Figure 14** shows the digital picture of *Shorea robusta* (Sal) tree.

Figure 14: *Shorea robusta* tree (Sal tree)

1.5. The rationale of the study

Forest is a precious wealth of Nepal and we are rich in finding the forest or plant/agro-waste everywhere. In that sense, it is reasonable to select this research topic. Among various plant resources *Shorea robusta* is one of the species which is available almost all over Nepal except in some places. The selection of such species is also another significant factor to rationalize the research topic. Besides this, the entire world is facing the scarcity of energy nowadays on one hand and the proper management of plant-wastage is also creating environmental pollutions as garbage in another hand. That's why, the sustainable use of these plant/agro-waste in energy storage gives us multiple benefits such as; protection of environment, production of energy sources and management of wastage garbage, etc.

This research has great significance in various grounds. First of all, this research incorporates various principles and methods of preparation and characterization of activated carbon//activated charcoal (AC) in general and its application in energy storage in particular. Furthermore, Activated-Carbon-Electrode derived from *Shorea robusta* could exhibit good electrochemical performances like high energy and power densities and good storage capacity.

Thus, it is anticipated that this research will be a milestone in the preparation and characterization of activated carbon in one way and energy storage application in another. Nepal is a flora-diversified country so applying such approaches in preparation, characterization and applications in different fields like energy storage, dye removal, etc. are greatly significant and have wide horizon in application. So, it helps to widen the scope, knowledge on various species of plant -wastage in pollution remediation, energy storage including wide scope.

Further, to the best of my knowledge, no study has been investigated on application of *Shorea robusta* derived activated carbon in energy storage till date.

1.6. Objectives

1.6.1. General objectives

ACs is highly sought after porous materials for applications in various emerging fields. In these days, the porosity with particular surface functionality is on the demand, the probable precursor candidate materials are being investigated. This study was undertaken aiming to prepare AC from an agro-waste, sawdust of *Shorea robusta* by carbonization technique. The chemical activation using phosphoric acid has been investigated and a complete characterization has been undertaken using X ray diffraction (XRD) Analysis, Raman Spectroscopy, Fourier Transform Infrared (FTIR) Analysis, X-ray photoelectron spectroscopy (XPS), Scanning Electron Microscope (SEM) Analysis, Thermogravimetric analysis/differential scanning colorimetry (TGA/DSC) etc. The well characterized materials were then investigated in energy related field.

1.6.2. Specific objectives

The specific objectives of the study are:

1. To prepare nanoporous AC from the agro-waste, sawdust of *Shorea robusta* (Sal), through carbonization following activation by the activating agent H_3PO_4.
2. To characterize different desired properties like phase state, functionalities, composition, surface area, pore size distribution, pore volume of as prepared AC, the instrumental techniques like thermogravimetric analysis/differential scanning colorimetry (TGA/DSC), X ray diffraction (XRD), Raman Spectroscopy, Scanning Electron Microscope (SEM), Fourier Transform Infra Red (FTIR), X-ray photoelectron spectroscopy (XPS), BET (Braunner, Emmet, Teller) method, BJH (Barrett, Joyner, Hallenda) Method will be used.
3. To fabricate carbon-electrode from well characterized as prepared AC.
4. To characterize laboratory fabricated AC-electrode electrochemically by (a) cyclic voltammetric (CV), (b) galvanostatic charge/discharge (GCD) and (c) electrochemical impedance spectroscopic (EIS) study. Then potential electrochemical performances such as energy density, power density, cyclic capability (% capability retention) of AC-electrode will be evaluated.
5. For further improvement of electrochemical performances like energy density, power density, cyclic capability of laboratory fabricated AC-electrode, hybrid composites (AC:MnO_2) will be fabricated by mixing as prepared AC with MnO_2 mechanically in three different ratios 1:1, 1:2 and 2:1 (AC: MnO_2) and then further investigation on electrochemical capacitive behaviors will be carried out.

CHAPETR –2

2. LITERATURE REVIEW

2.1 Historic outlook of carbon

In the stone age (from 35,000 to 11,000 BC), charcoal and carbon black were used as black color pigment for painting caves and to draw the black lines of the illustrations in the cave of Altamira (Spain) that represents the apogee of Paleolithic cave painting art developed across Europe. The Egyptians and Sumerians used charcoal in the reduction of copper, tin, and zinc minerals in the bronze manufacturing process and also as smokeless fuel in 3750 BC (Derbyshire et al. 1995; Greenwood & Earnshaw, 2006; Przepiórski, 2006) while Egyptian papyrus in 1,550 BC used charcoal as medicine for the adsorption of odors from purifying wounds and also to treat problems of the intestinal tract (Çeçen, 2011, 2014). The therapeutic value of carbon was later explored by the Greeks (Hippocrates, ca. 460–370 BC) and Romans (Pliny the Elder, AD 23–79) in the treatment of various diseases, including food poisoning, epilepsy, chlorosis, and anthrax. (Dąbrowski, 2001; Jäger et al., 2010).

In 1794, the carbon materials were used in industries for industrial processing in England. The wood charcoals were applied as bleaching agents in the processing of sugar. During that time, the wood charcoals preparation method was kept a secret (Jäger et al., 2010). Later, the first large-scale sugar refining facility was introduced in France by Gruillon, working with ground and washed wood char in 1805 (Allen et al., 2010). In French industry, Delessert demonstrated the effectiveness of charcoal for decolorizing sugar-beet liquor contributing for the growth of this industry from 1805-1808 (Allen et al., 2010). In 1808, all European sugar refineries were using charcoal as a decolorizer (Allen et al., 2010).

Figuier discovered bone-derived char as a more efficient raw sugar syrups decolorizing agent and consequently the sugar industry replaced wood charcoal by this improved material in 1811 (Allen et al., 2010; Çeçen, 2014). Later in 1815, the granular bone-derived char were used by sugar refinery factory (Allen et al., 2010).

During 1900 to 1903, Raphael von Ostrejko explored one of the most outstanding abilities of carbon materials, producing AC materials (Kim et al., 2013).

Nowadays, the uses of AC continue to grow in our daily life. Practically, it can be found to be used in every hospital, clinic or doctor's office in the world. It is used in a variety of industries like corn and cane sugar refining, gas adsorption, dry cleaning, pharmaceuticals, fat and oil removal, alcoholic beverage production etc. One of the most widely used area is for the purification of municipal water supplies. AC filters are used in water treatment or purification to remove organic compounds that produce carcinogens during the disinfection of water. Similarly, removal of heavy metals in the coal fire powder plants is another scope for AC (Thommes et al., 2015). Moreover, AC is also used at homes to remove the odor to keep air plash (a splashing sound). It seems that the demand of AC is due to rise over the coming few years with expectations of sales approaching 2 million metric tons per annum (Thommes et al., 2015). The reasons are varied, but regulatory changes in western economies are one of the primary causes.

Most of the commercial ACs is derived either from coal or from petroleum, which are very expensive. Therefore, the scientists are exploring new low cost precursors for the production of AC, mostly from the agricultural based lignocellulosic materials such as shells or stones of fruits, wood, coconut shells, coal peat, tobacco stems, bean husks, hazelnut shell, banana peels, mangosteen shells, sawdust, rice husk and so on which are lasting source for the production of activated carbon. Thus produced activated carbons are applied in different fields like environmental pollution remediation such as waste and ground water treatment process, adsorption of pollutant from air and water, removal of heavy and trace metal ions from water bodies, pesticides from air and water sources,etc. (Ioannidou & Zabaniotou, 2007, in industrial sector such as food, oil, pharmaceutical, chemical, mining and especially in water treatment processes and in energy storage and harvesting such as batteries, solar cells, sensors, supercapacitors.

2.2 Activated carbon//Activated charcoal (AC)

In 1999, AC was prepared from **pecan shells** and has got surface area ranging from 618 to 1149 m^2g^{-1} when steam activation was applied; while greater surface area of 1560 $m^2\ g^{-1}$ was obtained using CO_2 in the activation process (Mitchell et. al. 1999).
In another study on **apple pulp**, as precursor to produce AC was done in the year of 2002. Apple pulp was carbonized along with chemical activation with H_3PO_4. Thus obtained AC has surface area of 854 m^2g^{-1} (Suárez-García et. al., 2000).

Likewise, in another study, the AC was prepared from **almond nut shell** by chemical activation with H_3PO_4 as an activating agent. This study focused on the adsorption of chromium (VI) from aqueous solution on almond nut shell activated carbon with the adsorption parameters pH, agitation speed, agitation time, adsorbent dose were optimized. 98% of Cr (VI) was adsorbed at pH 2 and stirring speed 200 rpm. Surface morphology showed spongy type structure having large number of pores (Annadural et al., 2002).

Another study was carried in 2009 using **bamboo waste** as precursor to prepare AC and the AC was prepared by microwave-induced activation process using H_3PO_4 as an activating agent. The study focused on the effects of various factors, such as microwave radiation power, microwave radiation time, and H_3PO_4/carbon IR ratio, on the activation. The results revealed as in optimal activation conditions; a microwave radiation power of 350W, a microwave radiation time of 20 min, and H_3PO_4 / carbon IR ratio of 1:1, under which a surface area of 1432 m^2g^{-1} and a carbon yield of 48% could be reached. It was found that the microwave-induced activation exhibited a faster activation rate and a higher carbon yield compared with the conventional thermal process (Zhang et al., 2009).

Another study was reported by Oubagaranadin et al., (2009) on preparation of AC using **sawdust of *Shorea robusta* (Sal)** by thermal process and using H_2SO_4 as an activating agent to remove Pb (II) from aqueous solution. Adsorption equilibrium studies have been done at a pH of 4 and room temperature of 30°C. It was found that the adsorption isotherms are favorable and chemically activated carbons are better than physically activated carbon in terms of adsorption capacity (Oubagaranadin et al., 2009).

In the same year (2009), a study was conducted on AC produced from **waste tea** with potassium acetate (CH_3COOK) as the activating agent, on the conditions: activating agent to precursor (waste tea) ratio is (0.3 - 2.5), temperature of activation (500^oC to 800^oC), and time of activation (60 min -150 min). The statistical technique as a Response Surface Methodology was used to optimize the preparation conditions like activation temperature, activation time, production percentage and removal of dyes. The results indicated that the optimal conditions for good production percentage and removal of the dyes were 800^oC, ratio 1.4, and 120 minutes giving a high surface area of 854.30 m^2g^{-1}. The prepared mesoporous adsorbent exhibited good adsorption capacities of 453.12 and 554.30 mg g^{-1} for AB29 and MB, respectively (Zhang & Zhao, 2009).

Likewise, in 2009, AC was prepared from **corn cob** at the pyrolysis temperature of 500-800^oC and activated physically and chemically with CO_2 and KOH. The study focused on the effect of temperature and pyrolysis conditions on the efficiency of the carbon. The sorption properties were studied on NO_2 and hydrogen sulfide (H_2S). The surface area of the carbon was found to be varied from 337 to 1213 m^2g^{-1} (Zhang & Zhao, 2009).

Similarly, in the year of 2011, AC has been prepared from **olive seeds**, using KOH as activating agent. In the study, the ratio of KOH: precursor used was 4:1. The temperature varied from 800^oC to 900^oC and retention time varied from 1to 4 h. Thus obtained AC achieved a very high surface area up to 3000 m^2g^{-1}. This research is a pioneering work, which showed the co-relation between temperature and time with surface area. It showed that when temperature and retention time increases, the surface area too increases (Nabais et al., 2011).

Another study by Zhang et al. (2011) reported the preparation of a biomass-based AC from **bamboo scraps** and activated by the K_2CO_3, while the AC was treated in HNO_3 solution for the purpose of surface modification and ash removal. It was found that the BET surface area of the AC could reach 1264 m^2g^{-1} under the following conditions: activation temperature, 1173 K; activation time, 2 h; impregnation ratio, 1:1. The content and diversity of the surface oxygen functional groups of the AC could be well improved through the HNO_3 treatment, and the ash content was remarkably reduced. It was observed that the BET surface area was slightly reduced while the electrical resistivity was remarkably increased.

A study carried out by Ekpete et al. (2011), AC was prepared from **fluted pumpkin stem waste** and **c**arbonization was done at 350 °C for 2 hours and allowed to cool at room temperature for three hours before activation with 0.3M H_3PO_4 and heated to 300 °C for thirty minutes. Characterization of pH, bulk density, porosity and iodine number was conducted and compared to a commercial AC. The data was obtained when it was subjected to t-Test statistical analysis. It unveiled that the volatile matter, and phenol content of the ACs and particle density indicating no significant difference on both ACs. A significant difference in the properties of moisture, pH, porosity, ash content, iodine number, carboxylic acid content, lactones, and basic sites contents were observed on the activated carbons.

In 2011, an experiment was performed on agricultural **waste corn cob** as precursor to prepare AC. Corn cob granules were dried and KOH was used as an activating agent. Precursor material was analyzed for elemental analysis, and the effect of carbonization temperatures for 600, 700, 800 and 900^{o}C was examined. Higher BET surface area of 940 m^2g^{-1} was observed for temperature of 800^{o}C. The results showed that agricultural waste corn cob can be used as a promising precursor material for the production of low cost activated carbon (Prahas et. al., 2011).

Then, a comparative study on production of ACs from **date stone** was carried out and compared the effect of temperature, impregnation ratio and retention time on the production and iodine adsorption in 2012. In this study, ACs were prepared by activating with H_3PO_4 and $ZnCl_2$ which were then compared using the same equipment, and under similar conditions. It concluded that the high value of iodine number was obtained in case of H_3PO_4 activated carbon under following conditions; impregnation ratio 0.4 (4/10), activation time 60 min, activation temperature 800^{o}C. However, the production was found to be lower in case of H_3PO_4 AC than that $ZnCl_2$ AC. The research also revealed that Iodine Number (IN) increases significantly with increasing activation temperature while IN decreased sharply by increasing the impregnation ratio at the same temperature (Zhang & Zhao 2012).

A research on AC from **Lapsi (Choerospondias axillaris)** seed stone by chemical activation with $ZnCl_2$, in Nitrogen atmosphere at 400^{o}C was carried out in 2013. Chemical activation using a 1:1 ratio of Lapsi seed stone powder and $ZnCl_2$ followed by iron impregnation greatly enhanced the arsenic adsorption capacity for adsorption of arsenic from ground water. (Rajbhandari et al., 2012).

In another experiment conducted by Hiremath et al. (2012), AC was prepared from agricultural waste corn cob. Corn cob granules were dried, as a precursor material and activated by KOH. Precursor material was analyzed for elemental analysis, and the effect of carbonization temperatures for 600, 700, 800 and 900 °C is examined. Higher BET surface area of 940 m^2g^{-1} was observed for temperature of 800°C. The results unveiled that agricultural waste corn cob can be used as a promising precursor material for the production of low cost AC.

Likewise, AC from the same material, **Lapsi (Choerospondias axillaris)** seed stone was prepared as adsorbents for the removal of Pb (II) ions from aqueous solution. Two series of carbon have been prepared from Lapsi seed stones by treating with conc. H_2SO_4 and a mixture of H_2SO_4 and HNO_3 in the ratio 1:1 by weight for removal of metal ions. Chemical characterization of the resultant AC was studied by Fourier Transform Infrared Spectroscopy (FTIR) and Boehm titration which explored the presence of oxygen containing surface functional groups like carboxylic, lactonic, phenolic in the carbons. For this, the effect of pH and initial metal ion concentration on the adsorption was studied in a batch process mode, and the optimum pH for lead adsorption was found to be equal to 5. It was found that the maximum adsorption capacity of Pb (II) on the resultant activated carbons was 277.8 mg g^{-1} with H_2SO_4 and 423.7 mg g^{-1} with a mixture of H_2SO_4 and HNO_3 (Shrestha et al.,2013)

Similarly, the influence of activating agents on surface area and porosity of the **lapsi** derived AC was studied in 2013. A series of ACs from **lapsi seed stone** was prepared by chemical activation using different activating agents KOH, H_2SO_4, $FeCl_3$, $MgCl_2$, and $CaCl_2$.The iodine number and maximum adsorption capacity for methylene blue were determined. The SEM micrographs revealed that the AC was found to be mainly microporous and mesoporous. Among the different ACs, the KOH activated carbon showed the highest adsorption capacity for methylene blue and iodine (Joshi et al., 2013).

In the year 2013, a study on the preparation of AC using **tea waste** was conducted by Wankhade & Ganvir using the tea wastes directly collected from houses, cafeterias, tea stalls and hotels. This tea waste was first dried in the sunlight for 20 days. This naturally dried material was then kept in the oven for 12 hours at the temperature 50°C. Then 100 g of sample was crushed manually. Dilute sulphuric acid 70 mL was utilized to digest the tea waste. The digested tea wastes were washed with distilled water, 10 to 12 times. The whole sample is taken in a container and kept at 500 °C in a muffle furnace for 15 minutes. Finally, AC was obtained. Then, oversize and undersize particle is separated by using 300 sized meshes. Thus, the material showed good surface area and the material was found to be in crystalline phase (Wankhade & Ganvir, 2013).

Another research report on the preparation of ACs from a mixture of **sugar cane bagasse (SB)** and **corn husk** (CH) by the physical activation method was put forward by Billy et al. (2013). Initially, the SB and CH raw materials were processed into pellets to maintain a uniform size and shape during activation. Then carbonization was done at different temperature under a nitrogen atmosphere for 2 hours. This was followed by activation using air as a gasifying agent at different activation temperatures for 40 minutes. The activation temperature at 800°C gave the best quality with respect to the porosity of the carbon. The highest BET surface area was found to be 255.909 m^2g^{-1}.

In 2014**,** another study on **grape seed** was used for preparing AC using K_2CO_3 and KOH. The carbonization experiments were accomplished at 600 ºC and 800ºC. The results showed that AC with the highest surface area of 1238 m^2/g was obtained at 800ºC in K_2CO_3 concentration of 50 wt% while KOH produced the activated carbon with the highest surface area of 1222 m^2g^{-1} in a concentration of 25 wt% at 800ºC. The ACs were found to be mainly microporous (Okman et al., 2014).

In the year 2015, **olive stone was** used directly without any activation treatment to adsorb two dyes, MB and Alizarin Red (Albadarin A. B., Mangwandi C., (2015) Consequently, there were no significant surface groups available to adsorb the large positively charged basic dye coloured ions, resulting a very low uptake capacities of 13.2 and 16.1 mg/g, respectively.

Likewise, in the same year (2015), **olive stones** was steam activated to obtain an AC, which resulted surface area of 807 m^2g^{-1}. NO_2 adsorption was performed for different inlet gas compositions and temperatures and adsorption capacity of NO_2 was found to be 131 mg g^{-1} Both basic and acidic functional groups on the AC surface allow the reduction of NO_2 Ghouma et al. (2015). Several other olive industry wastes have undergone physical treatment/activation.

Another study was made in 2016 to produce AC from **olive stone** which was activated by H_3PO_4. As produced AC had a significant cadmium adsorption capacity of 51.1 mg g^{-1} and the surface area was found to be 1194 m^2g^{-1} at pH 5. According to a this study, the uptake of cobalt, nickel and copper on ACs obtained by treating olive stones with H_3PO_4 and H_3PO_4 with ozone provided capacities in the range 10 to 17.9 mg g^{-1}, but the treatment with H_3PO_4 and HNO_3 increased the nickel and copper capacities to 20.5 and 34.2 mg g^{-1}, respectively (Bohli & Ouederni, 2016). The result revealed that though the activated carbon had low surface area of 173 m^2g^{-1}, it showed better heavy metal ion adsorption and ion exchange capacity indicating the importance of surface functional groups on AC.

Many studies were reported for the adsorption of phenol from water using **olive stone-derived AC.** For example, the organic solvent washing of olive wood showed low capacities, less than 12 mg g^{-1}, for a range of chlorophenols and nitrophenols. In the study of Limousy et al., (2017) one interesting result is the adsorption of the pharmaceutical amoxicillin onto H_3PO_4 treated olive stone because of the recent awareness of the accumulation of pharmaceutical personal care products, in drinking water sources. An interesting study applying N_2 + plasma was performed Soudani et al. (2017) by using treatment times of 5, 10 and 30 min and produced ACs of surface areas 1140, 1055 and 988 m^2g^{-1}, respectively. The high phenol adsorption capacities for these three ACs were 226.4, 323.3 and 635.2 mg g^{-1}, respectively. Interestingly, the finding was the longer the treatment time, the lower the surface area, but the higher the phenol adsorption capacity. The prolonged treatment opened up micropores into mesopores causing the reduction in surface area with time and also changed the surface functionality, generating more nitrogen surface groups and decreasing the number of oxygen surface functional groups. Both of these effects favoured a high affinity for phenol adsorption (Soudani et al., 2017).

The present study has been focused on preparation, characterization and the use of laboratory prepared AC derived from agro-waste, sawdust of *Shorea robusta* (Sal) in energy related field. Hence, literatures were reviewed on AC and its application on energy related field.

2.3 Application of AC in energy related field

AC has been used in energy related fields such as batteries, solar cells, supercapacitors etc. Supercapacitors or Electrochemical capacitors (ECs) can be widely used as memory back-up systems in toys, cameras, video recorders, mobile phone (Winter & Brodd, 2008). It is also an attractive power source in electrical vehicles, military weapons, space equipment and a number of electrical devices (Zhang & Zhao, 2009). Now-a-day supercapacitors or ECs are broadly used in airbus for emergency door opening. Regarding the wide application of EC, many researchers have tried to investigate capacitive behavior of AC prepared from different precursors and by different activation processes.

Correspondingly, in the year 1991, a study has been made on carbon sample obtained from the processed **sunflower seed shell** and electrochemical studies have been made. The resulted specific capacitance was 244 Fg^{-1} in 0.1 M HCl electrolyte, surface area of 2585 m^2g^{-1}, pore volume of 1.4 cm^3g^{-1} and good cycle stability was obtained (Cartula et al., 1991). In the year of 2000, a breakthrough was done by Kotz and Carlen on devices which overcome the conventional devices/ batteries /capacitors. Those devices are available on the market for 100 years, have technically been optimized, and use elaborated manufacturing methods. However, due to the restriction of single cells to a low voltage, several dozens or even many hundreds of cells have to be connected in series. Capacitance as well as leakage resistance of the individual cells have to be very uniform during the whole life of the EC. Otherwise, in a series connected string some cells may see an overvoltage and get damaged. One single damaged cell may deteriorate the performance of the whole capacitor system. Precautions are therefore necessary to guarantee the balancing of cell-voltages. The balancing system should be very reliable, have low cost, and if ever possible, be integrated into the EC. (Kotz & Carlen, 2000).

An another work on AC nanospheres was reported in the year of 2001, in which AC was prepared after KOH activation and further post processing of **coconut shells.** It reported that though the surface area of 2000 m^2g^{-1}, total pore volume of 1.2 cm^3g^{-1}, the high specific capacitance of 250 Fg^{-1} in 1M H_2SO_4 electrolyte were obtained. The 93% capacitance retention was observed after 2000 cycles (Hu et al., 2001).

In 2004, in the research conducted by Wu et. al., AC prepared from **fire-woods**, using of a steam activation method at 900 °C for 1 to 7 h were used as promising materials for supercapacitors. The result showed that the carbons exhibited high-power, low equivalent series resistance and highly reversible characteristics between −0.1 and 0.9 V in aqueous electrolytes. All the steam-ACs of fire wood prepared at different activation times showed ideal capacitive performance in aqueous media. The average specific capacitance of an AC as estimated from cyclic voltammetic curves measured at 200 mVs^{-1} reached 120 Fg^{-1} between −0.1 and 0.9 V in acidic electrolytes. In the following year, a drastic change has been made by scientists by preparing composite of AC and metal oxides in order to have better performance in ECs. One of the metal oxide is nanometer-scale amorphous nickel oxide which was loaded into activated-carbon to enhance specific capacitance and energy density of carbon-based supercapacitor by suspending the activated-carbon in a $Ni(NO_3)_2$ solution followed by neutralization.

In the year, 2005, the activated-carbon loaded with nickel oxide was used as cathode material and activated-carbon was used as anode material to make a hybrid type electrochemical capacitor and it was tested. It was found that, when nickel oxide loading was increased, BET surface area of the activated-carbon was decreased compared to that of the starting material, its specific capacitance increased 10.84%, from 175.40 to 194.01 Fg^{-1} and the potential of oxygen evolution on the composite material electrode was 0.076 V higher than that of the pure activated-carbon electrode, in the electrolyte of 6 mol/L KOH solution, so the hybrid capacitor had larger energy density. Similar to the pure activated-carbon electrode, no obvious change appears on the specific capacitances of the composite material electrode at various discharge currents and the composite material electrode exhibiting good power characteristics (Yuan et al., 2005).

In the year 2006, nanostructured mesoporous non-graphitized carbon black (NMCB) powders were employed to fabricate symmetrical carbon/carbon double layer capacitors (EDLCs) and their EDLC behavior was studied using electrochemical techniques viz., cyclic voltammetry, a.c.-impedance, and constant current cycling. The cyclic characteristics indicating the double layer behavior of the NMCB carbon electrodes as rectangular shape were observed according to the research scholars. The mechanism of double layer formation and frequency dependent capacitance were deduced from the ac-impedance analysis. Specific capacitance, power density and energy density were derived from constant current charge/discharge measurements. NMCB powders demonstrated a specific capacitance of about $\sim 39\ Fg^{-1}$ and the power density of 782 $W\ kg^{-1}$ at a current density of 32 $mA\ cm^{-2}$. Nevertheless, at a low current density (3 $mA\ cm^{-2}$), the specific capacitance of $\sim 44\ Fg^{-1}$ was achieved, which corroborates with the values obtained by means of ac-impedance (40 Fg^{-1}) and cyclic voltammetry (41.5 Fg^{-1}). The test cells demonstrated the stable cycle performance over several hundreds of cycles (Prabaharan et al., 2006).

Additionally, **waste coffee beans** were also used to generate AC by treatment with $ZnCl_2$ to prepare high performance supercapacitors. According to Rufford et al., (2008) the results indicated that the supercapacitor electrodes exhibited energy densities up to 20 Whkg^{-1} in 1 M H_2SO_4, and exceptional stability at high charge–discharge rates. In a two-electrode cell, a specific capacitance as high as 368 Fg^{-1} was observed with rectangular cyclic voltammetry curves and stable performance over 10,000 cycles at a cell potential of 1.2 V and current load of 5 Ag^{-1}.

Similarly, in 2008 another study on **corn grains**-based activated carbon (CG-AC) was prepared and it was used successfully as an electrode in the electrical double layer capacitor (EDLC). The structural properties, energetic heterogeneities and surface functional groups of CG-AC were characterized using different techniques like nitrogen sorption data, adsorption energy distribution (AED) and X-ray Photoelectric Spectroscopy (XPS). The electrochemical properties of various CG-AC were evaluated by using cyclic voltammetry. The result showed that the specific capacitance value of 257 Fg^{-1} in 6 M KOH electrolyte solution (Balathanigaimani et al., 2008).

In the same way, AC was prepared from **cherry stone waste** for electrode material in supercapacitors by Marin et al. (2009). It was reported that the cherry stone waste precursor was activated with KOH at 800-900 ºC to obtain activated carbons with large specific surface areas (1100-1300 m^{2}g^{-1}), which makes them accessible to electrolyte ions. The findings showed that these features lead to capacitances at low current density as high as 230 Fg^{-1} (Marin et al., 2009).

Additionally, Zhao et al., (2009) studied the AC prepared from potato starch (PACS**)** by stabilization, carbonization followed by activation with KOH. The obtained PACS were hollow and retained the original morphology of potato starch with decreased size, as shown by scanning electron microscopy. The N_2 adsorption isotherms indicated that the samples prepared were mainly microporous. The electrochemical behaviors of the hollow PACS were studied by galvanostatic charge–discharge, cyclic voltammetry, and impedance spectroscopy. The results indicated that high specific capacitance of 335 Fg^{-1} was obtained at current density 50 mAg^{-1} for PACS with specific surface area 2342 m^{2}g^{-1} (Zhao et al., 2009). Similarly, Zhang et al. (2009) presented the activated carbon nanospheres obtained from carrageenan, which possesses a surface area of 1704 m^{2}g^{-1}, total pore volume of 0.9 cm^{3}g^{-1}, specific capacitance of 343 Fg^{-1} using KOH and CO_2 activation in 1 M H_2SO_4. And it has a cycle life of about 2500 cycles (Zhang & Zhao, 2009).

Likewise, a carbon-carbon composite electrode material for supercapacitors was prepared by KOH activation of **waste newspaper** by Kalpana et al., (2009). The composite was investigated by X-ray diffraction (XRD), N_2 adsorption/desorption and scanning electron microscopy while electrochemical characteristics were examined by cyclic voltammetry (CV) and charge–discharge tests. The CV results revealed a maximum specific capacitance of 180 Fg^{-1} at a 2 mVs^{-1} scan rate and the data explored a development of new use for waste paper into a valuable energy storage material (Kalpana et al., 2009).

Similarly, Wang et al. (2009) have reported that KOH as an activating agent showed better performance to obtain from honeycomb like **carbon foam**. It exhibited a large specific surface area of 1313 $m^2\ g^{-1}$ and a high specific capacitance of 473 F g^{-1}. In addition, porous carbon was converted from natural silk via coupled activation and graphitization process, which showed a high specific surface area of 2494 $m^2\ g^{-1}$ and a large pore volume of 2.28 $cm^3\ g^{-1}$. Further for supercapacitor application, the silk derived hierarchial porous carbon revealed a high specific capacitance of 242 F g^{-1}, a high-energy density of 102 Wh kg^{-1}, as well as exceptional cycling life stability (9% loss after 10,000 cycles).

In year 2010, the possibility of improving the hydrogen-storage capacity of mesoporous MCM-41 were investigated by research team of Park and Lee. In the study, MCM-41 containing nickel (Ni) oxides (Ni/MCM-41) prepares by hydrothermal process as a function of Ni content (2, 5, and 10 wt.% in the MCM-41). The surface functional groups of the samples were identified by using Fourier transforms infrared spectroscopy (FTIR). The structure and morphology of the samples were characterized by X-ray diffraction (XRD) and field emission transmission electron microscopy (FE-TEM XRD results showed a well-ordered hexagonal pore structure; FE-TEM also revealed, as a complementary technique, the structure and pore size. The textural properties of the samples were analyzed using N_2 adsorption isotherms at 77 K. The hydrogen-storage capacity of the sample was evaluated at 298 K/100 bar. It was found that the presence of Ni on mesoporous MCM-41 created hydrogen-favorable sites that enhanced the hydrogen-storage capacity by a spillover effect. It was concluded that the hydrogen-storage capacity was greatly influenced by the amount of nickel oxide, resulting in a chemical reaction between Ni/MCM-41 and hydrogen molecules. (Park & Lee, 2010).

Another study was conducted by Rufford et al. (2010) on AC prepared from **sugar cane bagasse** using chemical activation with $ZnCl_2$ for supercapacitor electrodes. The $ZnCl_2$ activation of bagasse was studied using thermogravimetric analysis and the carbon pore structures were characterized using N_2 and CO_2 adsorption. The results showed that in two-electrode, sandwich-type supercapacitor cells containing 1 M H_2SO_4, the sugar cane bagasse carbons (SCCs) exhibited specific energy up to 10 $Whkg^{-1}$ and specific capacitance close to 300 Fg^{-1}. On the other hand, the pyrolysis of bagasse without $ZnCl_2$ produced a carbon with low specific capacitance.

A high volumetric capacitance was studied by Xu et al., (2010) by preparing AC from **apricot shell** by optimizing the carbonization temperature prior to NaOH activation to balance the porosity and density. The outcome indicated that the carbonization temperature had a marked effect on both the pore structure and the electrochemical performances of the activated carbons. Moderate carbonization at 500 °C resulted in not only high gravimetric capacitance of 339 Fg^{-1} but also high apparent electrode density of 0.504 g/cm^3, and hence a highest volumetric capacitance of 171 F/cm^3 in 6 mol L^{-1} KOH aqueous electrolyte was obtained.

In 2012, Chen et al., studied the AC from **rice hull**, which had high specific surface area. It was carbonized at 400 ºC for 2 h, followed by alkali hydroxide activation and heating to 800ºC**.** The prepared AC was applied for EDLC and the CV measurement shows that the porous carbon exhibited supercapacitance of 368 Fg^{-1} at the scanning rate of 2 mVs^{-1} (Chen et al., 2012). Moreover, Elmouwahidi et al. (2012) have synthesized the ACs from Argan Seed Shells (ASS) activated by KOH. The AC with the largest surface area and the most developed porosity was superficially treated to bring together oxygen and nitrogen functionalities. Electrochemical measurements were carried out with three-electrode cell using 1 M H_2SO_4 as electrolyte and Ag/AgCl as reference electrode. The results showed that the O-rich AC showed the lowest capacitance (259 Fg^{-1} at 125 mAg^{-1}) and the lowest capacity retention (52% at 1 Ag^{-1}), due to surface carboxyl groups impeding electrolyte diffusion into the pores. On the contrary, the N-rich activated carbon showed the highest capacitance (355 Fg^{-1} at 125 mAg^{-1}) with the highest retention (93% at 1 Ag^{-1}), due to its well-developed micro-mesoporosity and the pseudocapacitance effects of N functionalities.

In the same year 2012, ordered mesoporous carbons (OMCs) with controllable pore sizes in the range of 4–10 nm were prepared by a template procedure using 2D hexagonal MSU-H and 3D cubic KIT-6 as hard templates and boric acid as the pore expanding agent. The electrochemical performances were characterized by cyclic voltammetry (CV), galvanostatic charge/discharge (GC) and electrochemical impedance spectroscopy (EIS) experiments in 30 wt% KOH electrolyte and measured using synthesized OMCs as electrode materials for electrochemical double layer capacitors (EDLCs). It was found that, the prepared OMCs exhibit good capacitive behaviors with the specific capacitance values ranging from 143 to 205.3 F g^{-1} at a voltage scan rate of 5 mV s^{-1} and 81 to 86% retained at a high scan rate of 100 mV s^{-1}. OMC-M-2 shows the highest specific surface capacitance value of 27.5 μF cm^{-2} at 5 mV s^{-1} with a peak pore size of 7.8 nm and a Brunauer–Emmet–Teller (BET) surface area of 729.3 m^2 g^{-1}. Both kinds of pore symmetries of OMCs with the same pore size of about 6.5 nm shows that the 3D cubic OMC exhibited superior capacitive performance than the 2D hexagonal OMC was found. (Lu et al., 2012).

Similarly, Verla et al. (2012) studied a series of ten samples of AC, which were successfully prepared by carbonization and activation of **fluted pumpkin seed shell**. In this study, thermal activation was achieved at 300°C, 400°C, 500°C, 600°C and 700°C, while chemical activation was achieved by first impregnating the prepared raw material with activating reagents, and then carbonization at 500°C. Characteristics of the ACs were determined using standard methods. Increasing the activation temperature from 300°C to 700°C showed improved characteristics. The optimum temperature for production of activated carbon was obtained at 500°C after 2 hours. The iodine values for physically prepared carbons were normally lower, compared to chemically prepared carbons. Phosphate removal efficiency and rates of phosphate removal were satisfactory for all prepared activated carbons though the chemically prepared samples had higher efficiencies. Results revealed that quality AC could be produced from these agricultural wastes.

The study of Peng et al. (2013) had presented an account of AC from **waste tea leaves** applied in supercapacitor electrode. AC was prepared under high temperature carbonization and KOH activation. As the electro-active electrode materials, the AC exhibits ideal capacitive behaviors in aqueous KOH electrolyte, and the maximal specific capacitance is as high as 330 F/g at the current density of 1 Ag^{-1}. Furthermore, excellent electrochemical cycle stability was shown by AC with ~92% initial capacitance being retained after 2000 cycles.

Additionally, an ultrahigh specific surface area (3164 m^2g^{-1}) and large pore volume (1.88cm^3g^{-1}) porous AC from **waste litchi shells** was synthesized by Zhang et al. (2014)**.** The AC was activated by KOH, which showed channel-like macropores. The macroporous structure of litchi shells was supposed to be favorable to distribute the activation agent, which enables sufficient activation. The prepared AC was developed as a conducting framework for lithium–sulfur battery cathode materials. The resulting activated carbon/sulfur composite cathode possesses a high specific capacity, good rate capability, and long-term cycling performance.

Similarly, the preparation of a three-dimensional (3D) honeycomb-like porous carbon (HLPC) by the simple carbonization of pomelo peel followed by KOH activation was reported by Liang et al. (2014). Structural characterization indicated that the as-prepared HLPC with a high Specific Surface Area (SSA) up to 2725 m^2g^{-1} was made up of interconnected microporous carbon walls. Chemical analysis presented that the HLPC was doped with nitrogen having oxygen-containing groups. Electro-chemical measurements showed that the HLPC reveals a high specific capacitance of 342 Fg^{-1} at 0.2 Ag^{-1} (Liang et al., 2014).

In a similar work by Jain & Tripathi (2014), presented the **coconut shell** AC was synthesized using chemical activation method using KOH as an activating agent. The specific surface area (mesopores size of 3 nm) was reported to be 1640 m^2g^{-1}. EDLCs fabricated using the samples as electrode material with polymer electrolyte exhibited energy and power density of 88.8 $Whkg^{-1}$ and 1.63 $Kwkg^{-1}$, respectively.

Literatures revealed that preparation of hybrid electrode by adding electrochemically active materials in carbon-particle-based electrode demonstrate higher specific capacitance and energy density (Conway, 1999; Ganesh et al., 2006; Wang et al., 2008). The attention has been given to generate a single-supercapacitor by accommodating both the EDLC and pseudo-capacitance in one component. Hybrid-composite materials of AC along with MnO_2 nanoparticles can be a good component. Activated carbon behaves non-faradiac EDLC and MnO_2 shows faradaic pseudo capacitance. Wang et al. (2015) had prepared hybrid composite of activated carbon and MnO_2, which demonstrated the high specific capacitance of 324.3 F g^{-1} at 0.1 A g^{-1} using three-electrode system, however impedance or charge transfer resistance was found to be 0.92 Ω, which is high (Wang et al., 2015).

Similarly, Qu et al. (2015) used **corncob residue** to prepare a porous carbon for supercapacitor electrodes, using a green and low-cost steam activation method. The carbon obtained at 850°C, which was further treated with ash removal and acid soaking exhibited SBET of 1210 m^2g^{-1} with a production of 23.2 wt.%. They reported a capacitance of 314 Fg^{-1} at a scan rate of 5 mVs^{-1} and a capacitance retention of 82%. The performance of the samples was attributed to the well-developed porosity and good conductivity. The same researchers made use of an organic and 6MKOH aqueous electrolyte to determine the electrochemical performance of corncob residue-derived carbon, which revealed an energy density of 5.3 $Whkg^{-1}$ at a power density of 8276 Wkg^{-1} in 6 M KOH, while the organic electrolyte exhibited energy and power density of 15 $Whkg^{-1}$ and 2827 Wkg^{-1}, respectively.

A research on porous AC from **fallen leaves**, were studied by Li Yin-Tao et al. (2015). They employed KOH, K_2CO_3 and mixed KOH, K_2CO_3 for activation and observed that the mixed activation produced enlarged pore sizes for the activated carbon (SBET of 1078 g cm^{-1}), noting that the surface area and hierarchical pore structures were related to the mass ratio of two activators. They reported a high specific capacitance of up to 242 Fg^{-1} (0.3 Ag^{-1}, 6 M KOH) in a two-electrode system, maintaining a high retention rate.

In another study, Yin et al. (2016) prepared AC from **coconut fibers** with a multi-tubular hollow structure using KOH for activation. The sample with 4:1 mass ratio of KOH to carbonized coconut fibers exhibited a specific surface of 2898 m^2g^{-1} with a pore volume of 1.59 cm^3g^{-1} (30% mesopores). The prepared supercapacitor electrode (with 6 M KOH electrolyte) exhibited a specific capacitance of 266 Fg^{-1} at a current of 0.1 Ag^{-1}, maintaining 76% of its capacitance at 100 Ag^{-1}. They found that the 3-dimensional hierarchical porous AC electrode exhibited a high capacitance of 155 Fg^{-1} at 0.1 Ag^{-1} and 142 Fg^{-1} at 10 Ag^{-1} and achieved a high-energy density of 53 $Whkg^{-1}$ and a high-power density of 8224 Wkg^{-1}.

In the same way, porous carbon material from **soybean roots** has been prepared by Guo et al. (2016). The roots were carbonized for 2 h at 500°C under nitrogen atmosphere and further functionalized for 2 h at 900°C under a nitrogen atmosphere. Using a symmetric two-electrode supercapacitor in 6 M KOH, it reported the existence of quasi-rectangular shapes for CV plots. The study found that the sample exhibited a specific capacitance of 276 Fg^{-1} at 0.5 Ag^{-1} and capacitance retention of 98% after 10,000 cycles. A supercapacitor was assembled using an ionic liquid electrolyte and reported an energy and power density of 100.5 $Whkg^{-1}$ and 4353 Wkg^{-1}, respectively.

In another novel work, AC tubes were prepared from biomass waste container **strobili fibers** (Su et al, 2018). It reported that the optimized material demonstrated a specific capacitance of 214.5 Fg^{-1} at 50 A g^{-1} in the three-electrode setup. A fabricated supercapacitor exhibited 84.21% capacitance retention at a significant specific energy of 33.04 $Whkg^{-1}$ at 160 Wkg^{-1}.

A work on carbon based nanofiber (CNF) has been performed by a research group in 2016 in Thailand (Sinprachim et al., 2016). They prepared CNF samples and hybrid composite along with metallic oxide namely CNF, AgOx/CNF, MnOx/CNF, AgOx-MnOx/CNF. Then morphological, structural, textural properties of CNF, AgOx/CNF, MnOx/CNF, AgOx- MnOx/CNF were carried out, and supercapacitor performances were studied by cyclic voltammetry, galvanostatic charge/discharge, and electrochemical impedance spectroscopy. Results revealed that calcined fibers were obtained as a paper-like sheet thickness of ∼30–60 μm, having several diameters of ∼237–643 nm depending on each composite. Among the samples, the AgOx-MnOx/CNF which had a high specific surface area of 812 m^2g^{-1} expressed the highest specific capacitance of nearly 204 Fg^{-1} and energy density of ∼28 $mWhg^{-1}$ at a power density of ∼250 mWg^{-1}. Moreover, it also displayed imposing cycling capability of more than 99% after 1000 cycles of charge/discharge. Concerning to this, extensive works have been undergoing to get better performance supercapacitor with high power density, energy density, longer life time and low charge transfer resistance but the quest for new materials are ongoing (Sinprachim et al., 2016).

Similarly, Maryati et al. (2017) also fabricated composite of activated carbon and MnO_2 nanoparticle, which showed the specific capacitance of 372 Fg^{-1} at the scanning rate of 10 mV in 3 M KOH having the charge transfer resistance of 0.88 Ω (Maryati et al., 2017).

In the studies reported successful preparation of nitrogen-doped AC from **orange peels**. The study investigated the properties of the fabricated capacitor cells using electrochemical impedance spectroscopy, cyclic voltammetry and galvanostatic charging-discharging. The electrochemical performance of the samples was tested in a two-electrode assembly using 6 M KOH as the electrolyte. They observed a surface area of 1577 m^2g^{-1} for the activated carbon and established a specific capacitance of 167 Fg^{-1} at 0.7 Ag^{-1}. The samples exhibited specific energy and power densities of 23.3 $Whkg^{-1}$ and 2334.3 Wkg^{-1}, respectively (Ahmed et al. 2018).

Na et al. (2018) in their unique study used a **broken eggshell** and **rice husks** to fabricate a novel egg white gel polymer electrolyte and green solid-state supercapacitor. It revealed that the specific capacitances decrease with increasing scan rate as expected. The sample exhibited good specific capacitance (214.3 Fg^{-1} at 0.2 Ag^{-1}) high flexibility and stable cycle performance.

Fu et al. (2019) obtained multi-hierarchical porous carbon from a typical food waste, **crab shell**.

The multi-hierarchical porous carbon exhibited a specific capacitance of 322.5 Fg^{-1} and 223.4 Fg^{-1} at current densities of 1 Ag^{-1} and 10 A g^{-1}, respectively. The same researchers reported that the crab shell-derived carbon/M-type hexagonal strontium ferrite ($SrFe_{12}O_{19}$) composites showed 94.5% capacitance retention over 10,000 cycles, exhibiting a specific capacitance of 690.4 Fg^{-1} at 1 Ag^{-1}, and 401.3 Fg^{-1} even at 10 A g^{-1} (Fu et al., 2019).

From the deep review of literatures, it was seen that there is a number of literatures regarding preparation of low cost AC from agricultural wastes and its application on capacitive behaviors. However, a significant results on the basis of present demand is still the matter of investigation. Hence, in this study, we tried to prepare AC from locally available agro-waste i.e., sawdust of *Shorea robusta* and well characterized by different techniques like XRD, FTIR, Raman, SEM, BET. Then it was electrochemically characterized in order to improve capacitive behaviors to get better supercapacitive behaviors.

CHAPTER –3

3. MATERIALS AND METHODS

This chapter dealt with the materials/reagents and methods used throughout the experiment. The methods of preparation of AC, hybrid composites, fabrication of AC electrodes, and hybrid composite electrodes were also described. Procedures adopted for their chemical and electrochemical characterization are also discussed.

3.1 Materials / Reagents used

3.1.1. Collection of splinters/sawdust of *Shorea robusta* (Sal)

Sawdust obtained from timber section of *Shorea robusta* tree were collected from local carpentry of Kathmandu valley, Nepal.

3.1.2. Phosphoric acid

Ortho phosphoric acid (85%H_3PO_4) has been purchased from Fischer Scientific, India and was used as an activating agent.

3.1.3. Double distilled water

Double distilled water has been used throughout the experiment.

3.1.4. Carbon black

Carbon black was purchased from Sigma-Aldrich (USA) and was used as conductor.

3.1.5. Polyvinylidine fluoride (PVDF)

PVDF was used as binder, which was obtained from Sigma-Aldrich (USA).

3.1.6. N-Methyl-2-pyrolidone (NMP)

NMP has been procured from Sigma-Aldrich (USA) and was used as dispersive agent to disperse PDVF.

3.1.7. Manganese dioxide (MnO_2)

MnO_2 was obtained from Wako Pure Chemical Industries Ltd. It was mixed with as prepared AC powder to prepare hybrid composite material.

3.1.8. Nickel foam

The three dimensionally porous, corrosion resistant and highly electrical conductor Ni-foam was obtained from PRED MATERIALS, International, USA. Ni-foam was used as electrode substrate and current collector.

3.2 Instrumentation

The following instruments were used in the entire experimental works.

3.2.1. Thermogravimetric analysis / Differential scanning colorimetry (TGA/DSC)

TGA/DSC of raw sawdust powder of *Shorea robusta* (Sal) was investigated by using "(DSC) (SDT Q600 V20.9 Build 20 USA)".

3.2.2. X-ray Diffractometer (XRD)

XRD analysis of as prepared carbon material was performed by using "RIGAKU Xray diffractometer, Japan".

3.2.3. Raman Spectroscopy

Defects of the carbon sample was investigated by Raman spectra using labRAM HR800 France, JOBIN YVON, Finland.

3.2.4. Scanning electron microscopy (SEM)

To record the surface morphology, SEM of as prepared carbon sample was performed by using "Mini SEM nanoeyes, Korea".

3.2.5. Fourier transform infrared spectroscopy (FTIR)

The surface functionality of as prepared AC was examined by Fourier Transform Infrared Spectroscopy using BRUKER- OPTIK GMBH, Germany, VERTEX 70/80, USA. The % of transmission of samples was recorded over 4000 to 400 cm^{-1}.

3.2.6. X-ray photoelectron spectroscopy (XPS)

The binding energy and oxidation states of the elements in the surface of the carbon sample was studied under "MultiLab 2000, Thermo Fischer, Scientific, USA system with an Al Kα source at 15 kV and. 200 W.

3.2.7. Brunauer-Emmett-Teller theory (BET)

The surface area of as prepared AC was measured by Brunauer–Emmett–Teller (BET) using Micromeritics ASAP 2020 system USA method.

3.2.8. Potentiostat/ Galvanostat

"Metrohm Autolab (PGSTAT 302 N) potentiostat/galvanostat" system was used to perform three electrochemical measurements techniques 1) potentiostatic cyclic voltammetry (CV), (2) galvanostatic charge/discharge (GCD) and (3) electrochemical impedance spectroscopy (EIS)

3.3. Methods

3.3.1. Preparation of sawdust powder

The collected splinters/sawdust of *Shorea robusta* was sun-dried for a few days. Then a few preliminary stages have been performed such as crushing, grinding and sieving through 150 µm sized sieve. Thus fine powder of sawdust was obtained and was used as a precursor for the preparation of AC.

3.3.2. Preparation of Activated Carbon

Based on the carbonization technique, AC has been prepared by two procedures.

3.3.2.1. Single-step carbonization procedure

In this case, carbonization has been done only for one time, after activation with the chemical agent, H_3PO_4 at 400°C in an inert atmosphere of N_2.

Details of procedure

The fine powder of precursor was impregnated chemically with H_3PO_4. The ratio of precursor to activating agent was 1:1 (w/w). They were left for 24 h at room temperature for proper soaking. After that, the impregnated sample was evaporated to dryness at 110°C for 2 h in an oven. Then it was inserted into the horizontal electric tubular furnace by using a steel boat and carbonized at 400°C for 3 h under the continuous N_2 flow of 100 mL/min. Then carbonized samples were cooled to room temperature maintaining inert atmosphere of nitrogen. The cooled sample was washed with hot distilled water for several times to dissolve impurities faster for removal and finally with double-distilled water till neutral pH. It was finally dried at 110°C. The dried sample was then grinded into fine powder and used for advanced characterization and electrochemical characterization. It was named as AC-(Sa-H_3PO_4).

Then, to optimize the carbonization temperature, carbonization has also been carried out at 500, 600 and 700°C separately for 3 h under the continuous N_2 flow of 100 mL/min. Further, to select better activating agent, other two activating agents KOH and Na_2CO_3 have also been tried, in addition to H_3PO_4, following same procedure of carbonization at 400°C for 3 h under the continuous N_2 flow of 100 mL/min.

3.3.2.2. Double-step carbonization procedure

In this case, carbonization has been done for two times; before and after activation with chemical agent, H_3PO_4. Here, sample was heated to 400°C for 1 h under the continuous N_2 flow of 100 mL/min. Then cooled and activated with H_3PO_4 (1:1) for overnight, then dried and again carbonized at 400°C for 1 h under the continuous N_2 flow of 100 mL/min.

Then again, to optimize the carbonization temperature, carbonization has also been carried out at 500, 600 and 700°C separately for 1 h before and after activation with H_3PO_4, under the continuous N_2 flow of 100 mL/min.

3.3.3. Preparation of hybrid composite

The hybrid-composites were prepared by mechanically mixing AC-(Sa-H_3PO_4) powder and MnO_2 in different mass ratios such as 1:1, 1:2 and 2:1. These hybrid composites are named as 1:1-(Sa-H_3PO_4:MnO_2), 1:2-(Sa-H_3PO_4:MnO_2) and 2:1-(Sa-H_3PO_4:MnO_2)-hybrid-composites respectively.

3.3.4. Fabrication of electrodes

3.3.4.1. Fabrication of Activated carbon electrode

Following procedure was applied for the fabrication of electrode:

3.3.4.2. Preparation of electrode substrate

At first, Ni-foam was taken and cut into small pieces having a size of 5 cm x 1cm, which is rectangular in shape. It is then used as electrode substrate.

3.3.4.3. Preparation of electrode material

Electrode material was prepared by grinding a mixture of 8 mg of as prepared AC-(Sa-H_3PO_4) powder, 1 mg of carbon black powder and 1 mg of PDVF in a mortar. Then 200 μL N-methyl pyroline (NMP) solution was added to the mixture in order to disperse PVDF. The mixture was again grinded thoroughly and thus slurry of electrode material was obtained.

3.3.4.4. Preparation of AC electrodes

A rectangular shaped Ni-foam was taken and 70 μL of slurry of carbon electrode material was applied on Ni-foam by covering only 1cm^2 area of it as shown in **Figure 15.**

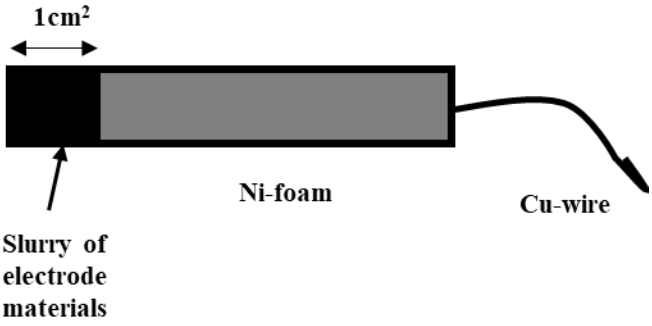

Figure 15: Preparation of Laboratory fabricated carbon electrode.

Then it was dried in an oven at 70°C for overnight. The electrical contact then has been made by using a cu-wire. Here, carbon black was used as conductor, PVDF as binder and Ni- foam as an electrode substrate and current collector.

Fabricated electrodes were then pressed at 10 kPa pressure for 1 min and soaked overnight in 6 M aqueous KOH solution prior to measurement.

3.3.5. Hybrid composite-electrodes

3.3.5.1. Preparation of hybrid electrode substrates

Hybrid electrode substrates have been prepared as described in **[section 3.3.4.2].**

3.3.5.2. Preparation of hybrid-composite-electrode material

Hybrid-composite-electrode materials were prepared by grinding a mixture of 4 mg of as prepared AC-(Sa-H_3PO_4), 4 mg of MnO_2 and 1 mg of carbon black and 1 mg of PVDF homogenously in a mortar. Then 200 μL N-Methyl-2-pyrolidone (NMP) solution was added to the mixture in order to disperse PVDF. The mixture was transferred into a micro tube and shaken for 48 h continuously.

3.3.5.3. Preparation of hybrid AC electrodes

A rectangular shaped Ni-foam (electrode substrate) was taken and 70 μL of slurry of hybrid composite electrode material was dropped on to Ni-foam of size 1cm^2 as shown in **Figure 15**. and dried in an oven at 70°C for overnight. Then a Cu-wire was connected at the bottom for electrical connection. Thus 1:1-(Sa-H_3PO_4:MnO_2)-HCE was fabricated. In the same way, 1:2 and 2:1 hybrid composite electrodes namely 1:2-(Sa-H_3PO_4:MnO_2)-HCE and 2:1-(Sa-H_3PO_4:MnO_2)-HCE were also fabricated by varying ratio of AC-(Sa-H_3PO_4) and MnO_2 respectively.

Fabricated hybrid-composite-electrodes were then pressed at 10 kPa pressure for 1 min and soaked overnight in 6 M aqueous KOH solution prior to measurement.

3.3.6. Manganese dioxide (MnO_2) electrode

3.3.6.1. Preparation of electrode substrates

Electrode substrates have been prepared as described in **section [section 3.3.4.2.].**

3.3.6.2. Preparation of MnO_2 electrode material

Manganese dioxide **(**MnO_2) electrode materials were prepared by grinding thoroughly a mixture of 8 mg of MnO_2 powder, 1 mg of carbon black and 1 mg of PVDF in a mortar. Then 200 μL NMP solution was added to the mixture to disperse PVDF. The mixture was transferred into a micro tube and shaken for 48 h continuously.

3.3.6.3. Preparation of Manganese dioxide (MnO_2)-electrode

Then the 70 μL mixture was dropped on Ni-foam of size $1cm^2$, and dried in an oven at 70^oC for overnight. Then a wire was connected at the bottom for electrical connection. Thus MnO_2-electrode was fabricated.

Fabricated MnO_2-electrodes were then pressed at 10 kPa pressure for 1 min and soaked overnight in 6 M aqueous KOH solution prior to measurement.

3.3.6.4. Preparation of electrochemical cell (Experimental setup)

The electrochemical properties of the phosphoric acid activated carbon electrode was tested in electrolyte of 6M KOH aqueous solution, using 3 electrode experimental set up, consisting of as prepared carbon electrode as working electrode, Pt-plate as counter electrode and Ag/AgCl as reference electrode. The cell was connected to “Metrohm Autolab (PGSTAT 302 N) potentiostat/galvanostat” system to perform the experiment under room temperature as shown in **Figure 16.**

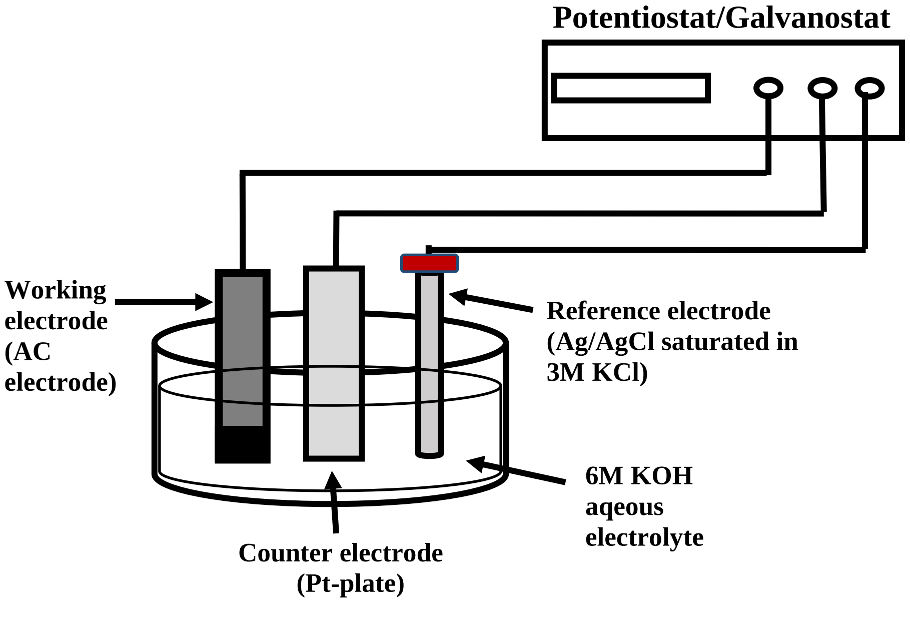

Figure 16: Three electrode experimental set

3.4. Characterization

3.4.1. Thermogravimetric analysis (TGA)/Differential Scanning Calorimetry

TGA/DSC experiment was carried out on TG/DSC instrument under nitrogen flow of 60 mL/min at heating rate of 100 °C/ min. About 10 mg of sample was placed in a vial which was present in the TGA/DSC analyzer. The vial was connected to sensors which detects the weight of the sample all times. The sample was heated from 50 to 900°.

3.4.2. X-ray Diffractometry

The phase state of as prepared sawdust derived AC (Sa-H_3PO_4) was examined by X-ray diffractometer which was operating at an accelerating voltage of 40 kV and current 40 mA with Cu-Kα radiation (λ=1.5418 Å) in the diffraction angles of 10 to 50 degrees.

3.4.3. Raman Spectroscopy

Raman scattering spectra of as prepared sawdust of *Shorea robusta* (Sa-H_3PO_4) derived AC were recorded on spectrometer has been used by using laser excitation at 514 nm and 0.06 mW power. The range of spectra obtained over Raman shift 1000-2000 cm^{-1}.

3.4.4. Fourier Transform Infrared Spectroscopy

FTIR spectra of as prepared AC (Sa-H_3PO_4) was recorded on spectrophotometer, over the wave number range 4000-400 cm^{-1} at 25 ºC.

3.4.5. X-ray Photoelectron Spectroscopy

The binding energy and oxidation states of the elements in the surface of the carbon sample was studied under “Multilab system with Al Kα source at 15 kV and 200 W.

3.4.6. Scanning Electron Microscope (SEM)

For SEM observation, samples were placed on a carbon tape and coated with gold in an ion coater prior to the measurements. SEM image was obtained at an accelerating voltage of 10 kV.

3.4.7. Nitrogen Adsorption-Desorption Isotherms/ Brunauer-Emmett-Teller theory (BET)

The Nitrogen adsorption-desorption isotherms were obtained at 77 K on Micromeritics ASAP 2020 system. For each measurement about 20 mg of AC was degassed for 24 h at 120 ºC prior to the measurement.

3.5. Electrochemical characterization

Three electrochemical measurements techniques 1) Potentiostatic Cyclic Voltammetry (CV), (2) Galvanostatic Charge/Discharge (GCD) and (3) Electrochemical Impedance Spectroscopy (EIS) were performed to test the electrochemical properties of as prepared AC-electrode. The electrochemical properties of the carbon-electrodes were tested in electrolyte of 6M KOH aqueous solution, using 3 electrode experimental set up, which consists of

i. Working electrode: As prepared carbon electrodes were used as working electrodes.
ii. Counter electrode: Platinum-plate was used as counter electrode.
iii. Reference electrode: Silver/silver chloride (Ag/AgCl) was used as reference electrode.

3.5.1. Cyclic Voltammetry

The Cyclic Voltammetric (CV) study was performed within a potential windows of (-1.0 to -0.2 V), ranging a scan rate of 2, 5, 10, 20, 50 and 100 mVs^{-1} using Nova 1.11 software.

3.5.2. Galvanostatic Charge–Discharge (GCD)

The Galvanostatic Charge–Discharge (GCD) testing was observed over the same potential window (-1.0 to -0.2 V) as the CV measurement at the current density ranges 1, 2, 3, 5, 10, 15 and 20 A g-1 using Nova 1.11 software.

3.5.3. Electrochemical Impedance Spectroscopy (EIS)

The Electrochemical Impedance Spectroscopy (EIS) was monitored over the frequency range 100 kHz to 0.1 Hz at the same potential range of CV and GCD. The equivalent circuits of the cells were evaluated using Nova 1.11 software.

The CV was measured within potential windows of -1.2 to 0 V, ranging a scan rate of 2, 5, 10, 20, 50 and 100 mVs^{-1}. The GCD testing was observed over the same potential window as the CV measurement at the current density ranges 1, 2, 3, 5, 10, 15 and 20 Ag^{-1}. The EIS was measured over the frequency range 100 kHz to 0.1 Hz at perturbation signal of 10 mV. The equivalent circuits of the cells were evaluated using Nova 1.11 software.

CHAPTER - 4

4. RESULTS AND DISCUSSION

The following materials have been prepared and characterized.

1. Raw sawdust powder: (Sa-Raw)
2. Activated carbon from raw sawdust powder: AC-(Sa-H_3PO_4)

(Sa-Raw) was analysed thermally by TGA/DSC and results are presented in **section 4.1.1.1.** Similarly AC-(Sa-H_3PO_4) was characterized by FTIR **[section 4.2.1.1]**, XPS **[section 4.2.1.2]**, XRD **[section 4.2.1.3]**, Raman **[section 4.2.1.4]**, SEM **[section 4.2.1.5]** and BET **[section 4.2.1.6]**

In order to investigate electrochemical supercapacitive performances, electrode from AC-(Sa-H_3PO_4) was prepared and named as (Sa-H_3PO_4)-electrode. Then electrochemical characterizations (a) CV, (b) GCD and (c) EIS were carried out to investigate the electrochemical performances; energy and power density, specific capacitance, cyclic stability and impedance and results of CV, GCD and EIS are presented in **[section 4.3.1, 4.3.2, 4.3.3, 4.3.4, 4.3.5, 4.3.6]**.

Then to improve electrochemical supercapacitive performances, hybrid composites were prepared by mixing AC-(Sa-H_3PO_4) and MnO_2 in 3 different ratios: 1:1, 1:2 and 2:1 which were used to prepare hybrid-composite electrodes (HCEs) namely,

1. 1:1-(Sa-H_3PO_4)-HCE
2. 1:2-(Sa-H_3PO_4)-HCE
3. 2:1-(Sa-H_3PO_4)-HCE

These electrodes were then electrochemically characterized by CV, GCD and EIS to investigate the electrochemical performances; energy and power density, specific capacitance, cyclic stability and impedance. The results of CV, GCD and EIS are presented in section **[section 4.4.1, 4.4.2, 4.4.3, 4.4.4, 4.4.5, 4.4.6].**

4. Results and Discussion

4.1. Raw sawdust powder (Sa-Raw)

Figure 17 shows the digital pictures of raw sawdust and sawdust powder.

Sawdust

Sawdust powder

Figure 17: Raw Sawdust and Sawdust Powder

4.1.1. Characterization of raw sawdust powder (Sa-Raw)

4.1.1.1. Thermo Gravimetric Analysis (TGA) / Differential Scanning Calorimetry (DSC) of raw sawdust powder (Sa-Raw)/precursor

TGA/DSC measurement was carried out to understand the pyrolytic behavior of the sawdust powder/precursor. Thermal decomposition behavior of raw saw dust powder (Sa-Raw) was displayed by TG curve which is shown in **Figure 18**. Three different phases could be seen in **Figure 18**.

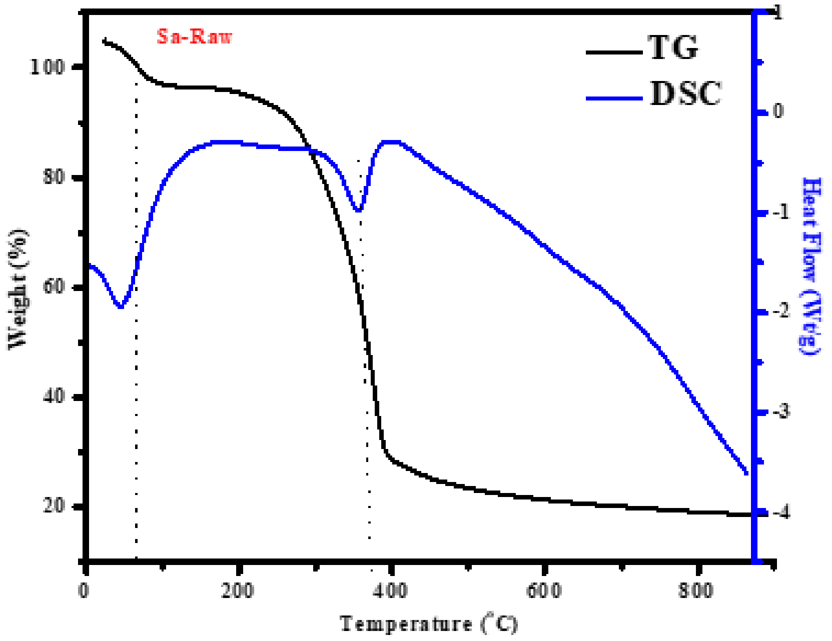

Figure 18: TGA/DSC curves of raw sawdust powder (Sa-Raw)

1. The first phase is at around 60 to 100 °C. This phase shows the slight loss of weight, which is probably due to desorption of residual moisture. It was further confirmed by a sharp endothermic peak of DSC curve at 100 °C.
2. The second phase is at around 200 to 300 °C. It demonstrates the reduction of weight. It may be due to decomposition of hemicellulose to CO_2 which might be caused by cracking and abscission of carboxyl group (C=O) and COOH (Yang et. al. 2007).
3. The third phase could be seen at around 300-400 °C in TG curve. This is attributed to the decomposition of cellulose/lignin into carboxyl, lactone, and carbonyl (Mohamed et al., 2015). It may be due to the desorption of CO_2 and CO by converting cellulose into volatile organic matters present in powder of *Shorea robusta*. This could also be seen in endothermic peak of DSC curve at 390 °C. Above 400 °C, no significant weight loss occurred which illustrates the completion of carbonization process (Shrestha et. al., 2019 a). Hence, in this study, 400 °C temperature has been used to carbonize sawdust powder. Similar carbonization temperature has also been reported by Wang et al. (Wang et al., 2012).

4.2. Activated carbon (AC)

Figure 19 shows the digital picture of as prepared AC-(Sa-H_3PO_4).

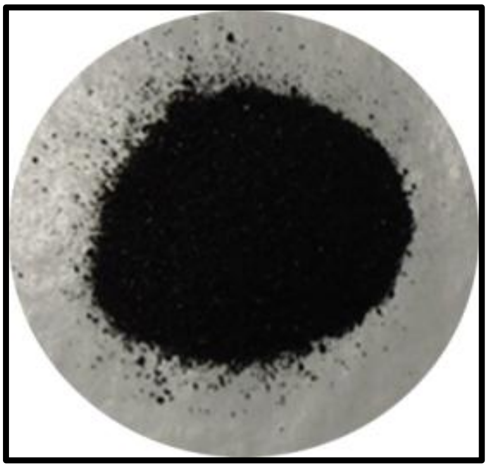

Figure 19: As prepared AC-(Sa-H_3PO_4).

4.2.1. Characterization of AC-(Sa-H_3PO_4)

4.2.1.1. Fourier transform infra-red (FTIR) analysis

The FTIR spectra of raw sawdust powder (Sa-Raw) and AC-(Sa-H_3PO_4) are shown in **Figure 20.**

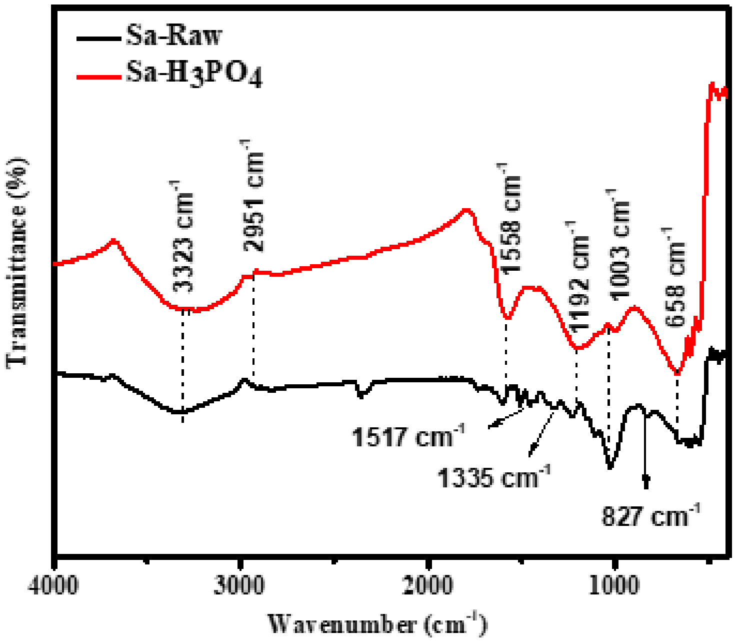

Figure 20: FTIR spectra of AC-(Sa-H_3PO_4) with raw sawdust powder (Sa-Raw)

As can be seen in the **Figure 20**, all spectra show a strong wide adsorption band at around 3323 cm^{-1}. The position of the band is characteristics of the stretching vibration of hydroxyl groups of carboxyl, phenol, alcohol. Such –OH band can also be correlated with adsorbed water present in raw sample as indicated by TG/DSC analysis, where, at around 100 °C, weight loss was clearly seen indicating the evaporation of water molecules. The band at around 2951 cm^{-1} is assigned to assymetric and symmetric C-H bands present in alkyl groups such as methyl and methylene groups. The band at around 1558 cm^{-1} is due to olefinic C=C vibrations in aromatic rings. The band at around 1192 cm^{-1} is due to asymmetric stretching of -C-O bond in acids, alcohols, phenols, ethers and esters. The band at around 658 cm^{-1} is attributed to C-C stretching in fingerprint region.

Similarly, in case of AC-(Sa-H_3PO_4), the band at around 3323 cm^{-1} was obviously due to –OH functional group which was found to be enriched in comparison to raw sample. It clearly pointed out for the functionalization occurred in raw sample after H_3PO_4 activation and carbonization (Shrestha et. al., 2019 a). The other band at around 1558 and 1192 cm^{-1} was also seemed to be enhanced in comparison to raw sample (Sa-Raw). It also indicates for the enhanced surface functionality occurred in raw sample. This might be due to the breakdown of cellulose into carboxyl, lactone and lacto groups (Cadenas-Perez et al. 2003).The band at around 1003 cm^{-1} was drastically reduced. This is due to the decomposition of the organic matter in sawdust and breakage of bonds. After the activation with H_3PO_4, some phosphate compounds might remain on the activated carbon surface. These results are in good agreement with the findings of many investigators (Shi, et al., 2014). The FTIR results clearly expressed that the as prepared AC-(Sa-H_3PO_4) was fully functionalized with oxygen containing functional groups such as carboxylic, phenolic, lactonic, ether groups by the use of activating agent.

4.2.1.2. X-ray photoelectron spectroscopy (XPS)

Chemical structure of as prepared AC-(Sa-H_3PO_4) was investigated by XPS.

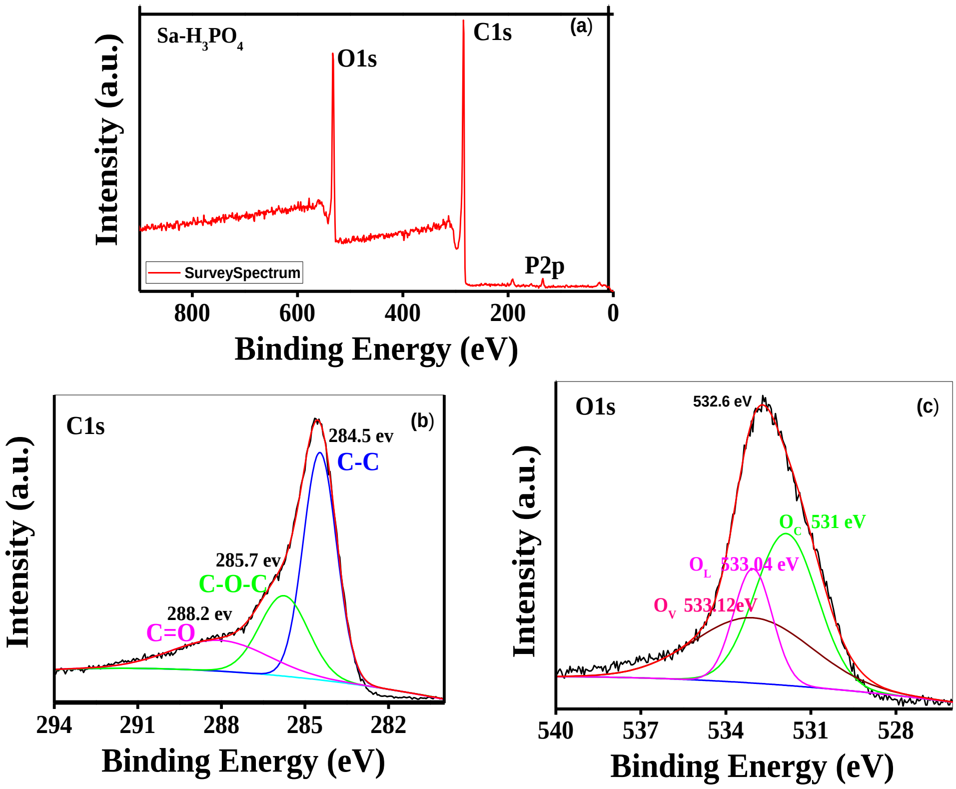

Figure 21: XPS spectra of AC-(Sa-H_3PO_4)

Figure 21 (a) depicts the XPS survey spectrum of AC-(Sa-H_3PO_4), showing the presence of carbon, oxygen. **Figure 21 (b)** shows high-resolution XPS spectra of C1s excitation having a broad peak which was deconvoluted into three peaks at binding energy (BE) 284.5 eV for C-C which is of pure or unfuntionalized carbon, 285.7 eV for ether and alcohol (R-O-R/ -OH) and 288.2 eV for ketone and aldehyde (C=O/ -CHO). Similarly, a broad peak at 532.6 eV for O1s could be seen in **Figure 21 (c)**, indicating the presence of different chemical states of oxygen. The three deconvoluted peaks for oxygen (O1s) at 531 eV for phosphatic oxygen (PO_4^{3-}), 533.04 eV for hydroxyl group (-OH) and 533.12 eV for silicon dioxide (SiO_2). The broad peak at 531 eV and 533.04 eV indicate the overlap of hydroxide and phosphate functional group. From **Figure 21 (b)** and **(c)**, it is confirmed that as prepared AC-(Sa-H_3PO_4) was well functionalized after H_3PO_4 activation and consists of more acidic functional groups as aldehydes/ketones, ethers, hydroxides (Shrestha et. al., 2019 a). Likewise, The oxygenated functional groups can also be seen in **Figure 20**, where one can see the high intensity spectra for hydroxyl (-OH), aldehyde/ketone (-CHO/C=O) and ether (C-O-C) functional groups. The results revealed that after carbonization and activation, breakdown of cellulose, hemicellulose and lignin occurs and cross linking of H_3PO_4 as well and functionalization occurred as a consequence (Shrestha et. al., 2019 a). There is a presence of C, O are obvious in XPS spectra.

4.2.1.3. X-ray diffraction (XRD) measurement

XRD was used to investigate the phase state of carbon sample.

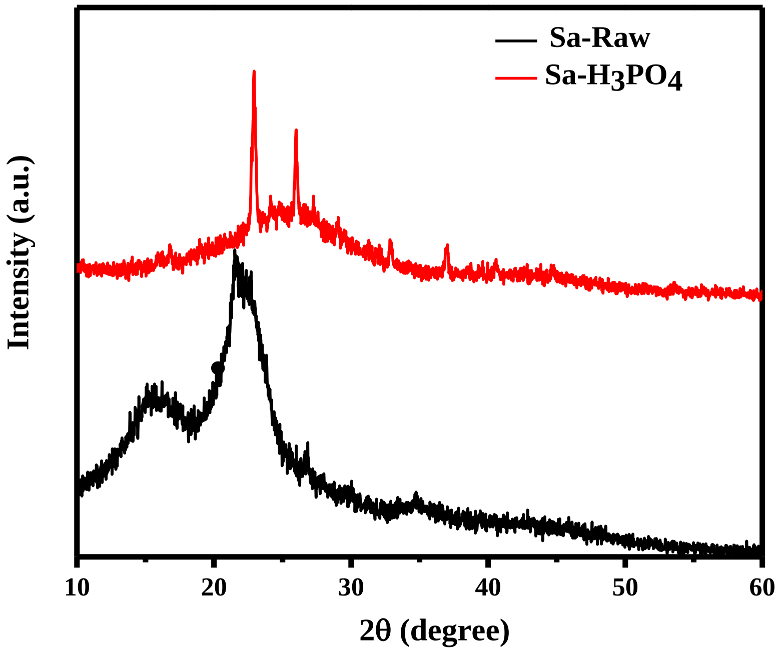

Figure 22: XRD pattern of AC-(Sa-H_3PO_4)

Figure 22 represents the XRD profiles for AC-(Sa-H_3PO_4) and raw sawdust powder (Sa-Raw) There are two broad peaks at around 16° and 22°, which are attributed to the reflection from the (002) and (100) planes respectively (Shrestha et. al., 2019 a). The (002) peak indicates stacking structure of aromatic layers of cellulose, while the (100) peak indicates the structure formed by sp^2 hybridised carbon (Puziy et al., 2003). But in the case of AC-(Sa-H_3PO_4), those two sharp peaks completely disappeared. But another broad peak was seen at around 26, 2θ degrees corresponding to (002), suggesting the disordered structure of layer. The broad peaks also indicated for the amorphous nature of carbon (Wang et al., 2013). No any other sharp peaks were observed which indicates the absence of degree of graphitization (Molina-Sabio et al., 1995). However, some insignificant peaks could be seen, that may be due to presence of some impurities or moisture associated with the sample.

4.2.1.4. Raman spectra analysis

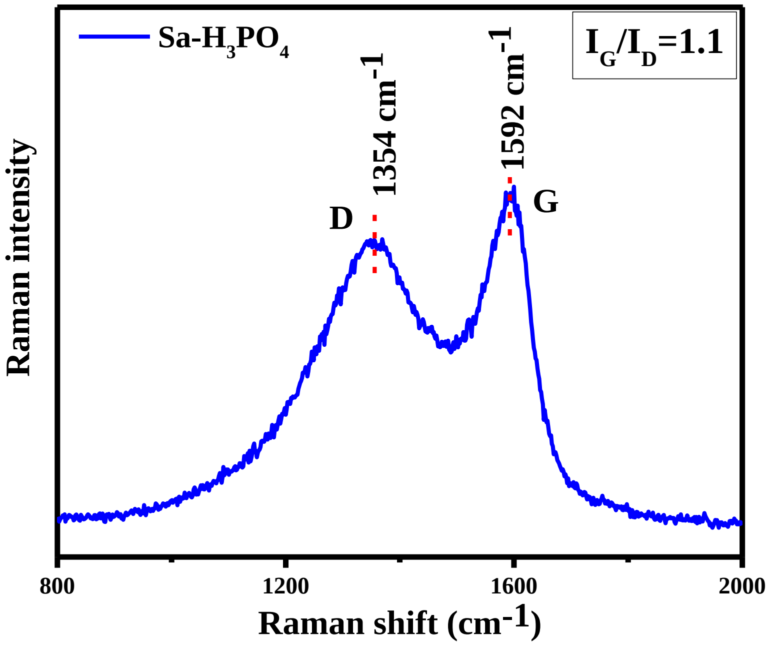

Figure 23: Raman spectra of AC-(Sa-H_3PO_4).

Figure 23 represents the Raman spectra of AC-(Sa-H_3PO_4). In **Figure 23**, two relatively sharp peaks are clearly seen at 1592 cm^{-1} and 1354 cm^{-1} which is assigned for G and D band respectively. The relative intensity ratio of D band to G band was found to be approximately 1, which indicates the irregularity in lattice space or a disordered carbon structure (Shrestha et. al., 2019 a). Hence, the amorphous nature of carbon as shown by XRD was further confirmed by Raman spectra.

4.2.1.5. Scanning electron microscope (SEM) analysis

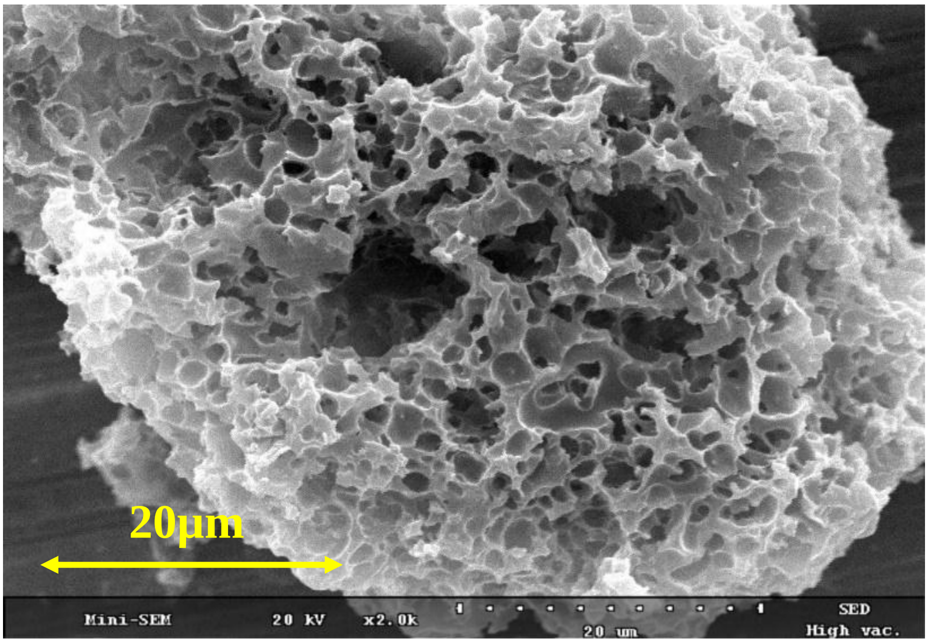

Sa-H_3PO_4

Figure 24: SEM image of AC-(Sa-H_3PO_4)

Figure 24 illustrates the SEM micrographs of AC-(Sa-H_3PO_4) at the magnification of 20 µm. It exhibited honeycomb like internal structure with well-developed pores. The pore development on the surfaces of the AC-(Sa-H_3PO_4) might be due to process of dehydration of H_3PO_4 (Shrestha et. al., 2019 a), and then react with oxygen to generate phosphoric anhydride (P_2O_5). Here, P_2O_5 sublimated from solid to gas at 360 °C and then gaseous P_2O_5 escaped from the surface of the AC creating pores (Sarkar et. al., 2015). In addition to this, during washing process, remaining P_2O_5 get hydrolysed and removed, creating vacant space or pores. Pores may be micro and mesopores with a volume corresponds to that of the removed phosphoric acid (Tawfik & Gaddafi, 2016), (Xie et al., 2018).

4.2.1.6. N_2 Adsorption/desorption isotherm/Brunauer-Emmett-Teller theory (BET)

The N_2 adsorption/desorption isotherms of AC-(Sa-H_3PO_4) at 77 K is shown in **Figure 25**.

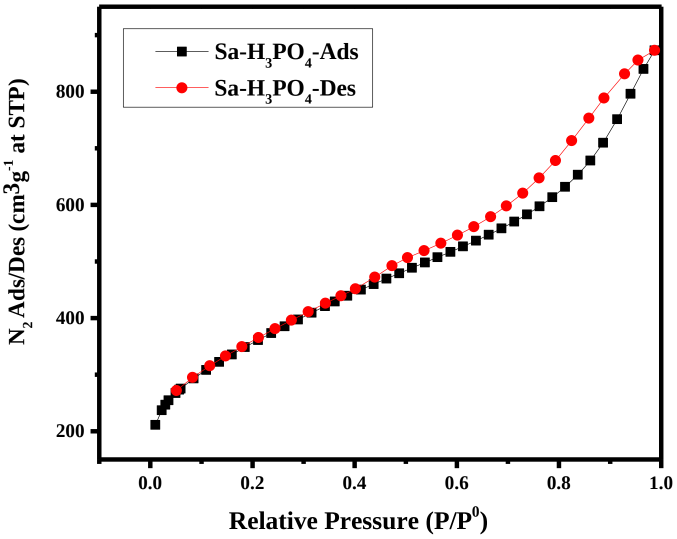

Figure 25: N_2 adsorption/desorption isotherm at 77 K of AC-(Sa-H_3PO_4)

In **Figure 25**, **Type II H_3** isotherm could be seen. At relatively lower pressure ($P/P^0 < 0.1$), the isotherms showed a minor uptake of nitrogen signifying the presence of a few micropores in AC-(Sa-H_3PO_4). However, at around $P/P^0 = 0.4$, the amount of nitrogen uptake has increased significantly showing hysteresis loop during adsorption and desorption of nitrogen. The adsorption volume of AC-(Sa-H_3PO_4) increased with the relative pressure until $P/P^0 \cong 0.6$. The slight hysteresis loops at the relative pressure of 0.6 to 1.0 indicated the presence of a considerable amount of mesopores having cylindrical shaped pores, where delayed capillary condensation occurred during N_2 adsorption/ desorption process. From the isotherm, it revealed that AC sample consists of a large amount of mesoporores, along with some micropores (Kondrat et al., 2012). Such pores could also be seen in SEM image (**Figure 24**).

Table 1: Surface area obtained after (i) single-step carbonization of AC-(Sa-Na_2CO_3), AC-(Sa-KOH), AC-(Sa-H_3PO_4) samples at 400°C and AC-(Sa-H_3PO_4)-5 sample at 500 °C, (ii) double step carbonization of AC-(Sa-H_3PO_4) 4-4 sample at 400 °C before and after activation, AC-(Sa-H_3PO_4) 5-5 sample at 500 °C before and after activation

S. No	Sample	Carbonization temperature (°C)	BET Surface Area (m^2g^{-1})
(i)	**Single step carbonization**		
1	AC-(Sa-Na_2CO_3)	400	58.9
2	AC-(Sa-KOH)	400	280.5
3	AC-(Sa-H_3PO_4)	400	1270.0
4	AC-(Sa-H_3PO_4)-5	500	1020.7
(ii)	**Double step carbonization**		
5	AC-(Sa-H_3PO_4) 4-4	400-400	967.5
6	AC-(Sa-H_3PO_4) 5-5	500-500	791.3

The BET specific surface area of AC-(Sa-H_3PO_4), AC-(Sa-KOH) and AC-(Sa-Na_2CO_3) in single-step carbonization procedure at 400°C and BET specific surface area of AC-(Sa-H_3PO_4)-5 at 500°C have been measured and results are given in Table 1. Similarly, Results revealed that, BET surface area was found to be lowest of 59 m^2g^{-1} from single-step carbonized Na_2CO_3 activated sample i.e. AC-(Sa-Na_2CO_3**)**. Then the second lower surface area was found to be 280 m^2g^{-1} for KOH activated carbon i.e. AC-(Sa-KOH). The highest BET surface area was found to be 1270 m^2g^{-1} for H_3PO_4 activated carbon i.e. AC-(Sa-H_3PO_4) (Shrestha et. al., 2019 a). This might be due to the fact that 400°C is insufficient carbonization temperature for both Na_2CO_3 and KOH activated samples as reported in literatures (Hussaro, 2014; Rwayhah et al., 2017; Yahya et. al. 2018). The Bet surface area obtained at 400°C for AC-(Sa-H_3PO_4) is found to be still higher than the sample carbonized at 500°C (1020 m^2g^{-1}). This might be due to the deterioration and destruction of wall between the adjacent mesopores at higher temperature of 500°C.

As can be seen in **Table 1,** Bet surface area was found to be still lower in double-step carbonized H_3PO_4 activated samples; [AC-(Sa-H_3PO_4) 4-4] and [AC-(Sa-H_3PO_4) 5-5]. It was found to have 967 m^2g^{-1} at 400°C before activation and after activation with H_3PO_4 at 400°C [AC-(Sa-H_3PO_4) 4-4]. The Bet surface area was found to be even lesser (791 m^2g^{-1}) in double-step carbonization at 500°C [AC-(Sa-H_3PO_4) 5-5]. This might be due to shrinkage of pores when heated to 400°C or 500°C before activation. After activation, further heat treatment may lead to breakdown of walls of pores to some extent.

In H_3PO_4 activated carbon i.e. AC-(Sa-H_3PO_4), it was observed that at temperature >500°C, more than 75% of the mass of precursor was converted into ash. Hence high temperature was found to be unfavorable to prepare H_3PO_4 activated carbon. While for preparing AC using activating agents KOH and Na_2CO_3, 400°C temperature was not sufficient and high temperature above 800 °C was required, as reported in literatures (Hussaro, 2014; Rwayhah et al., 2017; Yahya et. al. 2018).

The further pore size and pore volume of AC-(Sa-H_3PO_4) was calculated and are shown in **Table 2.** Porosity was also correlated with SEM images (**Figure 24** where honey comb like structure was obvious. Again, the reason may be due to escape of P_2O_5 during carbonization and washing steps, creating pores. At that time, oxidation of carbon was no more restrained. This is the reason why activated carbon has the largest BET surface area (Twafik & Gaddafi, 2016).

Table 2: BET specific surface area, pore size and pore volume of AC-(Sa-H_3PO_4)

Electrode	**Specific Surface Area (m^2g^{-1})**	**Pore size (BJH Ads) (nm)**	**Pore Volume (BJH Ads) (cm^3g^{-1})**
Sa-H_3PO_4	1270	5.1	1.1

Further electrochemical characterization have been carried out for AC-(Sa-H_3PO_4), AC-(Sa-KOH) and AC-(Sa-Na_2CO_3) by fabricating electrodes of each and supercapacitive performances like CV, GCD and EIS were evaluated by using three-electrode-system in aqueous 6M KOH. The specific capacitance acquired from GCD at $1Ag^{-1}$ were 136.3 Fg^{-1}, 42.2 Fg^{-1} and 59.1 Fg^{-1} for the electrode samples (Sa-H_3PO_4)-electrode, (Sa-KOH)-electrode and (Sa-Na_2CO_3)-electrode respectively. The energy density of (Sa-H_3PO_4)-electrode was found to be 3.0 $Whkg^{-1}$ at power density of 100.5 Wkg^{-1}. While, (Sa-KOH)-electrode showed 0.8 $Whkg^{-1}$ at power density of

95.2 Wkg^{-1}, and (Sa-Na_2CO_3)-electrode exhibited 1.8 Whkg^{-1} at power density of 95.1 Wkg^{-1}. Moreover, it also displayed imposing cycling life stability of about 97.5 %, 89.4% and 78.4 % after 1000 cycles of charge/discharge for the electrode samples (Sa-H_3PO_4)-electrode, (Sa-KOH)-electrode and (Sa-Na_2CO_3)-electrode respectively. The EIS result from Nyquist plot showed the lowest internal resistance of about 0.4 Ω for (Sa-H_3PO_4)-electrode, 0.5 Ω for (Sa-KOH)-electrode and 0.6 Ω (Sa-Na_2CO_3)-electrode, indicating that, (Sa-H_3PO_4)-electrode has still lower resistance than other two carbon electrodes namely (Sa-KOH)-electrode and (Sa-Na_2CO_3)-electrode (Shrestha et. al., 2019 b). The overall electrochemical performance of (Sa-H_3PO_4)-electrode showed outstanding capacitive behavior. Hence further work has been done on (Sa-H_3PO_4)-electrode only.

4.3. Electrochemical characterization of (Sa-H_3PO_4)-electrode: Supercapacitive performance

4.3.1. Cyclic Voltammetric study on (Sa-H_3PO_4)-electrode

From cyclic voltammetry (CV), current was measured against fixed potential window and scan rate to find optimum potential window.

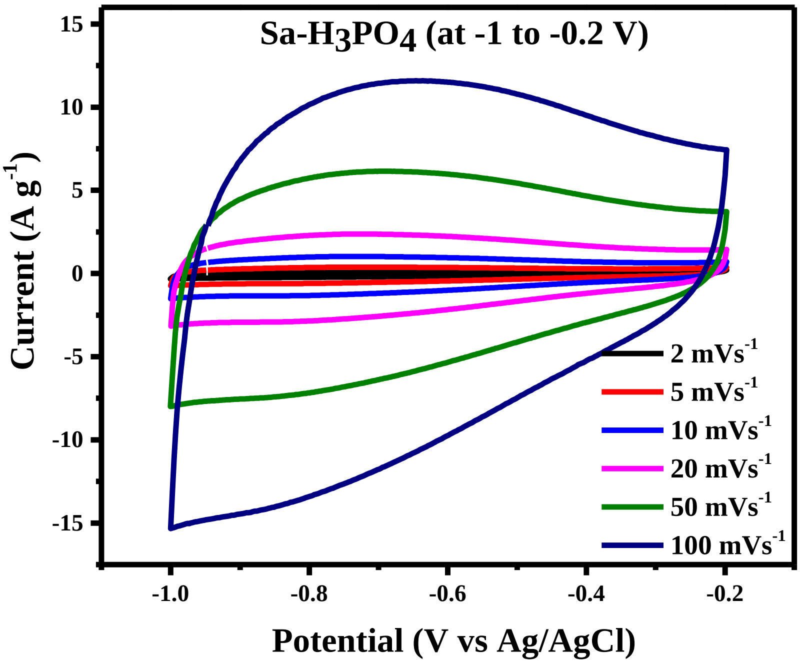

Figure 26: CV measurement of (Sa-H_3PO_4)-electrode at potential window (-1 to -0.2 V)

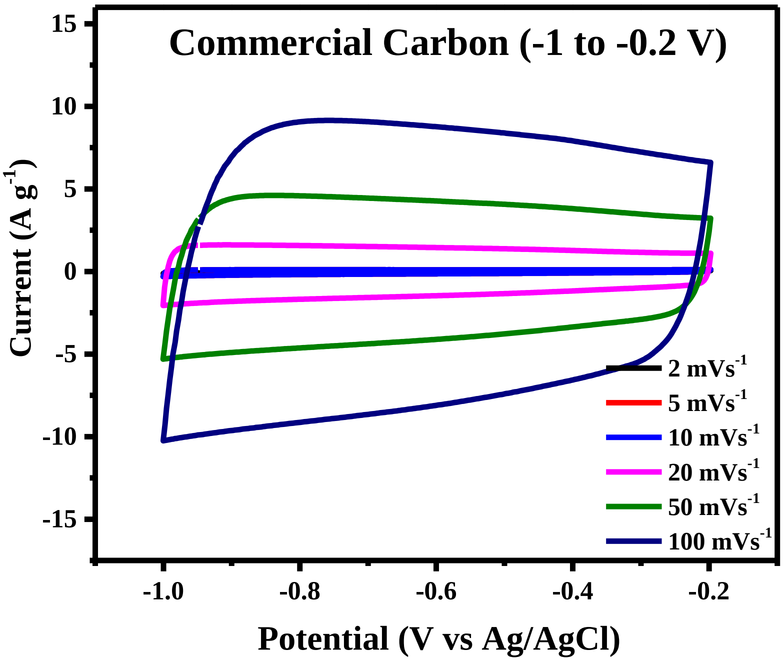

Figure 27: CV measurement of commercial-carbon-electrode at potential window (-1 to -0.2 V)

Figure 26 and 27 show the cyclic voltammogram of the as prepared (Sa-H_3PO_4)-electrode and commercial-carbon-electrode at different scanning rates of 2 mVs^{-1}, 5 mVs^{-1}, 10 mVs^{-1}, 20 mVs^{-1}, 50 mVs^{-1} and 100 mVs^{-1} using the potential window range -1 to -0.2 V in 6M KOH electrolyte (Shrestha et. al., 2019 a). These curves are nearly rectangular in shape, which is the characteristic of a double layer capacitor. The absence of any redox peaks is in agreement with FT-IR results, and interestingly, the shape of the CV curves was retained even at higher scan rates, suggesting high-rate performance of the (Sa-H_3PO_4)-electrode. At high scan rate of 100 mVs^{-1}, the curve was almost rectangular behaving similar to an ideal capacitor with no significant redox peak. Such performance even at a high scan rate may be due to porous structure and was expected for easy and smooth transportation of electrolyte ions. The charge-storage mechanism for (Sa-H_3PO_4)-electrode seems to be electrochemical double layer, as no redox peaks were observed in the CV curves. Such behavior is in agreement with the results reported by other scientists in other carbonized bio-mass (Guo et al., 2014). In electrochemical double layer charge storage mechanism, the electrolyte ions are reversibly adsorbing and desorbing inside the pores of (Sa-H_3PO_4)-electrode. From such process, higher surface area and energy storage capacity would be expected. Since in electrochemical double layer charge-storage mechanism, only adsorption and desorption took place, there is no chemical reaction or redox process involved, hence, the stability occurs and thus the better performance could be expected (Zequine et al., 2017). As can be seen in **Figure 26**, the current density was found to be about 13 Ag^{-1} which is significantly high.

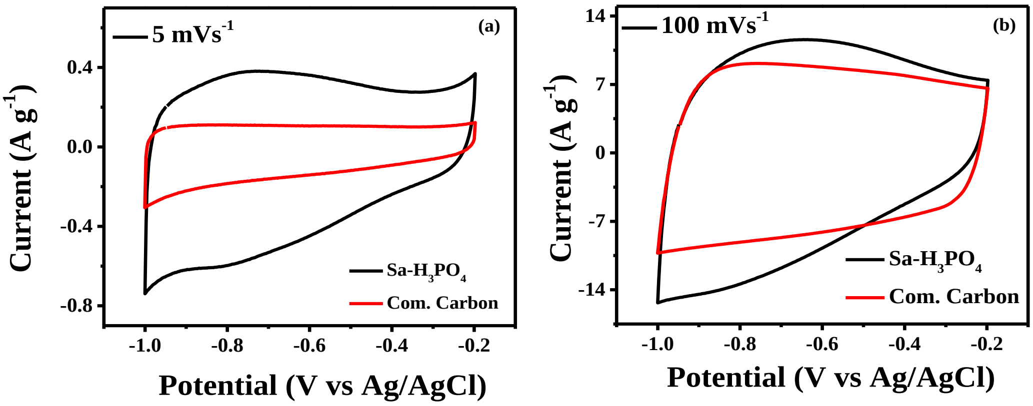

Figure 28: Comparative study of CV of (Sa-H_3PO_4)-electrode and commercial-carbon-electrode at **(a)** low scan rate of 5 mVs^{-1} and **(b)** high scan rate of 100 mVs^{-1}

Again, CV curves of as prepared (Sa-H_3PO_4)-electrode was compared with commercial carbon electrode at low scan rate of 5mVs^{-1} and high scan rate of 100 mVs^{-1} (Shrestha et. al., 2019 a). In both cases, the current density were found to be higher in **Figure 28 (a)** (Sa-H_3PO_4)-electrode, **Figure 28 (b)** than commercial-carbon-electrode. This revealed that, as prepared (Sa-H_3PO_4)-electrode exhibited better electrochemical performance than commercial-carbon-electrode.

4.3.2. Galvanostatic charge/discharge (GCD): time duration study on (Sa-H_3PO_4)-electrode

The potential application of as prepared AC-(Sa-H_3PO_4) as an electrode material for supercapacitor applications, was further investigated using galvanostatic charge-discharge measurements. It was operated at the same potential window range as CV (**Figure 29)** i.e. (-1 to -0.2 V), with different current densities of 1 A g^{-1}, 2 A g^{-1}, 3 A g^{-1}, 5 A g^{-1}, 10 A g^{-1}, 15 A g^{-1} and 20 A g^{-1}. It was found that the charge/discharge time duration for (Sa-H_3PO_4)-electrode decreased with increased in current density (Shrestha et. al., 2019 a). The potential versus time curves at various current densities were found to be triangular in shape and symmetrical in nature as well. Such a shape and nature were retained even at higher current densities, suggesting a high-rate performance. Small deviation (non-symmetrical) charge-discharge characteristics at low current density could be due to different rates of adsorption and desorption of electrolyte. It seems that desorption of electrolyte (discharge) is a lower process.

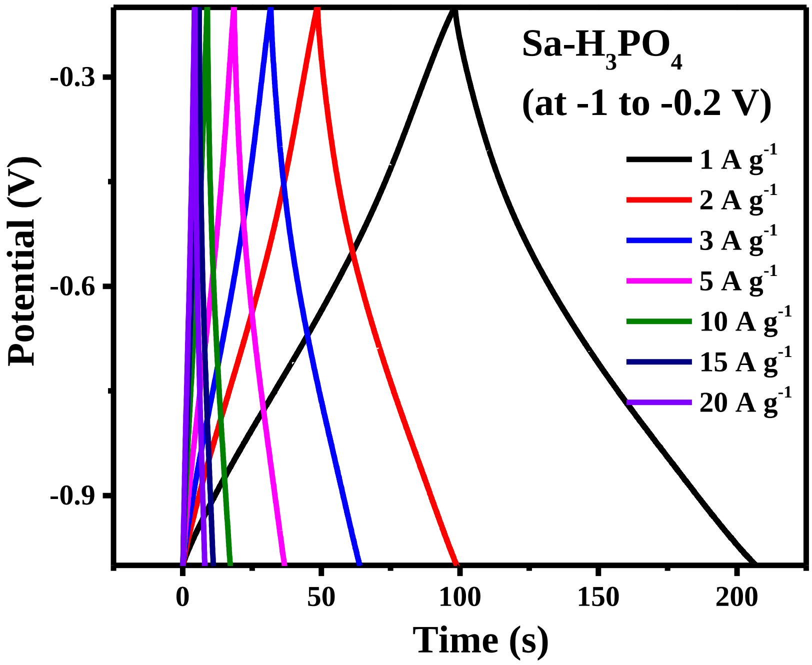

Figure 29: GCD measurement of ($Sa-H_3PO_4$)-electrode

In potential vs time curve, both charge/discharge curves, that both charge/discharge lines are straight making triangular in shape, which confirms the presence of EDLC behavior. It was also an indication of having low impurities and proper insertion between AC and electrolyte ions (Gomez & Kalu, 2013) inside the electrode material. Again it could be interconnected with high specific capacitance of ($Sa-H_3PO_4$)-electrode and high surface area as well. From the plots, we calculated the Specific capacitance (**C_S**) of ($Sa-H_3PO_4$)-electrode and commercial carbon electrode using the formula given **equation number (9).**

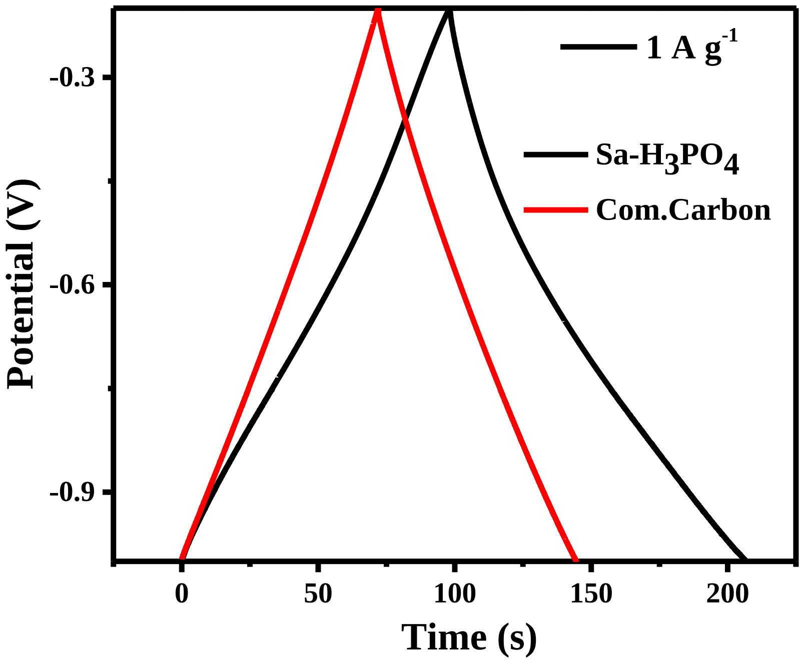

Figure 30: Comparative charge discharge curves of (Sa-H_3PO_4)-electrode and commercial-carbon-electrode at 1 A g^{-1} current density

Figure 30 shows the comparative charge discharge curves of (Sa-H_3PO_4)-electrode and commercial-carbon-electrode at 1 A g^{-1} current density. One can see the equivalent and triangular shape charge discharge curves. Here, the discharge duration was found to be 140 sec for commercial carbon while 230 sec for (Sa-H_3PO_4)-electrode. The duration of discharging time was found to be significantly longer in (Sa-H_3PO_4)-electrode (**Figure 30**). The Specific capacitance was also calculated which was found to be higher i.e.136.34 Fg^{-1} for (Sa-H_3PO_4)-electrode (Shrestha et. al., 2019 a) in comparison to commercial carbon electrode i.e. 91.68 Fg^{-1}, which are tabulated in **Table 3**. This is another evidence for better electrochemical performance of as prepared (Sa-H_3PO_4)-electrode than commercial carbon electrode.

Table 3: Charge/discharge time duration and specific capacitance

Electrodes	**Time duration of charge/discharge (sec)**	**Specific capacitance (Fg^{-1})**
(Sa-H_3PO_4)-electrode	230	136.3
Commercial carbon electrode	140	91.6

4.3.3. Energy density and power density of (Sa-H_3PO_4)-electrode

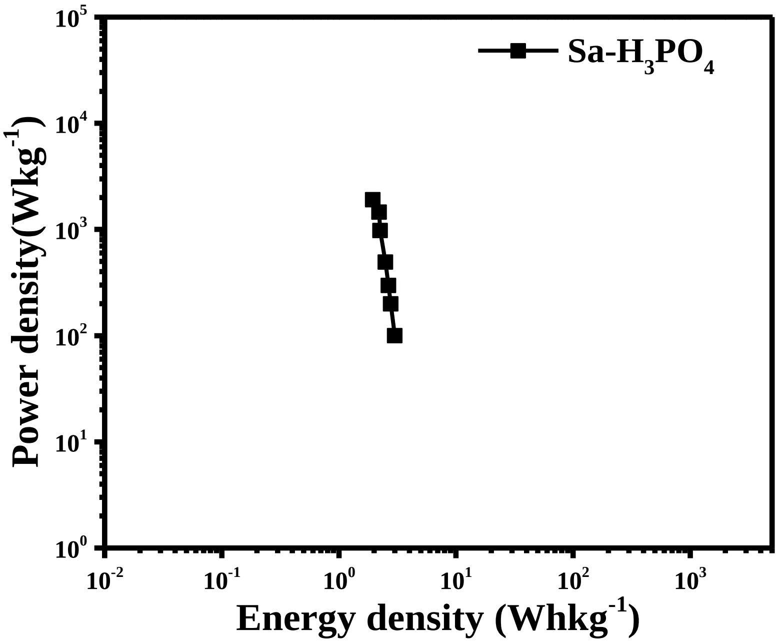

Figure 31: Ragone plot of (Sa-H_3PO_4)-electrode

Figure 31 shows the well-known Ragone plot determined from galvanostatic charge-discharge measurements. Energy density and Power density were calculated by using the formula given in **equation number (10) and (11).** In this study, since three electrode set up was used to measure electrochemical performances, the energy density should be calculated, dividing by 8 instead of 2, as per the rule of three electrode system. Hence, energy density has been calculated by using the formula $\mathbf{E = \frac{1}{8} C_{SP} \Delta v^2.}$ The results revealed that (Sa-H_3PO_4)-electrode showed the higher energy density of 12.03 Whkg^{-1} at a power density of 398.46 Wkg^{-1} (Shrestha et. al., 2019 a) than other reported values of energy density such as 5.3 Whkg^{-1} for the carbonized corncob in an alkaline medium (Qu et al., 2015), 4.8 Whkg^{-1} for KOH activated sunflower seed, (Li X, et al., 2011).

4.3.4. Specific capacitance studies on (Sa-H_3PO_4)-electrode

The specific capacitance (C_S) of carbon electrodes was calculated using **equation (9).** The specific capacitance value of as prepared (Sa-H_3PO_4)-electrode was found to be 136.34 Fg^{-1} (Shrestha et. al., 2019 a), which is even higher than commercial activated carbon (91.69 Fg^{-1}). In case of electrode materials for electrochemical capacitors, well-developed surface area significantly affects the growth of capacitance, by forming the electrical double layer at the electrode/electrolyte interface. However, the size and shape of the pores affect the transport of ions, hence the contribution of mesopores is necessary in order to receive good charge propagation (Ilona Acznik et al., 2014).

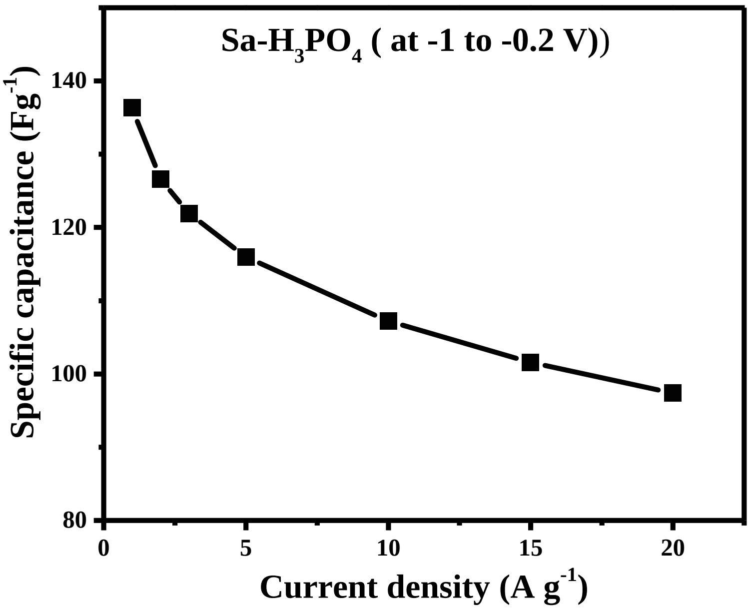

Figure 32: Specific capacitance of (Sa-H_3PO_4)-electrode as a function of current density

Figure 32 shows the plot of specific capacitances of (Sa-H_3PO_4)-electrode as a function of current density. The curve shows that there was a sharp decrease of specific capacitance with increase in current density up to 5 Ag^{-1}. Then after 5 Ag^{-1} specific capacitance was found to be approximately constant. As seen in **Figure 32**, decrease in the specific capacitance with increasing current density could be due to the diffusion limited process. At higher current density, the electrolyte ions do not get sufficient time for the diffusion into the inner pores and thus provides lower capacitance) (Shi et al., 2014). Qian *et al.* have also observed sharp decrease in specific capacitance with increase in discharge current density for the activated carbon produced from human hair.

The specific capacitance of (Sa-H_3PO_4)-electrode yielded a value of 136.3 Fg^{-1} at 1 A g^{-1} and kept a value of 127 Fg^{-1} at 2 A g^{-1}, 122 Fg^{-1} at 3 A g^{-1}, 116 Fg^{-1} at 5 A g^{-1}, 107 Fg^{-1} at 10 A g^{-1}, 102 Fg^{-1} at 15 A g^{-1} and 97 Fg^{-1}at 20 A g^{-1} which are tabulated in **Table 4**.

Table 4: Specific Capacitance from GCD at different Current Densities

AC- electrode	**Current densities ($A\ g^{-1}$)**	**Specific capacitance (C_S) (Fg^{-1})**
($Sa-H_3PO_4$)-electrode	1	136.3
	2	127
	3	122
	5	116
	10	107
	15	102
	20	97

4.3.5. Life cycle assessment (% retention capacity) of ($Sa-H_3PO_4$)-electrode

The stability of the as prepared ($Sa-H_3PO_4$)-electrode was investigated by % retention capacity. In this study, 1000 continuous charge/discharge cycle was applied at a current density of 3 A g^{-1}.

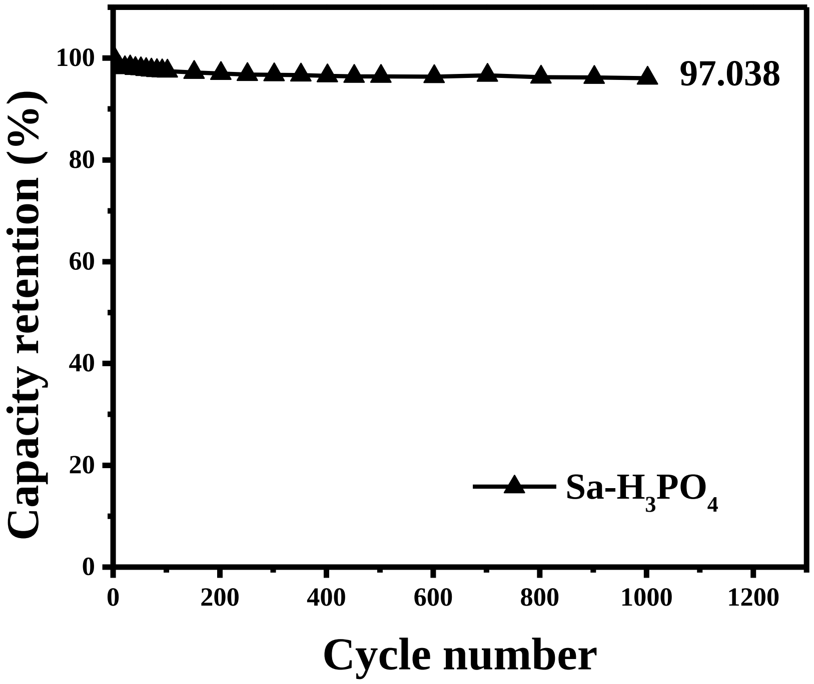

Figure 33: Life cycle assessment of ($Sa-H_3PO_4$)-electrode

As can be seen in **Figure 33** the retention capacity remains very high of 97%. Nearly 3 % of electroactive material got decomposed into electrolyte and sustained (1000) prolonged cycles without significant degradation. This revealed that, as prepared (Sa-H_3PO_4)-electrode has excellent cyclic stability and it is well fitted for supercapacitor application.

4.3.6. Electrochemical impedance spectroscopy (EIS) analysis

To investigate the reason of high electrochemical performance of (Sa-H_3PO_4)-electrode, electrochemical impedance spectroscopy (EIS) was carried out. From the Nyquist plot (**Figure 34**), two distinct part could be seen; one is the semi-circle at high frequency region, which indicates the total effective resistance or equivalent series resistance (ESR) including electrode, electrolyte and current collector interface. Another part is vertical line approximately 45° at low frequency region, indicating the diffusion and transportation of electrolyte in the porous sites of the electrode (Tawfik & Gaddafi, 2016). It is resulted that (Sa-H_3PO_4)-electrode, has low resistivity of about 0.44.Ω, which led to high conductivity (Shrestha et. al., 2019 a). This point attributed to high specific capacitance of (Sa-H_3PO_4)-electrode. The specific capacitance, energy density, power density, capacity retention and ESR values are tabulated in **Table 5**.

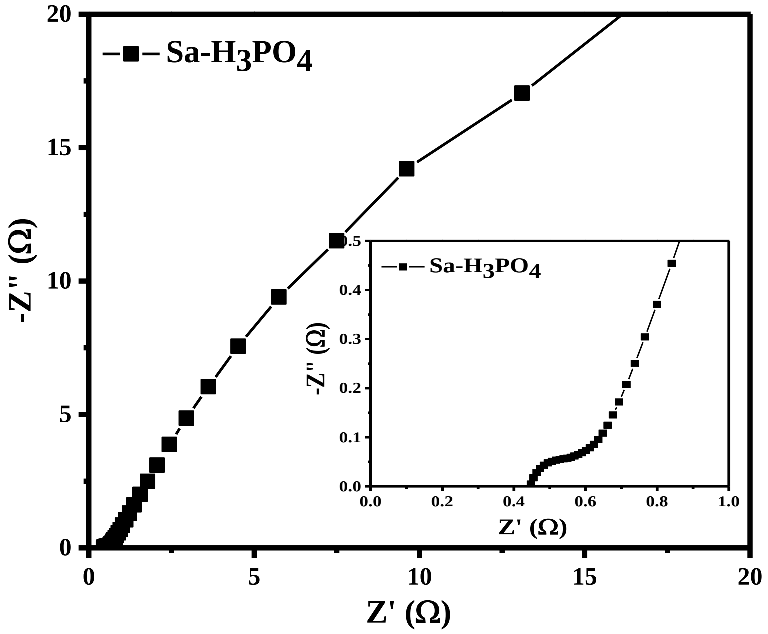

Figure 34: Nyquist plot of Sa-H_3PO_4-electrode and inset is an enlargement of Nyquist plot showing a semicircle at low frequency range

Table 5: Specific capacitance, Energy density, Power density, Capacity retention and ESR value of (Sa-H_3PO_4)-electrode

Electrode	**Specific Capacitance (Fg^{-1})**	**Energy density ($Whkg^{-1}$)**	**Power density (Wkg^{-1})**	**Capacity retention %**	**ESR (Ω)**
(Sa-H_3PO_4)-electrode	136.3	3.0	100.5	97	0.44

The results revealed that *Shorea robusta* derived AC-electrode i.e. (Sa-H_3PO_4)-electrode, provided the specific capacitance of 136.3 Fg^{-1} at 1 A g^{-1} in 6 M KOH electrolyte, high power and energy densities with excellent 97% retention of charge storage capacity during cyclic charge/discharge test (Shrestha et. al., 2019 a). Overall, evidences showed that **(**Sa-H_3PO_4)-electrode exhibited optimum electrochemical performances. Recent trends in supercapacitor research are focused on how to improve the energy density while maintaining high power density, fast charge/discharge and cycling stability (Gupta et. al., 2015). So, for further enhancement of electrochemical performances of as prepared (Sa-H_3PO_4)-electrode, hybrid composites were prepared by mixing AC-(Sa-H_3PO_4) with MnO_2 in different mass ratios as described in [**section 3.3.5.3]**. The hybrid composites are named as, 1:1-(Sa-H_3PO_4:MnO_2), 1:2-(Sa-H_3PO_4:MnO_2) and 2:1-(Sa-H_3PO_4:MnO_2).

Then hybrid-composite-electrodes (HCEs) have been prepared as described in [**section 3.3.5.3]** and named as: 1:1-(Sa-H_3PO_4:MnO_2)-HCE, 1:2-(Sa-H_3PO_4:MnO_2)-HCE and 2:1-(Sa-H_3PO_4:MnO_2)-HCE.

Then electrochemical supercapacitive performances were evaluated by three well known techniques: **(a)** cyclic voltammetry (CV), **(b)** galvanostatic charge/discharge (GCD) and **(c)** electrochemical impedance spectroscopy (EIS).

4.4 Electrochemical characterization of (Sa-H_3PO_4)-HCE: supercapacitive performance

4.4.1. Cyclic Voltammetric (CV) study on (Sa-H_3PO_4:MnO_2)-HCEs

First of all, to get best potential window, CV curve of hybrid composites (Sa-H_3PO_4:MnO_2) at potential windows (-1.2 to 0 V) (**Figure 35)**, (-1 to 0 V) (**Figure 36)**, and (-1 to -0.2 V) (**Figure 37)** has been investigated using current density (A g^{-1}) versus potential (V vs Ag/AgCl). Among the three potential windows, the potential window of (-1.2 to 0 V) was found to be the best one, since it showed the EDLC behavior as well as redox behavior, which is shown in **Figure 35**. Then (-1.2 to 0 V) potential window was chosen and CV was recorded for other two ratios, 1:2 and 2:1 [AC-(Sa-H_3PO_4):MnO_2] (Shrestha et. al., 2019 a), which is presented in **Figure 38** and **39** respectively. The rectangular EDLC curve as well as redox peak were obvious in all the three (1:1, 1:2 and 2:1)-HCEs. However, it was noticeable that when the amount of MnO_2 was increased to double, the capacitance was decreased, which either may be due to the aggregation of the MnO_2 particles within the composite or due to higher value of bulk resistance of pure MnO_2 [**Figure 39]** (Yu et al., 2011).

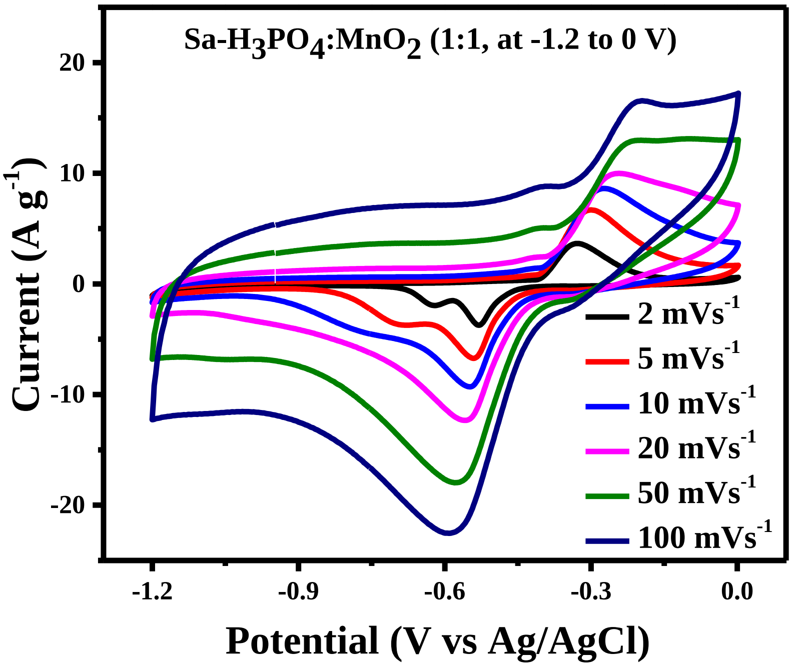

Figure 35: CV curves of 1:1-(Sa-H_3PO_4:MnO_2)-HCE at potential windows (-1.2 to 0 V)

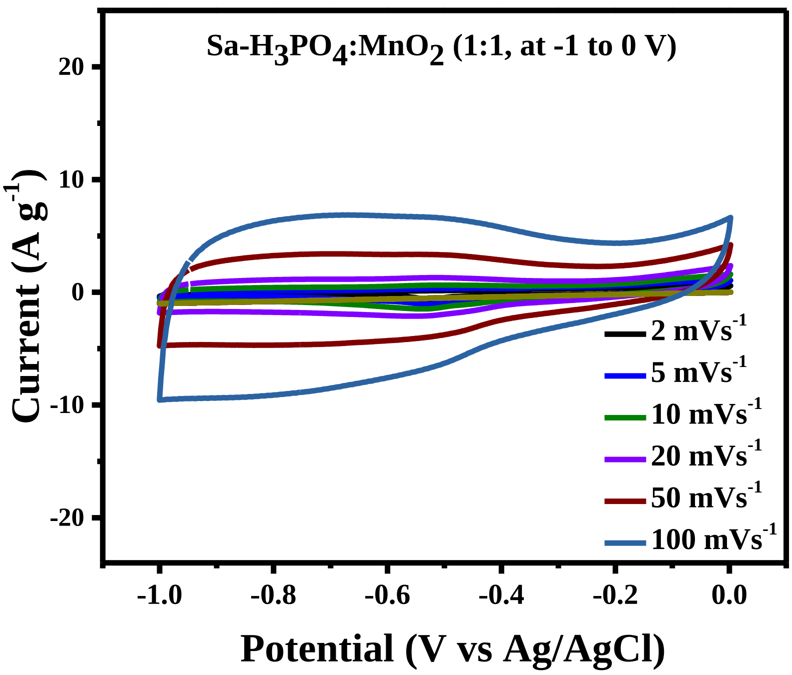

Figure 36: CV curves of 1:1-($Sa-H_3PO_4:MnO_2$)-HCE at potential windows (-1 to 0 V)

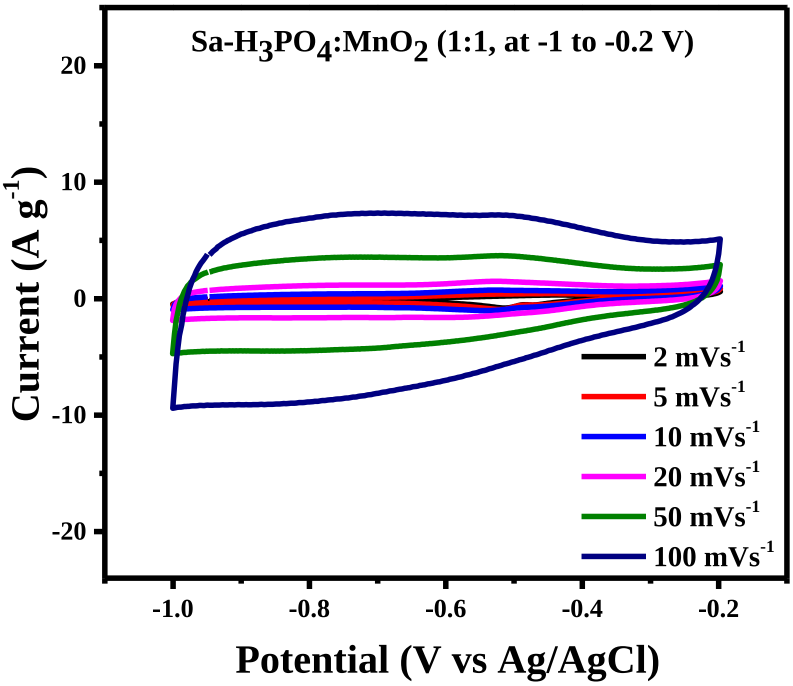

Figure 37: CV curves of 1:1-($Sa-H_3PO_4:MnO_2$)-HCE at potential windows (-1 to -0.2)

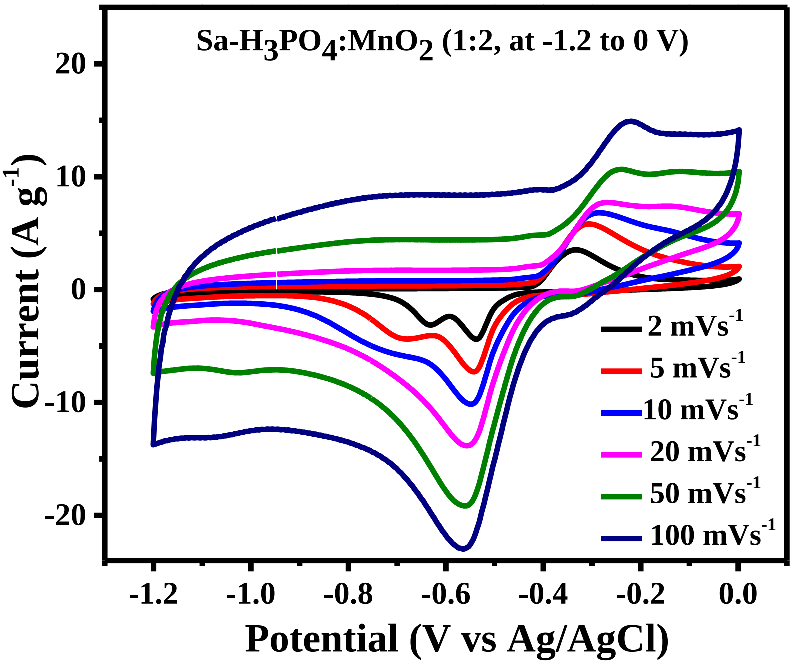

Figure 38: CV curves of 1:2-(Sa-H_3PO_4:MnO_2)-HCE at potential window (-1.2 to 0 V)

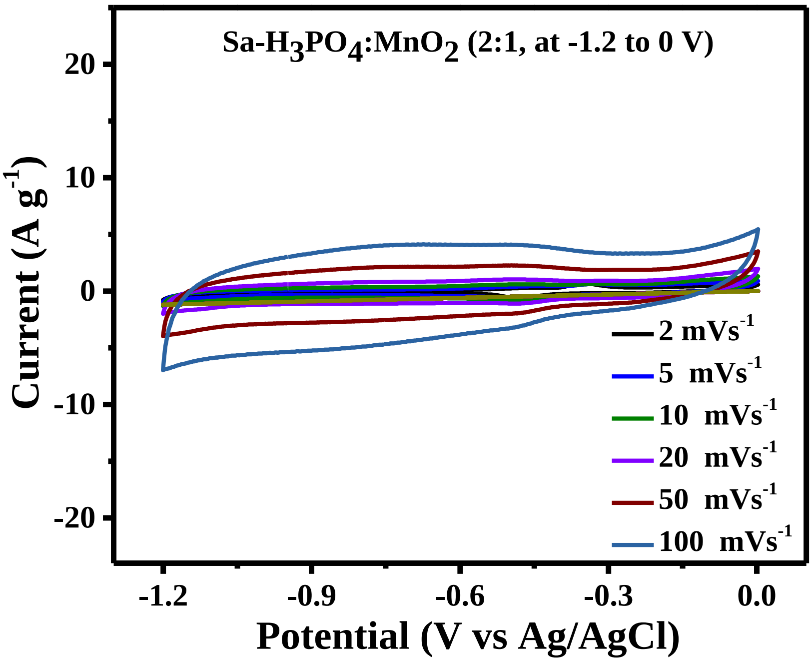

Figure 39: CV curves of 2:1-(Sa-H_3PO_4:MnO_2)-HCE at potential window (-1.2 to 0 V)

This fact was further explained in EIS analysis**.**

Nonetheless, when the amount of MnO_2 was reduced to half [**Figure 38]** the redox peak almost disappeared and the rectangular shape of EDLC became dominant. It demonstrated that the redox feature of the composite electrodes almost depend on the amount of MnO_2 as redox reactions arose on MnO_2. Here, the introduction of MnO_2 imparts the pseudocapacity. However, optimum redox behavior could be observed in 1:1-(Sa-H_3PO_4:MnO_2)-HCEs. It may be due to saturation of MnO_2 particles within the composite.

4.4.2. Galvanostatic Charge/Discharge (GCD) studies on (Sa-H_3PO_4:MnO_2)-HCEs

Galvanostatic Charge/Discharge (GCD) process was used to calculate energy and power densities of the carbon electrode. Hence, the electrochemical properties of composite electrodes were further studied using Galvanostatic Charge/Discharge (GCD) process in (-1.2 to 0 V) potential window and results are shown in **Figure 40, 41 and 42.** As can be seen in **Figure 40, 41 and 42,** at low current density, GCD curve appears to have nearly triangular. However, a bending nature could be observed which is similar to pseudo capacitor material as reported by Puziy et al., 2002. It is mainly caused by internal oxidation-reduction reaction in the material. However, the curve still showed good symmetry, indicating good charge–discharge reversibility of the material. Here, charge/discharge time was 1200 secs. When the discharge time of 1:1-(Sa-H_3PO_4:MnO_2)-HCE was observed (**Figure 40)**, it was found to be 600 secs. Similarly, in the case of 1:2-(Sa-H_3PO_4:MnO_2)-HCE too charge/discharge time was 1200 secs. but the discharge time was just 500 secs. (**Figure 41)**. In 2:1-(Sa-H_3PO_4:MnO_2)-HCE, charge/discharge time was only 1000 secs. and discharge time was 500 secs. (**Figure 42)**.The specific capacitance was also calculated and results are presented in **Table 3**. The specific capacitance was found to be 480.4 ($\underline{+}$ 0.15 %), 418.8 ($\underline{+}$ 0.52 %) and 404.4 ($\underline{+}$ 0.49 %) Fg^{-1} in 1:1, 1:2 and 2:1-(Sa-H_3PO_4:MnO_2)-HCEs respectively (Shrestha et. al., 2019 a), which are tabulated in **Table 6.** These values are also compared with the value of (Sa-H_3PO_4)-electrode and pure MnO_2-electrode. Though 1:2 and 2:1 (Sa-H_3PO_4:MnO_2)-HCEs showed quite good specific capacitance, however, 1:1-(Sa-H_3PO_4:MnO_2)-HCE (**Figure 40)** showed significantly good specific capacitance value (480.4 Fg^{-1}) in comparison to 1:2 and 2:1-(Sa-H_3PO_4:MnO_2)-HCEs. It may be due to equivalent mixture of AC-(Sa-H_3PO_4) and MnO_2, where non-faradaic and faradaic mechanism i.e. EDLC and redox behavior displayed well. The result clearly showed that the equivalent concentration of MnO_2

has improved the specific capacitance of 1:1-(Sa-H_3PO_4:MnO_2)-HCE via simultaneous EDLC and psedocapacitive charge storage mechanism. Whereas in 1:2, when MnO_2 concentration was increased in the electrode, capacitive performances was decreased and deteriorated the specific capacitance value (418.8 Fg^{-1}) (Shrestha et. al., 2019 a), which might be due to either aggregation of MnO_2 particle within the composite or due to higher value of bulk resistance of pure MnO_2. Similarly, in 2:1, due to less amount of MnO_2, psedocapacitive (redox) behavior might be dominated by EDLC behavior generated by AC, which has led to somewhat lower specific capacitance value (404.4 Fg^{-1}). This is further supported by low resistance observed in 1:1-(Sa-H_3PO_4:MnO_2)-HCEs which have also been discussed clearly in EIS analysis section **[section 4.4.4]**. Here, the specific capacitance (C_S) was calculated using the **equation no (9).**

Table 6: Charge/Discharge time duration and specific capacitance HCEs

Hybrid-composite-electrodes (HCE)	**Time duration of charge/discharge (sec)**	**Specific capacitance (Fg^{-1})**
1:1-(Sa-H_3PO_4)-HCE	600	480.4
1:2-(Sa-H_3PO_4)-HCE	500	418.8
2:1-(Sa-H_3PO_4)-HCE	500	404.4

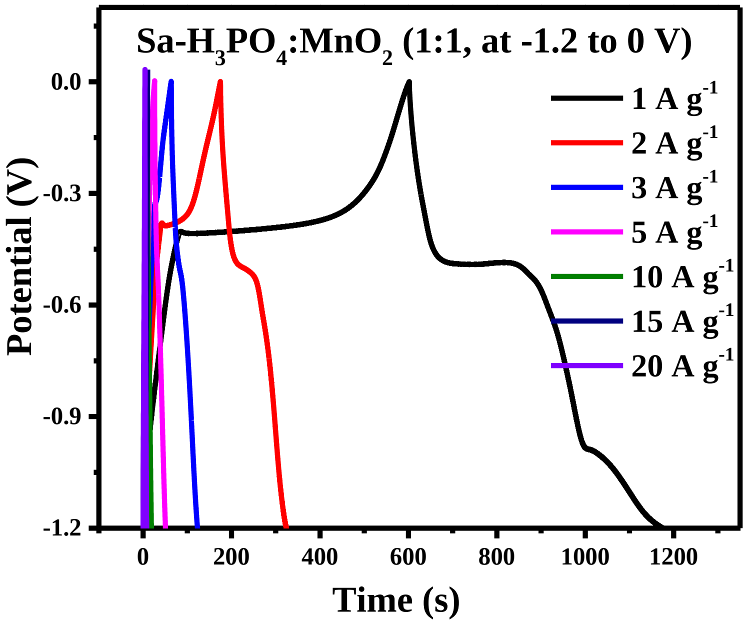

Figure 40: GCD of 1:1-(Sa-H_3PO_4:MnO_2)-HCE at potential window (-1.2 to 0 V)

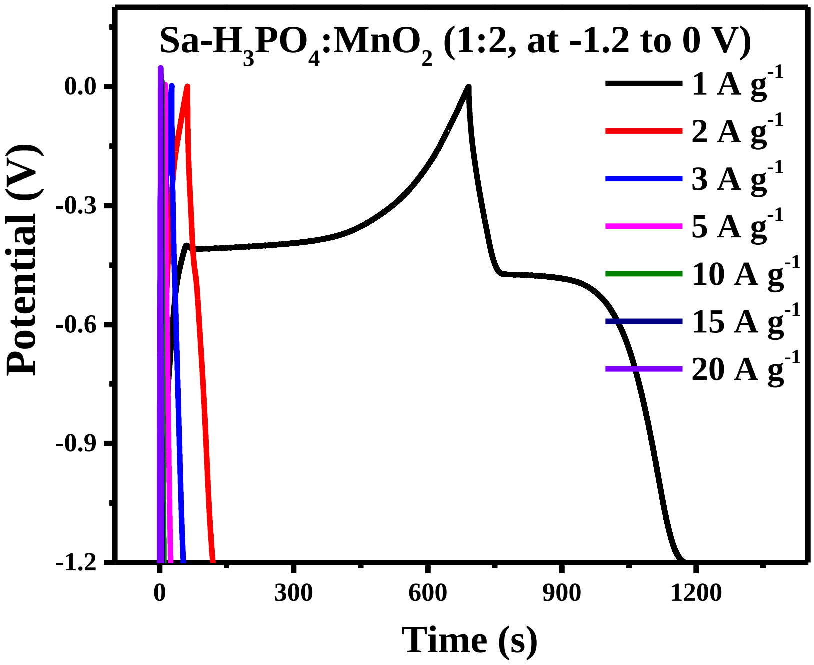

Figure 41: GCD of 1:2-(Sa-H_3PO_4:MnO_2)-HCE at potential window (-1.2 to 0 V)

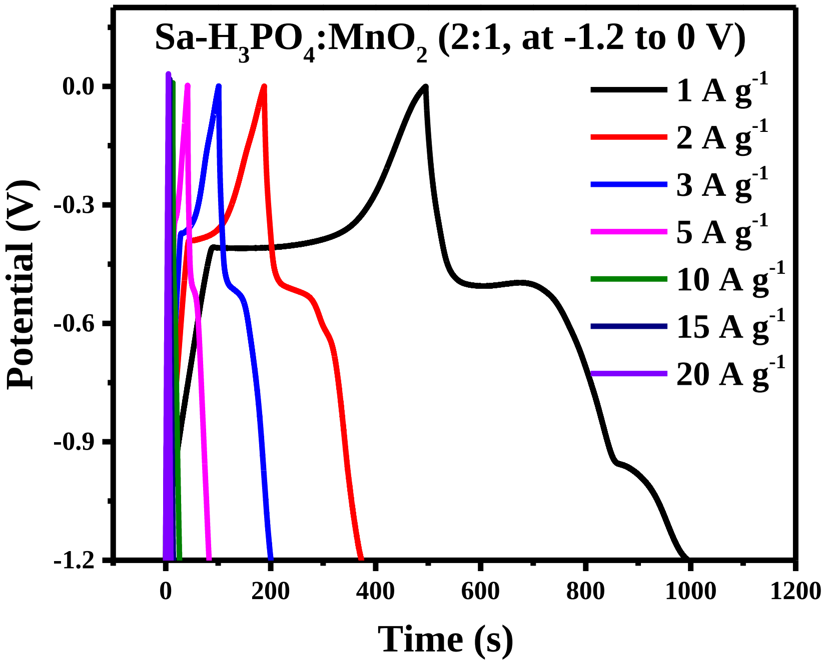

Figure 42: GCD of 2:1-(Sa-H_3PO_4:MnO_2)-HCE at potential window (-1.2 to 0 V)

4.4.3. Ragone plot of (Sa-H_3PO_4:MnO_2)-HCE

Figure 43 shows the Ragone plot of 1:1, 1:2 and 2:1 (Sa-H_3PO_4:MnO_2)-HCE, (Sa-H_3PO_4)-electrode and pure MnO_2-electrode at potential window range of (-1.2 to 0 V). The energy density of 1:1, 1:2 and 2:1 (Sa-H_3PO_4:MnO_2)-HCEs were found to be 24 ($\pm$ 0.26 %), 21($\pm$ 0.21 %) and 20 ($\pm$ 0.15 %) W h kg^{-1} respectively, which was significantly higher than the value of (Sa-H_3PO_4)-electrode which was found to be 3.0 W h kg^{-1} (Shrestha et. al., 2019 a). The results were presented in **Table 7.**

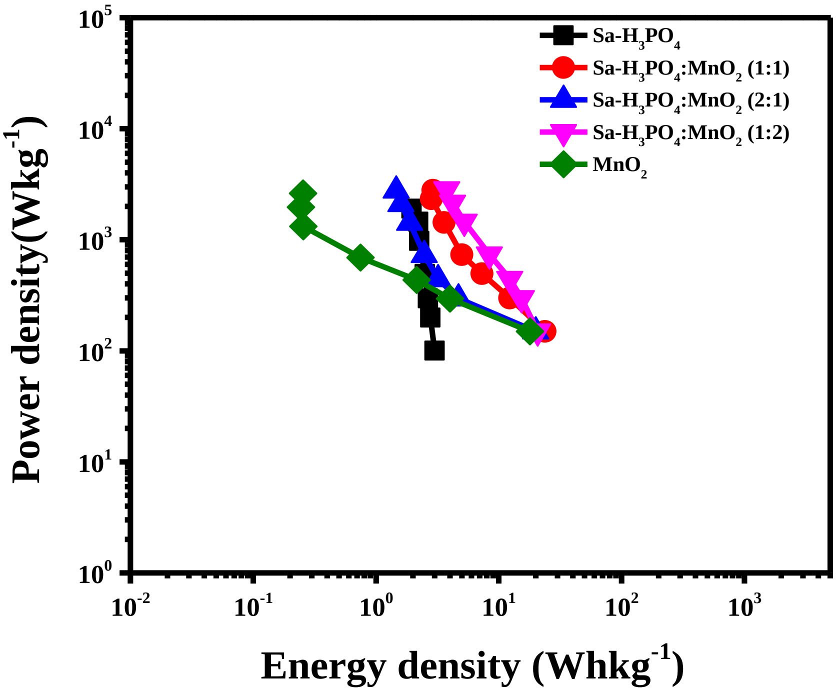

Figure 43: Ragone plots (Sa-H_3PO_4:MnO_2)-HCEs in three ratios, Sa-H_3PO_4–electrode and MnO_2-electrode

Similarly, power density was also found to be increased in HCEs than (Sa-H_3PO_4)-electrodes. Here MnO_2 in hybrid composite played the major source of pseudocapacitive characteristics and stores energy through fast and reversible faradiac surface (Xiong et al., 2011), (Sarangapani et al., 1996). This type of behaviors could be due to layer structure of MnO_2 where intercalation and deintercalation of alkali metal occurs during redox reaction between the III and IV oxidation states of Mn. The surface adsorption of (K^+) on MnO_2 may also be other possible mechanism.

$$\mathbf{MnO_2 + K^+ + e^- \leftrightarrow MnOOK \ldots\ldots\ldots\ldots\ldots\ldots\ldots..(12)}$$

$$\mathbf{(MnO_2)_{surface} + K^+ + e^- \leftrightarrow (MnO_2\text{-}\ K^+)_{surface}\ldots\ldots(13)}$$

Such type of the mechanisms has also explained by Lee et al. (Lee &. Goodenough, 1999). The other reason may be due to the use of higher range of potential window.

4.4.4. Electrochemical impedance spectroscopy (EIS) analysis of (Sa-H_3PO_4:MnO_2)-HCEs

Electrochemical Impedance Spectroscopy (EIS) of (Sa-H_3PO_4)-electrode, (Sa-H_3PO_4:MnO_2)-HCEs and pure MnO_2-electrode were performed to investigate the resistive component involved in electrochemical system and was measured in the frequency range of 100 KHz to 0.1 Hz at the perturbation signal with 10 mV AC voltage in 6M KOH aqueous solution. **Figure 44** represents the Nyquist plot of EIS measurements of electrodes. In the plot, the vertical axis is *Z*” imaginary component of the impedance and horizontal axis is the *Z*’ real component.

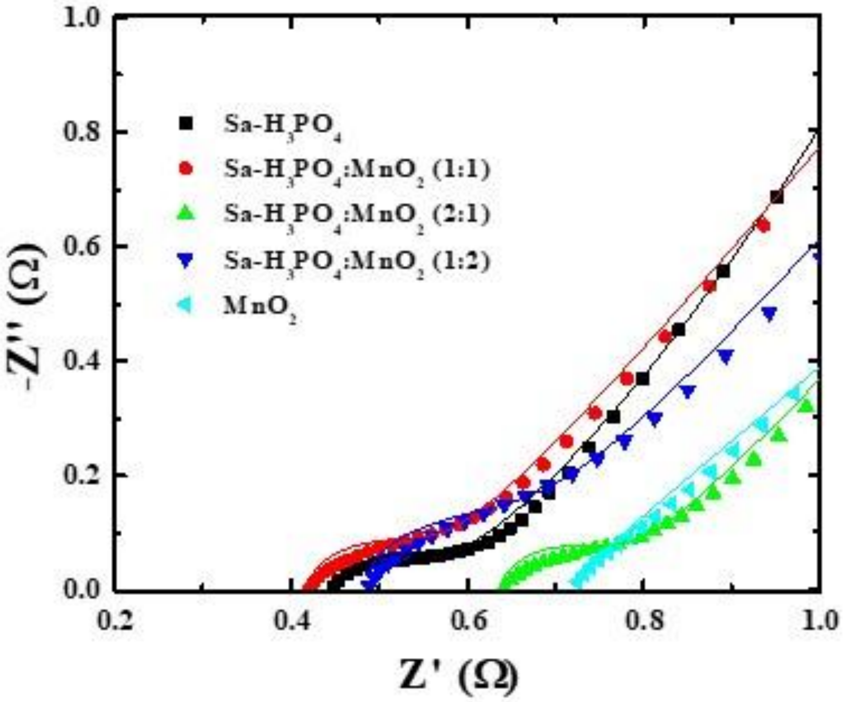

Figure 44: Nyquist plot of (Sa-H_3PO_4:MnO_2)-HCEs with (Sa-H_3PO_4)-electrode and MnO_2-electrode at frequency range of 100 KHz to 0.1 Hz at the perturbation signal with 10 mV AC voltage in 6M KOH aqueous solution.

EIS data were then analyzed in terms of equivalent circuit in order to match the measured data. In **Figure 44**, the points are the experimental data. At high frequency region, a small semicircle loop could be seen which was related to total effective series resistance (ESR) including solution resistance (Rs) and electrode resistance (Kötz & Carlen, 2000). At mid frequency region, a parallel combination of (i) charge transfer resistance (Rct) which was related to electrochemical reaction layer at the interfaces of active materials and (ii) double layer capacitance (Cdl) indicating stored charges on the electrode/electrolyte interfaces which is proportional to the electroactive surface area. The knee at low frequency region is a consequence of the semi-infinite linear diffusion and transporting of electrolyte to/from the electrode plane as well as in the porous electrode which is called as Warburg impedance (W). Behind W, at low frequency region, a vertical line having ~45° slope is a constant phase element (CPE) indicating the non-ideal capacitance of the double layer (Ra et al., 2009), and also represents the internal structures that are completely wetted by the electrolyte (Wang et. al., 2013), (Xing et al., 2014) .The proposed equivalent circuit model is shown in **Figure 45**.

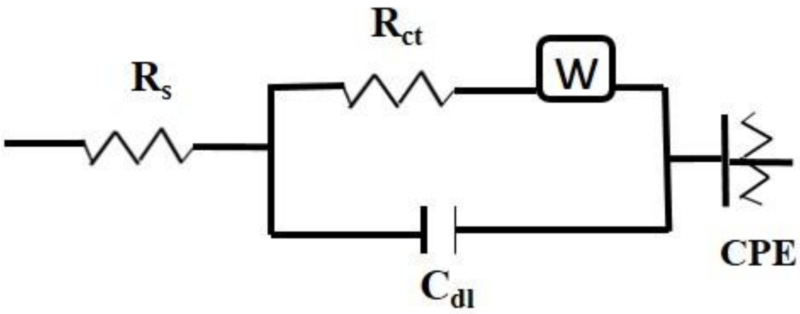

Figure 45: Equivalent circuit Model

The lines in **Figure 45** shows the fitted results by using equivalent circuit. It is obvious that a good fitting was obtained in all frequency range. From the fitted data, the fitted parameters are obtained and is presented in **Table 7**.

Table 7: Cs, Rs, Rct, W, Cdl and CPE value of (Sa-H_3PO_4)-electrode, (Sa-H_3PO_4:MnO_2)-HCE and MnO_2-electrode.

Ratio of Composite (Sa-H_3PO_4-4S:MnO_2)	Cs (Fg^{-1})	Rs (Ω)	Rct (Ω)	W (Ω)	Cdl (mF)	CPE (mMho)
1:0	136.3	0.44	0.11	4.3	54.3	1.53 24.6
1:1	480.4	0.41	0.12	2.8	0.583	81.9
1:2	418.8	0.63	0.12	3.4	0.316	86.4
2:1	404.4	0.49	0.16	4.3	0.546	42.9
0:1	362.7	0.72	0.98	25	5.64 0.101	

The Rs of the electrodes were found to be in the range of (0.41 to 0.72 Ω), which is attributed to the resistance of KOH electrolyte, indicating high electronic conductivity of the electrode. The Rct of all the electrodes were found to be < 1 Ω. Such a lower Rct value leads to the shortening of the ion diffusion path which reflects the higher charge-discharge performance. The W value of (Sa-H_3PO_4)-electrode, (Sa-H_3PO_4:MnO_2)-HCEs were found to be < 5 Ω which is relatively smaller and is the indication of the fast electron transfer within the mesopores of the electrode (Yeung et al., K.K., 2015) whereas in MnO_2-electrode it is relatively high. The Cdl value of (Sa-H_3PO_4:MnO_2)-HCEs was found to be 300 μF to 583 μF. Among them 1:1-(Sa-H_3PO_4:MnO_2)-HCE exhibited high Cdl value of 583 μF. The CPE 86.4 m Mho was also observed in 1:1 (Sa-H_3PO_4:MnO_2)-HCE which was consistent with the preceding specific capacitances of GCD results. The dependence of specific capacitance on composition of electrode is shown in **Figure 46.**

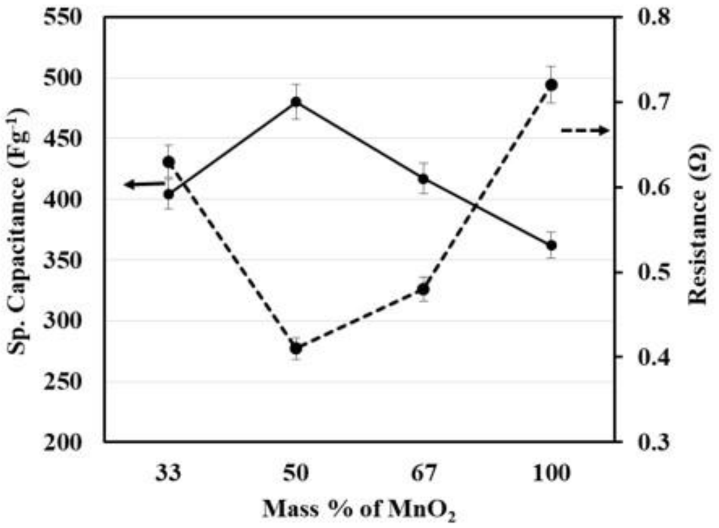

Figure 46: Variation of electrode capacitance and resistance with mass % of MnO_2.

In **Figure 46**, left x-axis indicates for specific capacitance in Fg^{-1} and y-axis represents for mass % of MnO_2 in 1:1, 1:2 and 2:1 (Sa-H_3PO_4:MnO_2)-hybrid-composite-electrode. Whereas, right x-axis indicates for resistance. As can be seen in **Figure 29** the specific capacitance seems to be decreasing when the mass percent of MnO_2 was varied in hybrid-composite-electrodes. In 1:1 composition (50% of AC and 50% MnO_2) specific capacitance was found to be high.

When the composition dependence of electrode/electrolyte resistance for different electrodes were investigated in **Figure 46,** it was found that, the resistance of MnO_2-electrode was abnormally high as compared to the resistance of other three hybrid composite electrodes and it was obvious that the resistances of electrodes increase with increasing mass percent of MnO_2. In conclusion, resistive component of the electrode depends on the composition of the electrode.

4.4.5. Life cycle assessment

Figure 47 shows the life cycle assessment of 1:1, 1:2, 2:1 (Sa-H_3PO_4-MnO_2)-HCEs (Sa-H_3PO_4)-electrode and pure MnO_2-electrode. As can be seen in **Figure 47**, (Sa-H_3PO_4)-electrode showed 97 percent capacity retention, almost no decay up to 1000 cycles, while pure MnO_2-electrode exhibited 61 percent only. The retention capacity was slightly affected by the amount of MnO_2 in the (Sa-H_3PO_4:MnO_2).hybrid-composites. However, in all three 1:1, 1:2 and 2:1 (Sa-H_3PO_4:MnO_2)-HCEs, 90 percent capacity retention was observed indicating good electrochemical stability due to excellent electrical conductivity (Shrestha et. al., 2019 a). The effect of ESR values on capacity retention was obvious. It is assumed that cycling of potential leads to degradation of active materials, presumably increasing the ESR value and decreasing the percentage retention capacity (Yeung et al., 2015).

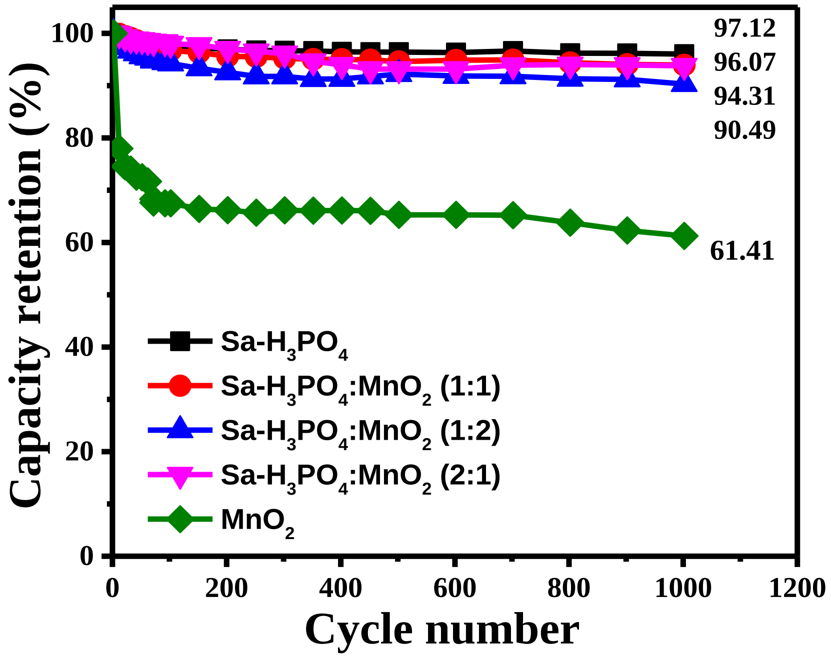

Figure 47: Life cycle assessment of ($Sa-H_3PO_4:MnO_2$)-HCEs along with ($Sa-H_3PO_4$)-electrode and MnO_2-electrode.

The overall results of specific capacitance, energy density, power density, % capacity retention and ESR value of ($Sa-H_3PO_4$)-electrode, ($Sa-H_3PO_4:MnO_2$)-HCEs and MnO_2-electrode are tabulated in **Table 8.**

Table 8: Specific capacitance, Energy density, Power density, Capacity retention and ESR value of ($Sa-H_3PO_4$)-electrode, ($Sa-H_3PO_4:MnO_2$)-HCEs and MnO_2-electrode

Ratio of Composite ($Sa-H_3PO_4$-4S:MnO_2)	**Potential window (V)**	**Specific Capacitance ((Fg^{-1})**	**Energy density (Whkg^{-1})**	**Power density (Wkg^{-1})**	**ESR (Ω)**
1:0	-1 to 0	136.3	3.0	100.5	0.44
1:1	-1.2 to 0	480.4	24	149.3	0.41
1:2	-1.2 to 0	418.8	21	149.5	0.63
2:1	-1.2 to 0	404.4	20	149.2	0.49
0:1	-1.2 to 0	362.7	72	597	0.72

CHAPTER- 5

5. CONCLUSION AND RECOMMENDATIONS

5.1 Conclusion

Activated carbon has wide applications in various fields. This study was undertaken to use agro-waste as precursor for the preparation of activated carbon to apply in energy storage device. From the results, following conclusions have been drawn:

1. The agro-waste, i.e. sawdust of *Shorea robusta* (Sal), can be used as good raw materials for the preparation of activated carbon (AC).
2. From Thermogravimetric analysis (TGA)/ Differential scanning colorimetry (DSC), the carbonization temperature of 400˚C was found to be adequate to prepare AC and the chemical, H_3PO_4 was found to be a good activating agent.
3. Scanning Electron Microscopy (SEM), X-ray diffraction (XRD), Raman spectra, Fourier Transform Infrared Spectroscopy (FTIR), Brunauer–Emmett–Teller (BET), and X-ray Photoelectron Spectroscopy (XPS) methods were carried out to characterize Sa-H_3PO_4 AC. Results revealed that prepared material was found to be amorphous having oxygenated surface functional groups with good porosity and the specific surface area of 1270 m^2g^{-1} (±0.57%) which is in good agreement with the reported value of olive stone derived AC having surface area 1218 m^2g^{-1} (Yakout, et al., 2016).
4. The experiments were performed in 6M aqueous KOH using Cyclic Voltammetry (CV), Galvanostatic Charge–Discharge (GCD) and Electrochemical Impendance Spectroscopy (EIS). The specific capacitance acquired from GCD at 1 Ag^{-1} was found to be 136.3 Fg^{-1} (±0.15%) with 0.44 Ω (±0.02%) ESR. Almost 100 % capacitance retention was observed after 1000 cycles. The energy density of carbon electrode was found to be 3.0 (±0.25%)Wh kg^{-1} at 100.5 (±0.20%)Wkg^{-1} power density which is quite comparable with carbon electrode of pine cone, reported by Bello et al., 2016. Bello et al. has reported the specific capacitance of 137 Fg^{-1} which was acquired from GCD at 1 Ag^{-1}, energy density was found to be 19 $Whkg^{-1}$ and power density was measured 100 Wkg^{-1} in pine cone. In addition to the excellent rate capability of this material, long cycling stability test was conducted under a constant charge at a current density of 5 A g^{-1} for 10,000

cycles. The capacitance retention was almost 100% retention. (Bello et al., 2016).

5. In this study, though, as prepared Sa-H_3PO_4-electrode exhibited good electrochemical performances However better supercapacitive performances can be achieved. Some improvements were done by making hybrid composites. From hybrid composites, HCEs were further fabricated by mixing AC-Sa-H_3PO_4 with MnO_2 in the various mass ratios (1:1, 1:2 and 2:1). Then improved results were obtained.

   (a) CV results concluded that, (-1.2 to 0 V) potential window was found to be the best one, since it showed the EDLC behavior as well as redox behavior. The rectangular EDLC curve as well as redox peak were obvious in all the three (1:1, 1:2 and 2:1)-HCEs. However, it was noticeable that when the amount of MnO_2 was increased to double, the capacitance was decreased, which either may be due to the aggregation of the MnO_2 particles within the composite or due to higher value of bulk resistance of pure MnO_2.

   (b) Among the three ratios, 1:1-(Sa-H_3PO_4:MnO_2)-HCEs, showed prominently high specific capacitance having 480.4 (±0.20%) Fg^{-1}, and high energy density 24 (±0.26%) $Whkg^{-1}$ at power density 149.3 Wkg^{-1} and low ESR value of 0.41 (±0.02%) Ω. The results showed that the desirable electrochemical capacitive performances enable the hybrid composite to act as a new potential bio material source for the preparation of high-performance supercapacitor material and low cost energy storage devices.

The overall results/ electrochemical performances showed excellent capacitive behavior of as fabricated hybrid composite electrodes (HCEs) prepared from agro-waste, sawdust of *Shorea robusta*. Hence they could be applied in supercapacitor devices as a core-electrode-material for the storage of electrochemical energy.

5.2 Recommendations/ Suggestion for Further Work

The following recommendations are made for further study:

1) In this thesis, AC was prepared by chemical activation using phosphoric acid (H_3PO_4). Other chemical reagents such as KOH, sulphuric acid (H_2SO_4), zinc chloride $ZnCl_2$ can also be tried on sawdust powder of *Shorea robusta* (Sal).

2) From this study, it was found that AC prepared from sawdust of *Shorea robusta* (sal) can be used as an electrode material for supercapacitor. Hence, this study can be further extended in preparing low cost supercapacitor as energy storage system.
3) Here, electrochemical measurement was carried out in aqueous electrolyte KOH. The electrochemical characterization can be investigated in other aqueous electrolytes like H_2SO_4, NaOH.
4) *Shorea robusta* is considered to be the most well-known representative tree for Nepal. The waste wood of other tree species can also be used to prepare activated carbon via same route and they will definitely be low cost energy storage materials having high- supercapacitive performance.

CHAPTER-6

6. SUMMARY

In the quest of exploring novel source of the preparation of AC, this study was carried out to prepare AC from an agro-forest waste; sawdust of *Shorea robusta* by chemical activation using phosphoric acid and characterize and apply this AC in energy related field. Activated carbon was prepared by carbonization of sawdust of *Shorea robusta* at 400°C in an inert environment which was chemically activated with H_3PO_4. It was successfully tested as supercapacitor materials for the first time for its application in energy storage device. Samples were characterized by Thermogravimetric Analysis (TGA)/Differential Scanning Calorimetry (DSC), Scanning Electron Microscopy (SEM), X-ray diffraction **(**XRD), Raman spectra, Fourier Transform Infrared Spectroscopy (FTIR), Brunauer–Emmett–Teller (BET), and X-ray Photoelectron Spectroscopy **(**XPS). Thermal decomposition behavior (TG curve) coupled with endothermic peak of DSC curve confirmed that 400^oC was the adequate temperature for completion of carbonization process from raw sawdust powder, since no significant weight loss occurred after 400^oC. FTIR spectra clearly confirmed the presence of oxygenated functional groups such as hydroxyl (-OH), aldehyde/ketone (-CHO/C=O) and ether (C-O-C), at the surface of as prepared AC. All the carbon samples were found to be amorphous in nature. The oxygen surface functionality was developed at the surface of sample (Sa-H_3PO_4). Similarly, XPS shows a broad peak at 532.6 eV for O 1s, indicating the presence of different chemical states of oxygen. The three deconvoluted peaks for oxygen at the binding energies 531 eV, 533.04 eV and 533.12 eV shows the presence of phosphatic oxygen (PO_4^{3-}), hydroxyl group (-OH) eV and silicon dioxide (SiO_2) respectively. XPS spectra assured that the prepared activated carbon (Sa-H_3PO_4) was well functionalized after the activation of H_3PO_4 and it consisted of more acidic functional groups as aldehydes/ketones, ethers, hydroxides and so on. This aligns with the FTIR results, where activated carbon (Sa-H_3PO_4) showed high intensities for hydroxyl (-OH), aldehyde/ketone (-CHO/C=O) and ether (C-O-C) functional groups. Likewise, XRD-pattern showed the amorphous structure of carbon having 002 and 100 plane, whereas Raman spectra clearly displayed G and D band, which further confirmed the amorphous nature of carbon. The G/D intensity ratio was found to be approximately 1 indicating the presence of graphitic degree and defects in equal proportion. BET method of surface area determination showed the high specific surface area of 1270 m^2g^{-1} (± 0.57 %), which is fairly higher than surface area of commercial activated carbon compared with 1000 m^2g^{-1}.The overall electrochemical performance of Sa-H_3PO_4 showed exceptional super-capacitive performance demonstrating the high potentials of this material to be used for the EDLC application in super-capacitive energy storage. Electrochemical characterization performed in 6M aqueous KOH using Cyclic Voltammetry (CV), Galvanostatic Charge-Discharge (GCD) and Electrochemical Impendance Spectroscopy (EIS). The specific capacitance acquired from GCD at 1 Ag^{-1} was found to be 136.3 Fg^{-1} (± 0.15 %) with 0.44 Ω (± 0.02 %) ESR. The 97 % capacitance retention was observed after 1000 cycles. The energy density of carbon electrode was found to be 3.0 (± 0.25 %) $Whkg^{-1}$ at 100.5 (± 0.20 %) Wkg^{-1} power density. Then the working carbon electrode was substituted by 'hybrid composite electrode' which displayed the ideal capacitive behaviors with specific capacitance of 480.4 (± 0.20 %) Fg^{-1}, specific energy density of 24 (± 0.26 %) $WhKg^{-1}$ and low ESR value of 0.41 (± 0.02 %) Ω. The obtained results unveiled that the desirable electrochemical capacitive performances enable the hybrid composite to act as a new bio-material for high performance supercapacitors and energy storage devices.

REFERENCES

Abdullah, A.H., & Kassim, A. Zainal, Z., Hussien, M. Z., Kuang, D., Ahmad F., Wooi, O.S. (2001). Preparation and characterization of AC from Gelam wood bark (melaleuca cajuputi). *Malay. J. Ana. Sci*., **7**(1): 65-68.

Acharya, J., Sahu, J.N., Mohanty, C.R, Meikap, B.C. (2009). Removal of lead (II) from wastewater by activated carbon developed from Tamarind wood by zinc chloride activation. *Chem. Eng. J.,* **149**:249–262.

Ahmed, S., Rafat, M., Ahmed, A. (2018). Nitrogen doped activated carbon derived from orange peel for supercapacitor application. *Adv. Nat. Sci. Nanosci. Nanotechnol*., **9**: 035008-035016.

Albadarin, A. B., & Mangwandi, C. (2015). Mechanisms of alizarin red S and methylene blue biosorption onto olive stone by-product: isotherm study in single and binary systems. *J. Environ. Manag.,* **164**: 86–93.

Allen, M. J., Tung, V.C., Kaner, R.B. (2010). Honeycomb carbon: A review of graphene. *Chem. Rev.,* **110:** 132–145.

Alslaibi, T.M., Abustan, I., Ahmad, M.A., Foul, A.A. (2013). A review: production of activated carbon from agricultural byproducts via conventional and microwave heating. *J. Chem. Technol. Biotechno.,* **88**:1183-1190.

Alvarez, J., Lopez, G., Amutio, M., Bilbao, J., Olazar, M. (2014). Upgrading the rice husk char obtained by flash pyrolysis for the production of amorphous silica and high quality activated carbon. *Bioresour. Technol.,* **170**:132-137.

Annadural, G., Juang, R. S., Lee, D. J. (2003). Adsorption of heavy metal from water using banana and orange peels. *Water Sci. Tech.,* **47**(1):185-190.

Asif, M., & Muneer, T. (2007). Energy supply, its demand and security for development and emerging economies. *Ren. Sust. Ener. Revie.,* **11** (7):1388-1413.

Ates, M., & Sarac, A.S. (2011). Electrochemical impedance spectroscopic study of polythiophenes on carbon materials. *Polym. Plast. Technol. Eng.,* **50**:1130–1148.

Auta, M. & Hameed B. (2011). Preparation of waste tea activated carbon using potassium acetate as an activating agent for adsorption of Acid Blue 25 dye. *Chem. Eng. J.,* **171**(7): 502-509.

Bae, W., Kim, J., Chung, J. (2014). Production of granular activated carbon from food-processing wastes (walnut shells and jujube seeds) and its adsorptive properties. *J. Air Waste Manage. Assoc*., **64**(8):879–886.

Balathanigaimani, M. S., Shim, W. G., Lee, M. J., Kim, C., Lee, J. W., Moon H. (2008). Highly porous electrodes from novel corn grains-based activated carbons for electrical double layer capacitors. *Electrochem. Commun.,* **10**:868–871.

Banerjee, K., Ramesh, S.T., Gandhimathi, R., Nidheesh, P.V., Bharathi, K.S. (2012). A novel agricultural waste adsorbent; watermelon shell for the removal of copper from aqueous solutions. *Iran, J. Ener. Environ*., **3**(2):143-56.

Baños, R., Manzano-Agugliaro, F., Montoya, F.G., Gil, C., Alcayde, A., Gómez, J. **(**2011**).** Optimization methods applied to renewable and sustainable energy: A review. *Ren. Sust. Ener. Review,* **159**(4):1753-1766.

Baral, S.S., Das, S. N., Rath, P. (2006). Hexavalent chromium removal from aqueous solution by adsorption on treated sawdust. *Biochem. Engine. J.*, **31**(3):216-222.

Bard, A. J., & Faulkner, L. R. (2000). *Electrochemical Methods: Fundamentals and Applications.* Wiley, New York.

Behnamfard, A., & Salarirad, M.M. (2013). Characterization of coconut shell-based activated carbon and its application in the removal of Zn (II) from its aqueous solution by adsorption. *Desalin. Water Treat.,* **52**:37–41.

Bello, A., Manyala, N., Barzegar, F., Khaleed, A., Momodua, D.Y., Dangbegnona J.K. (2016). Renewable pine cone biomass derived carbon materials for supercapacitor application. *RSC Adv.*, **6**: 1800-1809.

Benaddi, H., Legras, D., Rouzaud, J.N., Beguin, F. (1998). Influence of the atmosphere in the chemical activation of wood by phosphoric acid. *Carbon*, **36**:306-309.

Bernard, E., Jimoh, A., Odigure, J.O. (2013). Heavy metals removal from industrial wastewater by activated carbon prepared from coconut shell. *Res. J. Chem. Sci*.,**3** (8):3–9.

Billy, T. H., Puziah, A. L., Taufiq, Y. H. (2013). Physical preparation of activated carbon from sugar cane bagasse and corn husk and its physical and chemical characteristics. *Int. J. Eng. Res. and Sci. and Tech.*, **2**(3):1-14.

Biswas, G., Kumari, M., Adhikari, K., Dutta, S. (2017). Application of response surface methodology for optimization of biosorption of fluoride from groundwater using *Shorea robusta* flower petal. *Appl. Water Sci.*, **7**:4673–4690.

Bohli, T., & Ouederni, A. (2016). Improvement of oxygen-containing functional groups on olive stones activated carbon by ozone and nitric acid for heavy metals removal from aqueous phase. *Environ. Sci. Pollut. Res.*, **23:**15852–15861.

Bolotin, K. I., Sikes, K. J., Jiang, Z., Klima, M., Gudenberg, G., Hone, J., Kim, P., Stormer, H.L. (2008). Ultrahigh electron mobility in suspended graphene. *Solid State Commun*., **146:**351-355.

Boopathy, R., & Karthikeyan S. (2013). Adsorption of ammonium ion by coconut shell-activated carbon from aqueous solution: kinetic, isotherm, and thermodynamic studies. *Env. Sci. Pollut. Res.*, **20**:533–542.

Burke A**.**, & Miller M. **(**2010**).** Testing of electrochemical capacitors: capacitance, resistance, energy density, and power capability. *Electrochim. Acta*, **55**:7538-7548.

Burke A., (2007). R & D Considerations for the performance and application of electrochemical capacitors. *Electrochim. Acta*, **53**:1083-1091.

Cadenas-Perez, A. F., Maldonado-Hodar, F. J., Moreno-Castilla, C. (2003). On the nature of surface acid sites of chlorinated activated carbons. *Carbon*, **41**(3):473–478.

Cagnon, B., Py, X., Guillot, A., Stoeckli, F., Chambat, G. (2009). Contributions of hemicellulose, cellulose and lignin to the mass and the porous properties of chars and steam activated carbons from various lignocellulosic precursors. *Bioresour. Technol.,* **100**:292–298.

Cao, Z., Yang, H., Dou, P., Wang, C., Zheng, J., Xu X. (2016). Synthesis of three dimensional hollow SnO_2@PPy nanotube arrays via template-assisted method and chemical vapor-phase polymerization as high performance anodes for lithium-ion batteries. *Electrochim. Acta,* **209**:700–708.

Caturla, F., Molina-Sabio, M., Rodriguez-Reinoso, F. (1991). Preparation of activated carbon by chemical activation with $ZnCl_2$. *Carbon,* **29:** 999-1007.

Çeçen F. (2011). Water and wastewater treatment: Historical perspective of activated carbon adsorption and its integration with biological processes. In: Çeçen F, Aktaş Ö,(ed.), Activated carbon for water and wastewater treatment, Weinheim, Germany: Wiley- VCH Verlag GmbH & Co. KGaA, 1-11.

Çeçen F. (2014). *Activated carbon,* In: Kirk-Othmer Encyclopedia of Chemical Technology. John Wiley & Sons, Inc. 1-34.

Chaikittisilp, W., Hu, M., Wang, H., Huang, H.S., Fujita, T., Wu, K. C.W., Chin, L. C., Yamauchi, Y., Ariga K. (2012). Nanoporous carbons through direct carbonization of a zeolitic imidazolate framework for supercapacitor electrodes. *Chem. Commun.,* **58**: 7259-7261.

Chen, H., Wang, H., Yang, L., Xiao, Y., Zheng, M., Liu, Y., Fu, H. (2012**).** High specific surface area rice hull based porous carbon prepared for EDLCs. *Int. J. Electrochem. Sci.,* **7**:4889-4897.

Chen, T.C., Agripa, M. L., Lu, M.C., Dalida, M. L.P. (2016). Adsorption of sulfur compounds from diesel with ion-impregnated activated carbons. *Energy & Fuels,* **30** (5): 3870-3878.

Chen, W., Fan, Z., Gu, L., Bao, X., Wang, C. (2010). Enhanced capacitance of manganese oxide via confinement inside carbon nanotubes. *Chem. Commun*., **46**:3905-3907.

Choi, D. W., Blomgren, G. E., Kumta, P. N. (2006). Fast and reversible surface redox reaction in nanocrystalline vanadium nitride supercapacitors. *Adv. Mater.*, **18**:1178-1182.

Chuang, C. M., Huang, W., Teng, H., Ting, J. M. (2010). Effects of carbon nanotube grafting on the performance of electric double layer capacitors. *Energy Fuels*, **24**: 6476-6482.

Conway B. E. (1999). *Electrochemical supercapacitors: scientific fundamentals and technological applications.* New York. Kluwer Academic/Plenum Publishers.

Conway B. E. (1999). Transition from “supercapacitor” to “battery” behavior in electrochemical energy storage. *J. Electrochem. Soc.*, **138**: 1539-1548.

Conway, B. E., Birss, V. Wojtowicz, J. (1997). The role and utilization of pseudocapacitance for energy storage by supercapacitors. *J. Power Sources*, **66**(1-2): 1-14.

Dąbrowski, A. (2001). Adsorption from theory to practice. *Advances in Colloid and Interface Science*, **93**(1-3):135-224.

Danisha, M. & Ahmad, T. (2018). A review on utilization of wood biomass as a sustainable precursor for activated carbon production and application. *Rene. Sustain. Ener. Revi.*, **87**:1–21.

Dastgheib, S.A., Rockstraw, D.A. (2001). Pecan shell activated carbon: synthesis, characterization, and application for the removal of copper from aqueous solution. *Carbon*, **39**:1849-1855.

Derbyshire, F., Jagtoyen, M., Thwaites, M. (1995). *Porosity in carbons*, London: Edward Arnold U.K.

Diefendorf, R. J., (2000). *Pitch precursor carbon fibers*, Chapter 1.02" in comprehensive composite materials. Vol 1: reinforcement materials and general theories, T.W. Chou ed., Pergamon, Oxford, 107-145.

Dobrota, A.S., Pašti, I.A., Mentus, S.V., Johansson, B., Skorodumova, N.V., (2017). Functionalized graphene for sodium battery applications: the DFT insights. *Electrochim. Acta,* **250**:185–195.

Du, C., & Pan, N. **(**2006**).** Supercapacitors using carbon nanotubes films by electrophoretic deposition. *J. Power Sources,* **160:**1487-1494.

Ekpete, O., Horsfall, M. JNR. (2011). Preparation and characterization of activated carbon derived from fluted pumpkin stem waste. *Res. J. Chem. Sci.,* **1**(3):10-17.

Ellis, M.W., Spakovsky, M.R.V., Nelson, D. J. (2001). Fuel cell systems: efficient, flexible energy conversion for the 21st Century. *Proc. IEEE.* **89**:1808– 1818.

Elmouwahidi, A., Benabithe, Z. Z., Marin, F. C., Castilla, C. M. (2012). Activated carbons from KOH-activation of argan (*Arganiaspinosa*) seed shells as supercapacitor electrodes. *Bioresource Technol.,* **111**:185–190.

Faggioli, E., Rena, P., Danel, V., Andrieu, X., Mallant, R., Kahlen, H. (1999). Supercapacitors for the energy management of electric vehicles. *J. Power Sources,* **84**:261–269.

Fan, Z., Yan, J., Wei, T., Zhi, L., Ning, G., Li, T., Wei, F. (2011). Asymmetric supercapacitors based on graphene/MnO_2 and activated carbon nanofiber electrodes with high power and energy density. *Adv. Funct. Mater.,* **21**:2366–2375.

Fang, G., Gao, J., Liu, C., Dionysiou, D.D., Wang, Y., Zhou, D. (2014). Key role of persistent free radicals in hydrogen peroxide activation by biochar: implications to organic contaminant degradation. *Environ. Sci. Techno.,* **48**(3):1902-1910.

Floyd, E.L, Sapag, K, Oh, J., Lungu, C.T. (2014). Photothermal desorption of single-walled carbon nanotubes and coconut shell-activated carbons using a continuous light source for application in air sampling. *Annals of Occupational Hygiene,* **58**(7):877–888.

Frackowiak, E., Béguin, F. (2001). Carbon materials for the electrochemical storage of energy in capacitors. *Carbon,* **39** (6):937-950.

Fu, M., Chen, W., Zhu, X., Yang, B., Liu, Q. (2019). Crab shell derived multi-hierarchical carbon materials as a typical recycling of waste for high performance supercapacitors. *Carbon*, **141**:748–757.

Ganesh, V., Pitchumani, S., Lakshminarayanan, V. (2006). New symmetric and asymmetric supercapacitors based on high surface area porous nickel and activated carbon. *J. Power Sources*, **158** (2):1523–1532.

Gao, Z., Yang, W., Wang, J., Wang, B., Li, Z., Liu, Q., Zhang, M., Liu, L. (2013). A new partially reduced graphene oxide nanosheet/polyaniline nanowafer hybrid as supercapacitor electrode material. *Energy Fuels*, **27**:568–575.

Ghouma, I., Jeguirim, M., Dorge, S., Limousy L., Ghimbeu, C. M., Quedarni, A. (2015). Activated carbon prepared by physical activation of olive stones for the removal of NO_2 at ambient temperature. *Comptes. Rendus. Chim.*, **18** (1):63– 74.

Gomez, J., & Kalu, E.E. (2013). High-performance binder-free Co–Mn composite oxide supercapacitor electrode. *J. Power Sources*, **230**:218–224.

Gonzalez-Serrano, E., Cordero, T., Rodriguez-Mirasol, J., Cotoruelo, L., Rodriguez, J. J. (2004). Removal of water pollutants with activated carbons prepared from H_3PO_4 activation of lignin from kraft black liquors. *J. Water Res.*, **38**:3043–3050.

Gouy M., (1910). Sur la constitution de la charge électrique à la surface d'un electrolyte. *J. Phys. Theor. Appl.*, **9**(1):457-468.

Greenwood, N. N., & Earnshaw, A. (2006). *Chemistry of the elements*. 2nd ed. Butterworth- Heinemann Elsevier: Oxford, UK;

Gregg, S. J, Sing, K.S.W. (1982). *Adsorption, surface area and porosity*, 2nd ed. London: Academic Press Inc.

Guo, N., Li M., Wang Y., Sun X., Wang F., Yang R. (2016). Soybean root-derived hierarchical porous carbon as electrode material for high-performance supercapacitors in ionic liquids. *ACS Appl. Mater. Interfaces*, **8**: 33626–33634.

Guo, Y., Shi, Z.Q., Chen, M.M., Wang, C. (2014). Hierarchical porous carbon derived from sulfonated pitch for electrical double layer capacitors. *J. Power Sources,* **252**: 235–243.

Gupta, R. K., Candler, J., Palchoudhury, S., Ramasamy, K., Gupta, B. K. (2015). Flexible and high performance supercapacitors based on $NiCo_2O_4$ for wide temperature range applications. *Sci.Rep.,* **5**:15265**.** https://doi.org/:10.1038/srep15265.

Hassan, M. A. S., & Ashfaq, A. (2011). Synthesis and characterization of activated carbon from Saudi Arabian dates tree's fronds wastes, in 3rd international conference on chemical. *Bio. Env. Eng.,* **20**:124-146.

Hayashi, J. I., Kazehaya, A., Muroyama, K., Watkinson, A. P. (2000). Preparation of activated carbon from lignin by chemical activation. *Carbon,* **38**(13): 873-1878.

Hiremath, M. N., Shivayogimath, C.B., Shivalingappa, S.N. (2012). Preparation and characterization of granular activated carbon from corn cob by KOH activation. *Int. J. Res. Chem. Environ*., **2**(3): 84-87.

Hu, Z., Srinivasan, M.P., Ni, Y. (2001). Noval activation process for preparing highly microporous and mesoporous activated carbons. *Carbon*, **39**: 877-886.

Huang, Y., Peng, L., Liu, Y., Zhao, G., Chen, J.Y., Yu, G. (2016). Biobased nano porous active carbon fibers for high-performance supercapacitors. *J. ACS Appl. Mat. Interf.,* **8**:15205–15215.

Hussaro, K. (2014). Preparation of activated carbon from Palm oil shell by chemical activation with Na2CO3 and ZnCl2 as impregnated agents for H_2S adsorption. *American J. Environ. Sci.,* **10** (4): 336-346.

Ilona, A., Katarzyna L., Agnieszka S., Grzegorz L. (2014). Carbon-supported manganese dioxide as electrode material for asymmetric electrochemical capacitors. *Int. J. Electrochem. Sci.,* **9**:2518 – 2534.

Ioannidou, O., & Zabaniotou, A. (2007). Agricultural residues as precursors for activated carbon production: a review. *Renew. Sustain. Ener. Rev*., **11**(9):1966–2005.

Iqbal, S., & Ahmad, S. (2018). Recent development in hybrid conducting polymers: synthesis, applications and future prospects. *J. Ind. Eng. Chem.*, **60**:53– 84.

Jabit, N.A.B. (2007). *The production and characterization of activated carbon using local agricultural waste through chemical activation process* (Unpublished M. Sc. Thesis). School of Material and Mineral Engineering, USM, Malaysia.

Jäger, H., Frohs, W., Collin, G.V., Sturm, F., Vohler, O., Nutsch, G. (2010). *General. ullmann's encyclopedia of industrial chemistry*. Weinheim, Germany Wiley-VCH Verlag GmbH & Co. KGaA;

Jagtoyen, M., & Derbyshire, F. (1998). Activated carbons from yellow poplar and white oak by H_3PO_4 activation. *Carbon,* **36**:1085-1097.

Jain, A., & Tripathi, S.K. (2014). Fabrication and characterization of energy storing supercapacitor devices using coconut shell based activated charcoal electrode. *Mater. Sci. Eng. B,* **183**: 54–60.

Jankowska, H., Swiatkowski, A., Choma, J. (1985). *Active carbon,* West Sussex, England: Ellis Horwood, 64.

Janoš, P., & Coskun, S. (2009). Removal of basic (Methylene Blue) and acid (Egacid Orange) dyes from waters by sorption on chemically treated wood shavings. *Bioresour. Technol.*, **100**:1450–1453.

Jayalakshmi, M., & Balasubramanian K. (2008). Simple capacitors to supercapacitors - an overview. *Int. J. Electrochem. Sci.,* **3**:1196−1217.

Jian, Z., Liu, P., Li, F., He, P., Guo, X., Chen, M., Zhou, H. (2014). Core-shell-structured CNT@RuO_2 composite as a high-performance cathode catalyst for rechargeable Li-O_2 batteries. *Angew. Chemie. Int. Ed.,* **53**:442–446.

Jiang, H.L., Liu, B., Lan, Y. Q., Kuratani, K., Akita, T., Shioyama, H., Zong, F., Xu, Q. (2011.) From metal-organic framework to nanoporous carbon: toward a very high surface area and hydrogen uptake. *J. Am. Chem. Soc.,* **133**(31):11854-11857.

Jonglertjunya W. (2008). Biosorption of lead (II) and copper (II) from aqueous. *Chiang Mai J. Sci.*, **35**(1):69-81.

Joshi, S., Adhikari, M., Pokharel, B. P., Pradhananga, R. R. (2013). Effects of activating agents on the activated carbons prepared from Lapsi seed stone. *Res. J. Chem. Sci.,* **3**:19– 24.

Kalpana, D., Cho, S. H., Lee, S. B., Lee, Y. S., Mishra, R., Renganathan, N. G. (2009). Recycled waste paper—A new source of raw material for electric double-layer capacitors. *J. Power Sources,* **190**:587–591.

Kandalkar, S., Dhawale, D., Kim, C, Lokhande, C. (2010). Chemical synthesis of cobalt oxide thin film electrode for supercapacitor application. *Synth. Mater*., **160**:1299-1302.

Khan, A.M., & Ansari, R., (2009). Activated charcoal: preparation, characterization and applications: A review article. *Int. J. ChemTech. Res*., **1**(4): 859-864.

Khomenko, V., Frackowiak, E., Béguin, F. (2005). Determination of the specific capacitance of conducting polymer/nanotubes composite electrodes using different cell configurations. *Electrochim. Acta,* **50**: 499-2506.

Kim, K.H., Yang, M., Cho, K.M., Jun, Y.S., Lee, S.B., Jung, H.T. **(**2013). High quality reduced graphene oxide through repairing with multi-layered graphene ball nanostructures. *Sci. Rep*., **3**: 3251. https://doi.org/:10.1038/srep03251.

Kim, M., Hwang, Y., Min, K., Kim, J. (2013). Introduction of MnO_2 nanoneedles to activated carbon to fabricate high-performance electrodes as electrochemical supercapacitors. *Electrochem. Acta,* **113**:322-331.

Kini, S.M., Saidutta, M.B., Murty, R.V., Kadoli, S.V. (2015). Adsorption of basic dye from aqueous solution using HCl treated saw dust (Lagerstroemia microcarpa): kinetic, modeling of equilibrium, thermodynamic. *Int. Res. J. Environ. Sci. India,* **2**(8):6-16.

Kisacikoglu, M.C, Uzunoglu, M., Alam, M. S. (2009). Load sharing using fuzzy logic control in a fuel cell/ultracapacitor hybrid vehicle. *Int. J. Hydro. Ener.*, **34**:1497-1507.

Kondrat, S., Perez, C.R., Presser, C.R., Gogotsi, Y., Kornyshev, A. A. (2012). Effect of pore size and its dispersity on the energy storage in nanoporous supercapacitors. *En. Environ. Sci.,* **5**:6474-6479.

Kötz, R., & Carlen, M. (2000). Principles and applications of electrochemical capacitors. *Electrochem. Acta*., **45**:2483–2498.

Kumar, A.N., & Baek, J.B. (2014). Electrochemical supercapacitors from conducting polyaniline-graphene platforms. *Chem. Commun*., **50**:6298–6308.

Largeot, C., Portet, C., Chmiola, J., Taberna, P., Gogotsi, Y., Simon, P. (2008). Relation between the ion size and pore size for an electric double-layer capacitor. *J. Am. Chem. Soc.* **130** (9):2730-2731.

Le, Z. F., Liu, P., Nie, X., Li, X., Liu, Z., Bian, Z., Chen, G., Wu, H. B., Lu, Y. (2017). Pseudocapacitive sodium storage in mesoporous single-crystal-like TiO2-graphene nano composite enables high-performance sodium-ion capacitors. *ACS Nano.* **11**:2952–2960.

Lee, H.Y., & Goodenough J. B. (1999). Supercapacitor behavior with KCl electrolyte. *J. Solid State Chem*., **144** (1):220-223.

Lee, S.W., Kim, J., Chen, S., Hammond, P.T., Horn, Y.S. (2010). Carbon nanotube/manganese oxide ultrathin film electrodes for electrochemical capacitors. *ACS Nano*, **4**:3889.

Lewandowski, A., & Galinski, M. (2004). Carbon–ionic liquid double-layer capacitors. *J. Phys. Chem. Solids*, **64**:281-286.

Li, W., Probstle, H., Fricke, J. (2003). Electrochemical behavior of mixed C_mRF based carbon aerogels as electrode materials for supercapacitors. *J. Non-Cryst. Solids,* **325**:1−5.

Li, X., Xing, W., Zhuo, S., Zhuo, J., LI, F., Qiao, S. Z., Lu, G. Q. (2011). Preparation of capacitor's electrode from sunflower seed shell. *Bioresour. Technol.,* **102**:1118–1123.

Li, Y.T., Pi, Y.T., Lu, L.M., Xu, S.H., Ren, T.Z. (2015). Hierarchical porous active carbon from fallen leaves by synergy of K2CO3 and their supercapacitor performance. *J. Power Sources,* **299**:519–528.

Liang, Q., Ye, L., Huang, Z. H., Xu, Q., Bai, Y., Kang, F., Yang Q. H. (2014). A honeycomb-like porous carbon derived from pomelo peel for use in high performance supercapacitors. *Nanoscale,* **6:**13831-13837.

Limousy, L., Ghouma, I., Ouederni, A., Jeguirim, M. (2017). Amoxicillin removal from aqueous solution using activated carbon prepared by chemical activation of olive stone. *Environ. Sci. Pollut. Res.,* **24**:9993–10004.

Linares-Solano, A., & Carorla- Amoros, D. (2008). *Adsorption on activated carbon fibers.* Elsevier, Amsterdam: Holland.

Liu, T. C., Pell, W. G., Conway, B. E (1998). Behavior of molybdenum nitrides as materials for electrochemical capacitors comparison with ruthenium oxide. *J. Electrochem. Soc*., **145**:1882-1888.

Liu, Y., Wang, H., Zhou, J., Bian, L., Zhu, E., Hai, J. (2013). Graphene/polypyrrole intercalating nanocomposites as supercapacitors electrode. *Electrochim. Acta,* **112**:44–52.

Lu, H., Dai, W., Zheng, M., Li, N., Ji, G., Cao, J. (2012). Electrochemical capacitive behaviors of ordered mesoporous carbons with controllable pore sizes. *J. Power Sources*, **209**(1):243-250.

Lu, W. & Gleb, Y. (2012). Nanostructured activated carbons from natural precursors for electrical double layer capacitors. *Nano Energy*, **1**(4): 552-565.

Ma, S., Nam, K., Yoon, W., Yang, X., Ahn, K., Oh, K., Kim, K. (2007). A novel concept of hybrid capacitor based on manganese oxide materials. *Electrochem. Commun*., **9**:2807-2811.

Maharjan, M., Wai N., Veksha, A., Giannis A., Lim, M. T., Lisak, G. (2019). Sal wood sawdust derived highly mesoporous carbon as prospective electrode material for vanadium redox flow batteries. *J. Electroanalytical Chem*., **834**:94-100.

Mai, L., Dong, F., Xu, X., Luo, Y., An, Q., Zhao, Y., Pan, J., Yang, J. (2013). Cucumber-like V2O5/poly (3, 4-ethylenedioxythiophene) &MnO2 nanowires with enhanced electrochemical cyclability. *Nano Lett.,* **13**:740–745.

Marin, M.O., Fernandez, J.A., Lazaro, M. J., Gonzalez, C. F., Garcia, A. M., Serrano, V. G., Stoeckli, F., Centeno T. A. (2009). Cherry stones as precursor of activated carbons for supercapacitors, *Mater. Chem. Phys.*, **114**:323-327.

Marsh H. (1989). *Introduction to carbon science,* Butterworths.

Marsh, H., & Rodríguez-Reinoso, F. (2006). *Activated Carbon*, Elsevier: Science and Technology Books.

Marsh, H., Yan, D.S., O'Grady, T.M., Wennerberg, A, (1984). Formation of active carbons from cokes using potassium hydroxide. *Carbon,* **22**:603-611.

Maryati, D., Harjoso, Kuwat, T., Bambang, P. (2017). The effect of concentration nanoparticles MnO_2 doped in activated carbon as supercapacitor electrodes. *Inter. J. Appl. Eng. Res*. **12**(19):8625-8631.

Mastragostino, M., Arbizzani, C., Soavi, F. (2001). Polymer-based supercapacitors. *J. Power Sources,* **98**: 812 – 815.

Matzner, R., & Boehm, H. P. (1998). Influence of nitrogen doping on the adsorption and reduction of nitric oxide by activated carbons. *Carbon*, **36**(11):1697–709.

Mays T. J. (1999). *Active carbon fibers.* (chapter 3) in carbon materials for advanced technologies, 1st edition, (Elsevier Science Ltd, Oxford).

McKee D. W. (1991). *Oxidation protection of carbon materials.* In: Thrower PA, editor. Chemistry and physics of carbon, **23**: 173–232.

Mészáros, E., Jakab, E., Varhegyi, G., Bourke, J., Harris, M.M., Nunoura T., Antal, M. J. (2007). Do all carbonized charcoals have the same chemical structure? Implications of thermogravimetry-mass spectrometry measurements. *Ind. Eng. Chem. Res.,* **46**:5943-5953.

Miller, J. R., Outlaw, R. A., Holloway, B. C**. (**2010). Graphene double-layer capacitor with ac line-filtering performance. *Science*, **329:**1637-1639.

Mohamed, F. A. A, Zeid, A. A., Mohamad, A. H., Zlotea, C., Latroche, M., Cuevas, F. (2015). Hydrogen storage in pristine and d10-block metal-anchored activated carbon made from local wastes. *J. Energies*, **8** :3578-3590.

Molina-Sabio, M., Rodriguez-Reinoso, F. (2004). Role of chemical activation in the development of carbon porosity. *J. Coll. and Surf. Physicochem. Eng*., **241**: 15-25.

Molina-Sabio, M., RodRiguez-Reinoso, F., Caturla, F., Sellés, M. J. (1995). Porosity in granular carbons activated with phosphoric acid. *Carbon,* **33**:1105-1113.

Moreno-Castilla, C., Carrasco-Marin, F., Lopez-Ramon, M.V., Alvarez-Merino, M.A. (2001). Chemical and physical activation of olive-mill waste water to produce activated carbons. *Carbon*, **39**:1415-1420.

Na, R., Wang, X., Lu, N., Huo, G., Lin, H., Wang, G. (2018). Novel egg white gel polymer electrolyte and a green solid-state supercapacitor derived from the egg and rice waste. *Electrochim. Acta*, **274**:316–325.

Nabais, J. M. V., Laginhas, C. E. C., Carrott, P. J. M., Ribeiro, M. M. L. (2011). Production of activated carbons from almond shell, *Fuel Proc. Technol.,* **92**:234-240.

Nam, K. W., Lee, C. W., Yang, X. Q., Cho, B.W., Yoon, W.S. (2009). Electrodeposited manganese oxides on three-dimensional carbon nanotube substrate: Supercapacitive behavior in aqueous and organic electrolytes. *J. Power Sources*, **188**: 323-331.

Naoi K. (2010). Nanohybrid capacitor: the next generation electrochemical capacitors. *Fuel Cell*, **10** (5): 825-833.

Noor, A. B. M., & Nawi, M. A. B. M. (2008). Textural characteristics of activated carbons prepared from oil palm shells activated with $ZnCl_2$ and pyrolysis under nitrogen and carbon dioxide. *J. Phys. Sci.*, **19**(2):93-104.

Nuithitikul, K., Srikhun, S., Hirunpraditkoon, S. (2010). Influences of pyrolysis condition and acid treatment on properties of durian peel-based activated carbon. *Bioresour. Technol.*, **101**(1):426–429.

Okman, I., Karagoz, S., Tay, T., Erdem, M. (2014). Activated carbon from grape seed by chemical activation with potassium carbonate and potassium hydroxide. *Appl. Surf. Sci.*, **293**:138– 142.

Olabi, K.A.G., Orhan, S., Nafiz, A. (2017). Fuel cell and energy storage systems: a special issue section on 'the 9th international conference on sustainable energy and environmental protection. *Int. J. Hydro. Ener.*, **42**:25544–25549.

Olivares-Marin, M., Fernandez-Gonzalez, C., Macias-Garcia, A., Gomez-Serrano, V. (2006). Preparation of activated carbon from cherry stones by chemical activation with $ZnCl_{2.}$ *Sur. Sci*., **252**:5967-5971.

Oubagaranadin, J. U. K., & Murthy Z. V. P. (2009). Removal of Pb (II) fromaqueous solutions by carbons prepared from Salwood (*Shorea robusta*). *Eur. J. Wood Prod.,* 67:197–206.

Pandolfo, A. G., & Hollenkamp, A.F. (2006). Carbon properties and their role in supercapacitors. *J. Power Sources,* **157** (1):11−27.

Park, J. H., Park, O. O., Shin, K. H., Jin, C. S., Kim, J. H. (2002). An electrochemical capacitor based on a Ni $(OH)_2$/activated carbon composite electrode. *Electrochem. Solid-State Lett.,* **5** (2): H7. https://doi.org/10.1149/.

Park, S. J., & Jung, W.Y. (2003). KOH activation and characterization of glass fibers-supported phenolic resin. *J. Coll. Inter. Sci.*, **265**:245-250.

Peng, C., Yan, X., Wanga, R., Lang, J., Oub, Y., Xue, Q. (2013). Promising activated carbons derived from waste tea-leaves and their application in high performance supercapacitors electrodes. *Electrochim. Acta.,* **87**:401– 408.

Prabaharan, S.R.S., Vimala, R., Zainal, Z. (2006). Nanostructured mesoporous carbon as electrodes for supercapacitors. *J. Power Sources,* **161**(1):730-736.

Prahas, D., Yoga, K., Nani, I., Suryadi, I. (2011). The use of activated carbon prepared from jackfruit peel for methylene blue removal. *J. Env. Pro. Sci.,* **2**:1-10.

Prahas, D., Kartika, Y., Indraswati, N., Ismadji, S. (2008). Activated carbon from jackfruit peel waste by H_3PO_4 chemical activation: Pore structure and surface chemistry characterization. *Chem. Eng. J.,* **140**:32-42.

Przepiórski J. (2006). *Activated carbon filters and their industrial applications*. In: Bandosz T.J, (ed), Activated carbon surfaces in environmental remediation, New York: Elsevier.

Puziy, A. M., Poddubnaya, O. I., Martı´nez-Alonso, A., Sua´rez-Garcia, F., Tascon, J. M. D. (2002). Synthetic carbons activated with phosphoric acid; surface chemistry and ion binding properties. *Carbon,* **40**(9):1493–1505.

Puziy, A.M., Herbst, A, Poddubnaya, O.I, Germanus, J., Harting, P. (2003). Modeling of high-pressure adsorption using the bender equation of state. *Langmuir*, **19**:314–320.

Puziy, A.M., Poddubnaya, O.I., Gawdzik, B., Sobiesiak, M., Tsyba, M.M. (2007). Phosphoric acid activation – functionalization and porosity modification. *Appl. Surf. Sci.,***253**(13):5736–5740.

Puziy, A.M., Poddubnaya, O.I., Martı´nez-Alonso, A., Castro Muniz, A., Suarez-Garcia, F., Tascon, J. M. D. (2007) Oxygen and phosphorus enriched carbons from lignocellulosic material. *Carbon,* **45**(10):1941–1950.

Qu, D., & Shi, H. (1998). Studies of activated carbons used in double-layer capacitors. *J. Power Sources*, **74**:99-107.

Qu, W.H., Xu, Y.Y., Lu, A.H., Zhang, X.Q., Li, W.C. (2015). Converting biowaste corncob residue into high value added porous carbon for supercapacitor electrodes. *Bioresour. Technol.*, **189**:285–291.

Ra, E. J., Raymundo-Pinero, E., Lee, Y. H., Beguin, F. (2009). High power supercapacitors using polyacrylonitrile-based carbon nanofiber paper. *Carbon*, **47** (13):2984–2992.

Rahman, M. M., Bari, Q. H., Mohammad, N., Ahsan, A., Sobuz, H. R., Uddin, M.A. (2013). Characterization of rice husk carbon produced through simple technology. *Adv. Mater. Sci. Appl* **2**(1):25–30.

Rajbhandari, R., Shrestha, L. K., Pradhananga, R. R. (2011). Preparation of activated carbon from Lapsi seed stone and its application for the removal of arsenic from water. *J. Inst. Eng.*, **8**:211-218.

Rajbhandari, R., Shrestha, L. K., Pradhananga, R. R. (2012). Nanoprous activated carbon derived from lapsi seed stone (Choerospondiasaxillaris) seed stone for the removal of arsenic from water. *J. Nanosci. Nanotechnol.*, **12**:7002– 7009.

Rivera-Utrilla, J., & Ferro-Garcia, M.A. (1986). Effect of carbon–oxygen and carbon–nitrogen surface complexes on the adsorption of cations by activated carbons. *Adsorpt. Sci. Technol.*, **3**: 293–302.

Rodríguez-Reinoso, F., & Molina-Sabio, M. (1998). Textural and chemical characterization of microporous carbons. *Adv. Col. Inter. Sci.*, **76-77**:271-294.

Rufford, T. E., Jurcakova, D. H., Khosla, K., Zhu, Z., Lu, G. Q. (2010). Microstructure and electrochemical double-layer capacitance of carbon electrodes prepared by zinc chloride activation of sugar cane bagasse. *J. Power Sources*, **195**:912–918.

Rufford, T. E., Jurcakova, D. H., Zhu, Z., Lu G. Q. (2008). Nanoporous carbon electrode from waste coffee beans for high performance supercapacitors. *Electrochem. Commun.*, **10**:594–1597.

Rwayhah, Y.M.N., Hassan M. L., Shehata, M.R. (2017). Nanoporous activated carbon from olive stones waste. *J. Sci. Indus. Res*., **76**:725-732.

Salunkhe, R.R., Karmachi, Y., Torad, N.L., Hwang, S.M., Sun, Z., Dou, S.D., Kim, J..H., Yamauchi, Y. (2014). Fabrication of symmetric supercapacitors based on MOF-derived nanoporous carbons. *J. Mater. Chem. A*, **46**:19848. http://www.yamauchi-labo.com.

Sarangapani, S., Tilak, B.V., Chen, C. P. (1996). Materials for electrochemical capacitors theoretical and experimental constraints. *J. Electrochem. Soc*., **143**:3791-3799.

Sarkar, A., Singh, A. K., Sarkar, D., Khan, G.G., Mandal, K. (2015). Three-Dimensional Nano-Architecture of $BiFeO_3$ anchored TiO_2 Nanotube Arrays for Electrochemical Energy Storage and Solar Energy Conversion. *J. ACS Sust. Chem. Eng.*, **3**(9) :2254-2263.

Saueprasearsit P. (2011). Adsorption of chromium (Cr+6) using durian peel. In: *Intl Conf. Biotech. Environ. Manage. Singapore*, **18**:33–38.

Shaheed, R., Azhari, C. H., Ahsan, A., Mohtar, W.H.M.W. (2015). Production and characterization of low-tech activated carbon from coconut shell. *J. Hydro. Environ. Res*. **3**(1):6–14.

Shaikh, W. A., Chakraborty, S., Islam, R.U. (2019). Photocatalytic degradation of rhodamine B under UV irradiation using *Shorea robusta* leaf extract-mediated bio-synthesized silver nanoparticles. *Int. J. Environ. Sci. Technol.*, 1–14.

Sharma, P. & Bhatti, T. S. (2010). A review on electrochemical double-layer capacitors. *J. Ener. Conv. Manage.*, **51**(12):2901-2912.

Shi, K., Ren, M., Zhitomirsky, I. (2014). Activated carbon-coated carbon nanotubes for energy storage in supercapacitors and capacitive water purification. *ACS Sust. Chem. Engine.*, **2**:1289–1298.

Shrestha, D., Maensiri, S., Wongpratat, U., Lee, S.W., Rajbhandari, A. (2019 a). Shorea robusta derived activated carbon decorated with manganese dioxide hybrid composite for improved capacitive behaviors. *J. Environ. Chem. Engine.*, Elsevier,**7**: 103227. https://doi.org/10.1016/j.jece.2019.10322.

Shrestha, D., Maensiri, S., Wongpratat, U., Lee, S.W., Rajbhandari, A. (2019 b). Nanoporous activated carbons for supercapacitive energy storage. *I. J. Chem. Pharm. Sci.*, **7**(7):168–176.

Shrestha, R.M. Varga, M., Yadav, A.P., Pokharel, B.P., Pradhananga R.R., (2013). Removal of Ni (II) from aqueous solution by adsorption onto activated carbon prepared from Lapsi (*Choerospondias axillaris*) seed stone. *J. Ins. Engine*., **9**(1):166–174.

Sieminski A. (2013). US energy information administration independent statistics & analysis. *Inter. Ener. Outlook 2013* for US Senate Briefing. Washington, DC.

Simon, P., & Gogotsi, Y. (2008). Materials for electrochemical capacitors. *Nat. Mater*., **7**: 845–854.

Simon, P., & Gogotsi, Y**. (**2013**).** Capacitive energy storage in nanostructured carbon–electrolyte systems. *Acc. Chem. Res.*, **46**(5):1094-1103.

Simon, P., Gogotsi, Y., Dunn, B. (2014). Where do batteries end and supercapacitors begin? *Science,* **343**: 1210-1211.

Sinprachim, T., Phuming, S., Maensiri, S. (2016). Electrochemical energy storage performance of electrospum AgOx-MnO2/CNF composites. *J. Alloys Compd*., **677**: 1–11.

Soudani, N., Najar-Souissi, S., Abderkader-Fernandez, V. K., Ouederni, A. (2017). Effects of nitrogen plasma treatment on the surface characteristics of olive stone-based activated carbon. *Environ. Technol.*, **38**:956–966.

Spahis, N., Addoun, A., Mahmoudi, H., Ghaffour, N. (2008). Purification of water by activated carbon prepared from olive stones. *Desalination*, **222**:519-527.

Srikun, S, Hirunpraditkoon, S., Nuithitikul, K. (2011). Lead adsorption of activated carbon synthesized from durian peel. *Adv. Flu. Mech. Heat Mass Transf.*, 66–71.

Stoller, M. D., & Ruoff, R.S. (2010). Best practice methods for determining an electrode material's performance for ultracapacitors. *Ener. Environ. Sci.*, **3** (9):1294–1301.

Stoller, M. D., Park, S., Zhu, Y., An, J., Ruoff, R. S. (2008). Graphene-based ultracapacitors. *Nano Let.*, **8**:3498–3502.

Su, X.L., Li, S.H., Jiang, S., Peng, Z. K., Guan, X.X., Zheng, X.C. (2018). Superior capacitive behavior of porous activated carbon tubes derived from biomass waste-cotonier strobili fibers. *Adv. Powder Technol*. **29**:2097–2107.

Suárez-García, F., Martínez-Alonso, A., Tascon, J. M. D. (2000). Pyrolysis of apple pulp: chemical activation with phosphoric acid. *J. Anal. App. Pyro.*, **63(2)**:283-301.

Sugumaran, P., Susan, V. P., Ravichandran, P., Seshadri, S. (2012). Production and Characterization of Activated Carbon from Banana Empty Fruit Bunch and *Delonix regia* Fruit Pod. *J. Sustain. Ener. Environ.*, **3**:125-132.

Taberna, P. L., Simon, P., Fauvarque, J. F. (2003). Electrochemical characteristics and impedance spectroscopy studies of carbon-carbon supercapacitors. *J. Electrochem. Soc.*, **150** (3):A292- A300.

Taer, E., Deraman, M., Talib, I. A., Awitdrus, A., Hashmi, S. A., Umar, A.A. (2011). Preparation of a highly porous binderless activated carbon monolith from rubber wood sawdust by a multi-step activation process for application in supercapacitors. *Int. J. Electrochem. Sci*., **6**:3301– 3315.

Tawfik, A. S., & Gaddafi I. D. (2016). Adsorptive desulfurization of dibenzothiophene from fuels by rubber tyres-derived carbons: Kinetics and isotherms evaluation. *Proc. Safe Environ. Prot.*, **102**:9-19.

Thommes, M., Kaneko, K., Neimark, A. V., Olivier, J. P., Rodriguez-Reinoso, F., Rouquerol, J., Sing, K. S. W. (2015). Physisorption of gases, with special reference to the evaluation of surface area and pore size distribution (IUPAC technical report). *Pure & App. Chem.*, **87**(9-10):1051-1069.

Troshin, P.A., Hoppe, H., Peregudov, A.S., Egginger, M., Shokhovets, S., Gobsch, G., Sariciftci N.S., Razumov V. F. (2011). Fullerene-based materials for organic solar cells. *Chem. Sus. Chem*., **4**:119–124.

Tyagi, A., Tripathi, K.M., Gupta, R. K. (2015). Recent progress in micro-scale energy storage devices and future aspects. *J. Mater. Chem. A.,* **3**:22507–22541.

Verla, A. W., Horsfall, M., Verla, E. N., Spiff, A.I., Ekpete, O. A. (2012). Preparation and characterization of activated carbon from fluted pumpkin seed shell. *Asi. J. Nat. & Appl. Sci*., **1**(3):39-50.

Wang, C., Li, H., Zhao, J., Zhu, Y. (2013). Graphene nanoribbons as a novel support material for high performance fuel cell electro catalysts. *Int. J. Hydro***.** *Ener.,* **38**: 13230–13237.

Wang, D.W., Li, F., Cheng, H.M. (2008). Hierarchical porous nickel oxide and carbon as electrode materials for asymmetric supercapacitor. *J. Power Sources*, **185** (2):1563–1568.

Wang, G., Wang, H., Lu, X., Ling, Y., Yu, M., Zhai, T., Tong Y., Li, Y. (2014). Solid-state supercapacitor based on activated carbon cloths exhibits excellent rate capability. *Adv. Mater.,* **26**:2676–2682.,

Wang, H., Hao, Q., Yang, X., Lu, L., Wang, X. (2009). Graphene oxide doped polyaniline for supercapacitors. *Electrochem. Commun.,* **11**:1158-1161.

Wang, J. G., Yang, Y., Huang, Z. H., Kang, F. (2012). Incorporation of nanostructured manganese dioxide into carbon nanofibers and its electrochemical performance. *Mat. Lett.,* **72**:18–21.

Wang, J. G., Yang, Y., Huang, Z. H., Kang, F. (2013). Effect of temperature on the pseudocapacitive behavior of freestanding MnO_2@carbon nanofibers composites electrodes in mild electrolyte. *J. Power Sources*, **224**:86–92.

Wang, J. W., Chen, Y., Chen B. Z. (2015). A synthesis method of MnO_2/activated carbon composite for electrochemical supercapacitors. *J. Electrochem. Soc*., **162** (8): A1654–A1661.

Wang, J., & Kaskel, S. (2012). KOH activation of carbon-based materials for energy storage. *J. Mater. Chem.,* **22** (45): 23710-23725.

Wang, L., He, X., Li, J., Gao, J., Fang, M., Tian, G., Wang, J., Fan, S. (2013). Graphene-coated plastic film as current collector for lithium/sulfur batteries. *J. Power Sources*, **239**: 623–627.

Wankhade, A. A., & Ganvir, V.N. (2013). Preparation of low cost Activated carbon from Tea wasting using sulphuric acid as activating agent. *Int. Res. J. Environ. Sci*., **2** (4):53-55.

Wei, H., Gu, H., Guo, J., Cui, D., Yan, X., Liu, J., Cao, D., Wang, X., Wei S., Guo, Z. (2017). Significantly enhanced energy density of magnetite/polypyrrole nanocomposite capacitors at high rates by low magnetic fields. *Adv. Compos. Hybrid Mater.,* **1**:127–134.

Winter, M., & Brodd, R. J. (2008). What are batteries, fuel cells, and supercapacitors? *Chem. Rev.,* **104**:4245– 4270.

World Resources Institute (1996). *World Resources 1996–1997*, Oxford University Press, New York, 1996.

Wu, F. C., Tseng, R. L., Hu, C. C., Wang, C. C. (2004). Physical and electrochemical characterization of activated carbons prepared from firwoods for supercapacitors. *J. Power Sources*, **138**:351–359.

Xie, K., Zhang, M., Yang, Y., Zho, L., Qu, W. (2018). Synthesis and supercapacitor performance of polyaniline/nitrogen-doped ordered mesoporous carbon composites. *Nanoscale Res. Lett.*, **13:**163. doi: 10.1186/s11671-018-2577-3.

Xing, Y., Fang, B., Bonakdarpour, A., Zhang S., Wilkinson D.P. (2014). Facile fabrication of mesoporous carbon nanofibers with unique hierarchical nanoarchitecture for electrochemical hydrogen storage. *Int. J. Hydro. Ener.,* **39** (15):7859–7867.

Xiong, W., Liu, M., Gan, L., Lu, Y., Li, Y., Yang, L., Xu, L., Hao, Z., Liu, H., Chen, L. **(**2011). A novel synthesis of mesoporous carbon microspheres for supercapacitor electrodes. *J. Power Sources,* **196:**10461-10464.

Xu, A.N., Sun, X., Zhao, F. (2017) The role of pre-lithiation in activated carbon/ $Li_4Ti_5O_{12}$ asymmetric capacitors. *Electrochim. Acta,* **236**:443–450.

Xu, B., Chen, Y., Wei, G, Cao, G., Zhang, H., Yang, Y. (2010). Activated carbon with high capacitance prepared by NaOH activation for supercapacitors. *Mater. Chem. Phys*., **124**:504–509.

Yahya, M.A., Mansor, M.H., Zolkarnaini W.A.A.W., Rusli, N.S., Aminuddin, A., Mohamad, K., Sabhan F. A. M., Atik A. A. A., Ozair L.N. (2018). A brief review on activated carbon derived from agriculture by-product, *Recent Advancement on Applied Physics, Industrial Chemistry and Chemical Technology. AIP Conf. Proc., 1972,* 030023-1–030023-8.

Yakout, S.M., Sharaf El-Deen, G., (2016). Characterization of activated carbon prepared by phosphoric acid activation of olive stones. *Arab. J. Chem.,* **9**:S1155–S1162.

Yan, J., Fan, Z., Wei, T., Qian, W., Zhang, M., Wei, F. (2010). Fast and reversible surface redox reaction of graphene–MnO2 composites as supercapacitor electrodes. *Carbon,* **48**: 3825-3833.

Yang, H., Yan, R., Chen, H., Lee, D. H., Zheng, C. (2007). Characteristics of hemicellulose, cellulose and lignin pyrolysis. *Fuel,* **86**:1781–1788.

Yang, J., & Qiu, K. (2010). Preparation of activated carbons from walnut shells via vacuum chemical activation and their application for methylene blue removal. *Chem. Engine. J.,* **165**:209–217.

Yang, X., Cheng, C., Wang, Y. Qiu, L., Li, D. (2013). Liquid-mediated dense integration of graphene materials for compact capacitive energy storage. *Science,* **341**: 534-537.

Yeung, K. K., Zhang, X., Kwok, S.C.T., Ciucci, F., Yeun, M.M.F. (2015). Enhanced Cycle life of lead-acid battery using graphene as a sulfation suppression additive in negative active material. *RSC Adv*., **5**:71314–71321.

Yin, L., Chen, Y., Li, D., Zhao, X., Hou, B., Cao, B. (2016). 3-Dimensional hierarchical porous activated carbon derived from coconut fibers with high-rate performance for symmetric supercapacitors. *Mater. Des*., **111:** 44–50.

Yu, G., Hu, L., Liu, N., Wang, H., Vosgueritchian, M., Yang, Y., Cui, Y., Bao, Z. (2011). Enhancing the supercapacitor performance of graphene/MnO_2 nanostructured electrodes by conductive wrapping. *J. Nano Lett*., **11**:4438- 4442.

Yuan, G.H., ,Jiang, J. H., Aramata, A., Gao, Y. Z.(2005). Electrochemical behavior of activated-carbon capacitor material loaded with nickel oxide. *Carbon,* **43**(14): 2913-2917**.**

Zequine, C., Ranaweera, C.K., Wang Z., Dvornic, P. R., Kahol, P. K., Singh, S., Tripathi, P., Srivastava, O.N., Singh, S., Gupta, B.K., Gupta G., Gupta R.K. (2017). High-performance flexible supercapacitors obtained via recycled jute: bio-waste to energy storage approach. *J. Sci. Rep*., **7**: 1174. https://doi.org/10.1038/s41598-017-01319-w.

Zhang, J. T., & Zhao, X. S. (2012). On the configuration of supercapacitors for maximizing electrochemical performance. *Chem. Sus. Chem*., **5**:818-841.

Zhang, J., Zhong, Z., Shen, D., Zhao, J., Zhang, H., Yang, M., Li W. (2011). Preparation of bamboo-based activated carbon and its application in direct carbon fuel cells. *Energy Fuels,* **25**:2187–2193.

Zhang, L. L., & Zhao, X. S. (2009}. Carbon based materials as supercapacitor electrodes. *Chem. Soc. Rev.,* **38**:2520– 2531.

Zhang, S., Zheng, M., Lin, Z., Li, N., Liu, Y., Zhao, B., Pang, H., Cao, J., He, P., Shi, Y. (2014**)**. Activated carbon with ultrahigh specific surface area synthesized from natural plant material for lithium–sulfur batteries. *J. Mater. Chem. A*, **2:**15889-15896.

Zhang, Y., Feng, H., Wu, X. B., Wang, L. Z., Zhang, A. Q., Xia, T. C., Dong, H. C., Li, X. F., Zhang, L. S. (2009). Progress of electrochemical capacitor electrode materials: a review. *Int. J. Hydro. Ener.*, **34**:2467-2470.

Zhao, C., Zheng, W., Wang, X., Zhang, H., Cui, X., Wang, H. (2013). Ultrahigh capacitive performance from both $Co(OH)_2$/graphene electrode and $K_3Fe(CN)_6$ electrolyte. *Sci. Rep.*, **3**:2986. https://doi.org/:10.1038/srep02986.

Zhao, F., Dai, S., Wu, Y., Zhang, Q., Wang, J., Jiang, L., Ling, Q., Wei, Z., Ma, W., You, W., Wang, C., Zhan, X. (2017). Single-junction binary-blend nonfullerene polymer solar cells with 12.1% efficiency. *Adv. Mater.*, **29**(18):1700144. https://doi.org/10.1002/adma.201700144.

Zhao, S., Wang, C. Y., Chen, M. M., Wang, J., Shi, Z. Q. (2009). Potato starch-based activated carbon spheres as electrode material for electrochemical capacitor. *J. Phys. Chem. Solids*, **70**:1256–1260.

Zhu, Y., Murali S., Stoller, M. D., Ganesh, K. J., Cai, W., Ferreira, P. J., Pirkle, A., Wallace, R. M., Cychosz, K. A., Thommes, M., Su, D., Stach, E. A., Ruoff, R. S. (2011). Carbon-based supercapacitors produced by activation of graphene. *Science*, **332**: 1537-1541.

APPENDIX

Scientific Publications

1. **Dibyashree Shrestha**, Santi Maensiri, Unchista Wongpratat, Soo Wohn Lee, Armila Rajbhandari Nyachhyon, Shorea robusta derived activated carbon decorated with manganese dioxide hybrid composite for improved capacitive behaviors (2019) Journal of Environmental Chemical Engineering, **7,** 103227.

2. **Dibyashree Shrestha**, Santi Maensiri, Unchista Wongpratat, Soo Wohn Lee, Armila Rajbhandari Nyachhyon, Nanoporous Activated Carbons for Supercapacitive Energy Storage, (2019) International Journal of Chemistry and Pharmaceutical Sciences, **7**(7): 168–176.

3. **Dibyashree Shrestha**, Govinda Gyawali, Armila Rajbhandari, Preparation and Charecterization of Activated Carbon from Waste Sawdust from Saw Mill (2018) Journal of Science and Technology (JIST) **22**(2), 103- 108.

4. P. Pokhrel, **D. Shrestha**, A. Rajbhandari (Nyachhyon), Microwave Preheated Saw Dust Power an Efficient Precursor for Activated Carbon (2018) Lumbini Engineering College Journal (LCDJ) **1** (1): 44-51

APPENDIX – A

PAPER IN INTERNATIONAL JOURNAL

Title of Journal**: Journal of Environmental Chemical Engineering**

Title of Paper: **Shorea robusta derived activated carbon decorated with manganese dioxide hybrid composite for improved capacitive behaviors**

Published Date:

Received 12 April 2019; Received in revised form 10 June 2019

; **Accepted** 21 June 2019; **Available online** 15 July 2019

Published by

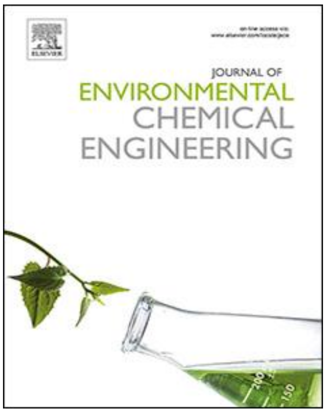

APPENDIX – B

PAPER IN INTERNATIONAL JOURNAL

Title of Journal: International Journal of Chemistry and Pharmaceutical Sciences

Title of Paper:

Nanoporous Activated Carbons for Supercapacitive Energy Storage

Published Date:

Received : 29 May 2018, **Accepted** 10 December 2018, **Available Online** 27 July 2019

Published by

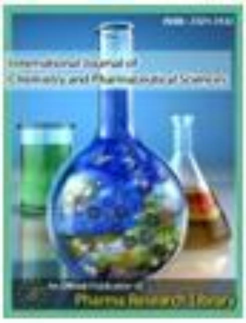

APPENDIX – C

PAPER IN NATIONAL JOURNAL

Title of Journal: **Journal of Science and Technology (JIST)**

Title of Paper:

PREPARATION AND CHARACTERIZATION OF ACTIVATED CARBON FROM WASTE SAWDUST FROM SAW MILL

Published Date:

January 2018

Published by

Institute of Science and Technology
Tribhuvan University
Kirtipur, Kathmandu, Nepal

Volume 22 Issue 2 January 2018

JOURNAL OF INSTITUTE OF SCIENCE AND TECHNOLOGY

Published by
Institute of Science and Technology
Tribhuvan University
Kirtipur, Kathmandu, Nepal

APPENDIX – D

PAPER IN NATIONAL JOURNAL

Title of Journal: **LEC Journal**

Title of Paper:

MICROWAVE PREHEATED SAW DUST POWDER AN EFFICIENT PRECURSOR FOR ACTIVATED CARBON

Published Date:

Received: 7 July, 2018; **Revised:** 14 September, 2018; **Accepted:** 9 October, 2018

Published by

Lumbini Engineering College
Pokhara University
Rupandehi, Nepal

APPENDIX – E

Participation in National and International conferences

1. International Conference on Advances in Polymer Science and Technology", held in Kathmandu, Nepal from 1-3 November, 2018 for Oral presentation, titled 'Wood Derived Nanoporous Activated Carbon, a promising Material for Supercapacitor'.
2. "5th Microsymposium on Applied Sciences [Nano/Bio]" April 29, 2017, held in Hotel Woodland, Kathmandu, Nepal. Poster Presentation, titled 'Electrochemical characterization of Wood Derived Nanoporous Activated Carbon'.
3. "International Conference in Functional Nanomaterials and Nanoscience" (ICFNN-2017), held in Hotel Yak and Yeti from 10-13 October 2017. (Poster Presentation)
4. Participation in four days "First Kathmandu Autumn School on Chemistry and Chemical Technologies" (KAS Chem - 2014), held on September 4 – 7, 2014 Kathmandu.
5. 5. Participation in four days "Kathmandu Symposia on Advance Material" (KaSAM - 2014), held on September 7 – 10, 2014, Kathmandu, Nepal.
6. 6. Participation in three days "16th International Symposium on Ecomaterials Processing and Design" (ISEPD - 2015), held on January 12 – 15, 2015 Kathmandu, Nepal.

APPENDIX – F

NAME OF THE SAMPLES

(1) (Sa-Raw):

Raw sawdust powder prepared from splinters of *Shorea robusta.*

(2) AC-(Sa-H_3PO_4):

As prepared activated carbon from sawdust of *Shorea robusta.*

(3) AC-(Sa-H_3PO_4)-electrode:

Electrode prepared from AC-(Sa-H_3PO_4).

(4) 1:1-(Sa-H_3PO_4:MnO_2)-hybrid-composite:

Hybrid composite prepared by mixing AC-(Sa-H_3PO_4) and MnO_2 powder in the ratio 1:1 i.e. (50 %: 50 %).

(5) 1:2-(Sa-H_3PO_4:MnO_2)-hybrid-composite:

Hybrid composite prepared by mixing AC-(Sa-H_3PO_4) and MnO_2 powder in the ratio 1:2 i.e. (33 %: 66 %).

(6) 2:1-(Sa-H_3PO_4:MnO_2)-hybrid-composite:

Hybrid composite prepared by mixing AC-(Sa-H_3PO_4) and MnO_2 powder in the ratio 2:1 i.e. (66 %: 33 %).

(7) 1:1-(Sa-H_3PO_4:MnO_2)-HCE:

Electrode prepared from 1:1-(Sa-H_3PO_4:MnO_2)-Hybrid-Composite.

(8) 1:2-(Sa-H_3PO_4:MnO_2)-HCE:

Electrode prepared from 1:2-(Sa-H_3PO_4:MnO_2)-Hybrid-Composite.

(9) 2:1-(Sa-H_3PO_4:MnO_2)-HCE:

Electrode prepared from 2:1-(Sa-H_3PO_4:MnO_2)-Hybrid-Composite.